DEFINING THE MOLECULAR MECHANISMS OF THE CEREBRAL CAVERNOUS MALFORMATION PROTEINS.

Bryan Timothy Richardson

A dissertation submitted to the faculty of the University of North Carolina at Chapel Hill in partial fulfillment of the requirements for the degree of Doctor of Philosophy in the Department of Pharmacology

Chapel Hill
2013

Approved by:

Gary L. Johnson, Ph.D.

Victoria L. Bautch, Ph.D.

Lee M. Graves, Ph.D.

Christopher Mack, Ph.D.

Robert A. Nicholas, Ph.D.

ABSTRACT

BRYAN TIMOTHY RICHARDSON: Defining the molecular mechanisms of the Cerebral Cavernous Malformation proteins.
(Under the Direction of Gary L. Johnson, Ph.D.)

Cerebral cavernous malformations (CCM) are the second most common class of cerebrovascular brain malformations affecting .1-.5% of the population. The disease is manifested in endothelial cells as lesions of thin, dilated, and leaky capillaries lacking normal blood vessel-stromal interactions. Lesions cause varied symptoms ranging from minor headaches to seizure and hemorrhagic stroke. CCMs can be incurred sporadically or inherited in an autosomal dominant manner from loss of function mutations in one of three genes, *ccm1/krit1*, *ccm2/osm*, or *ccm3/pdcd10*. These mutations affect the actin cytoskeleton due to deregulated RhoA/ROCK signaling, which increases stress fiber incidence, reduces endothelial cell barrier function, and decreases angiogenesis in vitro. We demonstrate through global kinome profiling that numerous kinases controlling the actin cytoskeleton are deregulated. Of these, we demonstrate that the RhoA/ROCK effector LIM kinase is overactive and phosphorylates and in activates the actin depolymerizing factor cofilin. Importantly, in vitro CCM phenotypes are rescued with knock down of LIM kinase in CCM protein deficient cells. We further show that a potential molecular mechanism governing the elevated RhoA levels and activity is through the E3 ubiquitin ligase

Smurf1, which associates with CCM2 but not CCM1 or CCM3 and is responsible for ubiquitinating GTP bound RhoA. Current cell culture and animal models of CCM have given insight into CCM phenotypes, but the study of patient cells are needed to validate these models and to test potential therapeutics. Thus, we provide proof of principle studies demonstrating the utility of both endothelial progenitor derived endothelial cells and pluripotent stem cells in CCM disease modeling for the ultimate goal of producing a library of patient induced pluripotent stem cells. Overall, our findings elaborate on and provide insight into the complex molecular pathways involved in CCM phenotypes while also making the first steps towards in vitro patient specific CCM disease modeling.

TABLE OF CONTENTS

LIST OF TABLES

TABLE

LIST OF FIGURES

FIGURE

LIST OF ABBREVIATIONS

AQUA: Advanced Quantitative Analysis

bEND.3: Mouse brain Endothelial cell

bFGF: Basic fibroblast growth factor

BMP4: Bone morphogenic protein 4

CCM: Cerebral cavernous malformations

CCM1: Cerebral Cavernous Malformation 1 gene

CCM1: Protein encoded by Cerebral Cavernous Malformation 1 gene, also known as KRIT1

CCM2: Cerebral Cavernous Malformation 2 gene

CCM2: Protein encoded by cerebral cavernous malformation 2 gene; also known as OSM, malcavernin

CCM2L: CCM2-Like protein

CCM3: Cerebral Cavernous Malformation 3 gene

CCM3: Protein encoded by cerebral cavernous malformation 3 gene; also known as PDCD10

EC: Endothelial Cell

EPC: Endothelial Progenitor Cell

EP-EC: Endothelial progenitor-derived endothelial cell

FAT: Focal Adhesion Targeting

FDA: Food and Drug Administration

FERM: Four point one band Ezrin Radixin Moesin

FLAG: Polypeptide tag consisting of DYKDDDDK

GAP: GTPase Activating Protein

GCKIII: Germinal Center Kinase 3

GDI: Guanine nucleotide dissociation inhibitor

GEF: Guanine nucleotide exchange factor

GEMM: Genetically engineered mouse model

GFP: Green fluorescent protein

H1/H7/H9: Human embryonic stem cell lines (1,7,9)

HEG1: Heart of glass

hESC: Human embryonic stem cell.

Huvec: Human umbilical vein endothelial cell

ICAP1: Integrin cytoplasmic adapter protein-1

IHC: Immunohistochemistry

IPS: Induced pluripotent stem cell

KRIT1: Krev Interaction trapped 1

LIMK: LIM kinase

LOH: Loss of heterozygosity

MEEC: Mouse embryonic endothelial cell

MEKK3: Mitogen-activated protein kinase kinase kinase 3

MLC2: Myosin light chain 2

MLCK: Myosin light chain kinase

MLCP: Myosin light chain phosphatase

mM: millimolar

MRI: Magnetic resonance imaging

mRNA: message RNA

MSH2: MutS homolog 2 protein

MST4: Mammalian Ste20-like Kinase 4

NuDiX: Nucleoside Diphosphate linked to X

OMIM: Online Mendelian inheritance in man

OSM: Osmosensing scaffold for MEKK3; also known as CCM2, malcavernin

PECAM1: Platelet endothelial cell adhesion molecule 1

PCR: Polymerase chain reaction

PDCD10: Programmed cell death 10 protein

PKA/C: Protein kinase A or C

PTB: Phosphotyrosine binding

RNA: Ribonucleic acid

RNAi: RNA interference

ROCK: Rho kinase

RT-PCR: Reverse transcription polymerase chain reaction

SDS-PAGE: Sodium dodecyl sulfate polyacrylamide gel electrophoresis

shRNA: short hairpin RNA

siRNA: small interfering RNA

SMURF1/2: Smad ubiquitination regulatory factor 1/2

STK24/5: Serine/threonine kinase 24/25

TGF-β: Tumor derived growth factor beta

VECadherin: Vascular endothelial cadherin

VEGF: Vascular endothelial growth factor

VEGFR2: Vascular endothelial frowth factor receptor

I. Introduction

CCM prevalence and pathophysiology

Stroke is a leading cause of death in the United States behind heart disease and cancer. Cerebral cavernous malformation (CCM; OMIM 116860) is the second most prevalent intracranial vascular malformation (IVM), which has symptoms ranging from mild headaches to epileptic seizure to hemorrhagic stroke [1]. Lesions appear principally in the central nervous system vasculature, but there have been reports of peripheral lesions in the retina, liver, and spinal cord [2]. Pathologically, CCM lesions are clusters of leaky capillaries, and the only treatment option for CCM is through invasive surgery or radiation therapy. Recent in vitro and in vivo experiments have attributed lesion generation to a break down of normal vascular remodeling and the blood brain barrier (BBB) linked to deregulation of the actin cytoskeleton of endothelial cells (EC)s through aberrantly high levels of the small GTPase RhoA [3-8].

CCM inheritance

CCM can be inherited in an autosomal dominant fashion or incurred sporadically [9]. In nearly all cases, loss of function gene mutations that lead to non-sense mediated mRNA decay have been mapped to three genes, *krit1 (ccm1), osm (ccm2), or pdcd10 (ccm3)*. CCMs are found in .4-.8% of the population with a higher

prevalence in Hispanic populations due to the presence of a founder mutation [10-12]. Mutation rates of the three genes have been estimated at 40%, 20%, and 40% for CCM1, CCM2, and CCM3, respectively [13-16]. Both genders are affected equally, and lesions are detected at a mean age of 35 with 25% of the cases presenting in childhood [17-19]. However, broad ranges, 10-40% of patients with CCM lesions remain asymptomatic [1, 20]. CCM symptom severity is a function of lesion location, size, and likelihood of hemorrhage [21]. CCM disease occurs sporadically and familially in an inherited form with 10-40% and over 50% in the Caucasian and Hispanic populations, respectively [2, 9]. There is some debate on the prevalence of familial CCM lesions as a study determined that 75% of reported sporadic CCMs were actually familial [22]. These numbers are skewed to more sporadic reporting of CCM lesions because CCM patients typically aren't genetically tested for germ-line mutations and typically do not receive genetic counseling. Interestingly, 22% of CCM patients that have multiple lesions have no mutation in any of the *CCM* genes, suggesting that other deregulated genes may cause CCM lesions to form [23]. This finding may also result from inadequate older generation PCR gene mutation identification strategies, which do not identify potential point mutations that can inhibit *CCM* gene function without complete protein loss. The identification of familial patients is important with over 50% of familial patients accruing multiple lesions, which are larger and more severe. In contrast, only 12% of sporadic patients have multiple lesions [1, 24]. Early lesion identification allows for the careful MRI monitoring of CCM lesions, which improves morbidity. Thus, recent advances in deep sequencing technology will make CCM patient gene

mutation identification more commonplace and accurate, which will expand current knowledge of familial vs. sporadic CCM formation and which CCM gene is mutated.

CCM pathophysiology

CCMs are characterized as well-circumscribed lesions that have a mulberry-like appearance ranging in size from one millimeter up to nine centimeters [25, 26]. Most all of CCM lesions are located within the subcortical cerebrum [27, 28]. Histologically, the endothelium has thin dilated walls with an intact basal lamina lacking any intervening brain parenchyma often with signs of prior microhemorrhages and hemosiderin deposition [25, 29, 30]. Typically, lesions have clots of blood in the endothelial lumen [30]. Endothelial cells maintain contacts with pericytes and astrocytes for the establishment of the blood brain barrier (BBB). However, CCM protein deficient ECs are void of these intracellular contacts, which decreases BBB stability and increases vascular leak [30]. Lesions are stratified into two stages; stage 1 lesions have enlarged blood vessels with hemosiderin deposits, and stage 2 lesions have more clusters of tangled blood vessels with calcification and astrogliosis [31]. Lesions increase both in size and severity with age, and they principally occur in areas of de-novo angiogenesis following surgical intervention [2, 32, 33].

CCM lesions are diagnosed through MRI as multi-lobule structures with a peripheral hemosiderin ring and are monitored yearly; they are observed until symptoms require treatment. Epilepsy and seizure symptoms are pharmacologically treated; however, numerous side effects occur, and up to 50% of CCM patients do

not respond to anti-epileptics [34]. In these cases, surgery is recommended, but many CCM lesions are surgically inaccessible. Radiation surgery is an alternative, but this method has increased complication rates with 16% of patients displaying permanent neurological deficits [35, 36]. These facts highlight the importance of understanding the basic signaling mechanisms contributing to CCM, which will promote the generation of non-invasive pharmacological agents for the treatment of CCM.

Knudson two hit hypothesis of loss of heterozygosity.

Specific inactivation of the mutated CCM protein in endothelial cells from patient lesion samples but not in surrounding normal brain tissue has given rise to the notion of CCM as a disease defined by a loss of heterozygosity, similar to the Knudson "two-hit" hypothesis for neoplastic cancer progression [37, 38]. Further evidence for LOH as a mechanism for inherited CCM phenotypes comes from mouse models, which show that homozygous knock out of CCM1, 2, or 3 are embryonically lethal [3, 39-41]. Furthermore, studies with CCM1 and CCM2 heterozygous mice in a p53 or Msh2 null background developed normally but displayed lesion formation with increasing age, phenocopying the human disease [8, 42, 43]. Two studies, however, have demonstrated that there is a CCM protein haplo-insufficiency related increase in vascular leak in the brain and lung in CCM1 and CCM2 heterozygous mice [3, 7]. This vascular leak was described post mortem through Evan's blue dye extravasation and suggests that there is a defect in endothelial barrier, which may not be enough to result in lesion formation. Further

histological analysis of human sections and tissue specific inactivation of CCM proteins in endothelial cells, neurons, and smooth muscle cells in mouse models have demonstrated that CCM phenotypes are isolated to endothelial cells [3, 37, 41]. However, A recent study, utilizing a tissue specific conditional knock out of CCM3 specifically in astrocytes from mice results in CCM lesion generation [44]. Therefore, it is widely accepted that the LOH mechanisms contribute to CCM lesion development; however, whether there are cells other than ECs affected by CCM protein loss remains controversial, and new models to describe these differences are needed.

CCM lesion initiating cell(s)

The cell of origin for the development of CCM lesions is unknown, and lesion formation most likely is a multifactorial process. It is possible that CCMs arise from the loss of CCM-1, -2, or -3 in an endothelial cell which undergoes uncontrolled proliferation and sprouting angiogenesis or groups of endothelial cells accrue mutations concomitantly or slowly over time. Increased proliferation remains controversial with several reports both in cell culture and in mouse models demonstrating an increased and decreased cell proliferative effect after loss of the CCM proteins [8, 40, 41, 45, 46]. These conflicting differences, at least in vivo, may be associated with the lesion stage and developmental timing [8, 46] (Table 1). A new mouse model, which investigated the developmental timing loss of CCM2, showed that lesions only formed during times of active angiogenesis in murine development and loss of CCM2 did not affect already formed quiescent blood

vessels [46]. This indicates there is a peripheral signaling cue that may promote lesion generation in cells lacking CCM proteins. An attractive hypothesis, which has not been tested, is whether a circulating endothelial progenitor stem cell could lead to CCM lesion formation in adult tissues. Along these lines, there have been numerous reports of circulating endothelial progenitor cells leading to adult angiogenesis and recruited bone marrow-derived circulating cells that can lead to adult neovascularization [47]. Thus, it would be possible that a circulating stem cell, which has accrued a mutation in one of the CCM proteins, could hone to a site of active adult angiogenesis and form a CCM lesion. While speculative, this hypothesis could explain why CCM lesions form and from what cell they originate. The identification of the CCM cell(s) of origin will present an important discovery for the CCM field and may shed light into specific treatment paradigms for the prevention of lesions in familial CCM patients.

CCM protein structure, function, and signaling

CCM1

The three genes CCM1, CCM2, and CCM3 are associated with global cytoskeletal mediated cell shape and polarity regulation by regulating RhoA and ROCK signaling (Fig 1.0 and 1.1). CCM1 was mapped as the first known gene to cause CCM through linkage analyses to 7q21.2 [48, 49]. CCM1 knock out is developmentally lethal from improper primary branchial arch artery formation [40]. There have been over 100 independent germ line mutations that have been mapped to CCM1 and [14, 48-57]. The CCM1 gene product is a 51 KD protein that was first

discovered in a yeast-2-hybrid screen as an interactor with the small G-protein Rap1A [58]. This interaction was direct and occurred through its FERM (band 4.1 Ezrin, Radixin, Moesin) domain, which was specific for Rap1A and not Ras [58]. The presence of four ankrin repeat domains within CCM1 are thought to establish additional protein-protein interactions. Interestingly, there are differently spliced isoforms of CCM1, which abrogate binding of CCM1 to Rap1A, and the expression of these different isoforms have been sequenced in familial CCM1 patients [59-61].

This CCM1/Rap1A interaction led researchers to investigate whether CCM1 was a regulator of Rap1A signaling. It was shown that CCM1 associates with the membrane proteins β-catenin, AF-6, and p120catenin, which was dependent upon the FERM domain dependent interaction of activated Rap1A and CCM1 [62]. Functionally, the loss of this membrane protein association with CCM1 led to the delocalization of β-catenin, increased membrane permeability, and increased F-actin stress fiber formation. It was further shown that CCM1 moves through the cell through an association with microtubules, and it is subsequently displaced from the microtubule network at the membrane by GTP bound Rap1A [63]. An additional yeast two-hybrid screen demonstrated that CCM1 binds to the integrin binding protein ICAP-1 through an n-terminal NPXY motif within CCM1 [63]. Binding of ICAP-1 to CCM1 converts CCM1 from a closed to open form by displacing an intramolecular interaction between the CCM1 C-terminal FERM domain and an N-terminal NPAY motif, promoting a ternary interaction between CCM1, ICAP-1, and Rap1A [63]. Overall, these experiments have delineated an important role for CCM1 in regulating membrane junctions, integrin signaling, and F-actin formation [64].

CCM1 was further established as a scaffolding protein after it was demonstrated that CCM1 directly binds to the CCM2/MEKK3 complex endogenously [65]. This binding is dependent upon the functional CCM2 PTB domain as a single point mutation abrogates the interaction [65]. Functionally, the CCM1/ICAP1/CCM2 complex promotes cytoplasmic accumulation of CCM1 and ICAP1, which is further enhanced during hyperosmotic stress [65]. This phenotype has ascribed CCM2 as having a nuclear shuttling role for CCM1. The CCM1 scaffolding complex may also be functionally restricted to the endothelium. Data supporting this idea was generated after the discovery of the mammalian ortholog to the zebrafish heart of glass receptor 1 (HEG1) [39]. HEG1 is required for the formation of a patent blood vascular network and is only expressed in endothelial cells [39]. The malformation following HEG1 knock out phenotypically copied CCM lesions with increased aberrant endothelial junctions [39, 66]. The CCM1/CCM2 complex co-immunoprecipitates with HEG1 with CCM1 binding directly and CCM2 indirectly through its interaction with CCM1 [39]. These data suggest that CCM1 is further regulating the endothelial junctions through its association with HEG1, CCM2, and β-catenin.

CCM is a multifactorial disease process; therefore, it is not surprising that there have been reports of CCM1 function outside of the more investigated Rap1A/CCM2/HEG signaling (Table 1). Recently, CCM1 has been described as promoting low reactive oxygen species (ROS) through FoxO1 mediated upregulation of the antioxidant protein SOD2 [67]. This functionally resulted in a transition from proliferative growth to quiescence [67]. The function of CCM proteins on cellular

growth has remained a point of contention with some groups reporting positive or negative growth promoting effects of CCM proteins (Table 1). Recently, it was reported that CCM1 functions to activate NOTCH signaling through increased PIP2/3 induced AKT phosphorylation signaling to reduce aberrant angiogenesis and cell proliferation through inhibition of phospho-ERK1/2 [45]. Because CCM1 loss increased phospho-ERK1/2 the multi-kinase inhibitor Sorafenib, which is a potent ERK1/2 inhibitor, was used as a potential therapeutic to reduce aberrant endothelial sprouting [45]. In contrast to these results, our lab has consistently observed decreased proliferation after shRNA knock down of CCM1; these results may differ based upon the type of RNAi knock down technology employed. Thus, a better approach may be to assess the in vitro proliferation potential of endothelial cells from CCM1 null mouse embryos

Loss of CCM1 protein increases F-actin stress fiber formation, which is one of the hallmarks of an epithelial to mesenchymal transitions (EMT). EMT is a normal developmental process, which becomes aberrantly occurs in metastatic cancer and fibrosis. In general, an EMT involves a loss in cell polarity and increased migratory capability accompanied by a loss in epithelial cell markers. These epithelial markers include adherens and tight junction proteins such as E-cadherin, ZO-1, Occludin, and Laminin. Mesenchymal cells gain expression of the EMT promoting transcription factors Snail, Slug, Twist, Goosecoid, Lef-1 and FOXC2 with a concomitant increase in the expression of mesenchymal markers α-SMA, N-cadherin, and Vimentin. A major upstream driver behind EMT is through tumor derived growth factor beta (TGF-β) signaling. TGF-β binds the TGF-βR1 and TGF-βR2 receptor tyrosine

kinases, which elicit a cellular response through phosphorylation of the Smad proteins. Smads function as transcription factors promoting EMT gene expression. Endothelial to mesenchymal transition (EndMT) is a highly related process, and during embryogenesis endothelial cells undergo an EndMT to form the endocardial cells and heart valves [68].

Interestingly, an inducible murine CCM1 knock out model generated lesions, which had highly disorganized VE-cadherin staining and an increase in the EMT markers N-cadherin, Slug, ID1, α-SMA CD44 and stem cell markers Sca1, CD44, and Klf4. The expression of these markers were proportional to lesion size and were not present in the normal surrounding brain vascular tissue [69]. TGF-β signaling through BMP6 was found to be the upstream driver of this process selectively in brain endothelial cells. BMP6 is a strong mesenchymal inducer and in line with previous results, CCM1 loss reduced Notch signaling, which functioned to inhibit BMP6 expression [45, 69]. Importantly, small molecule inhibition of TGF-β signaling with either SB-431542 or LY-364947 reduced the number of lesions, prevented vascular leak, and restored correct astrocyte endothelial connections. This EndMT phenotype was further visualized in mouse CCM3 lesions and in human CCM lesions from CCM1 and CCM2 patients [69]. These data suggest that the CCM1 is playing an important role in promoting the Notch pathway, which antagonizes mesenchymal differentiation programs by blocking TGF-β signaling. With CCM2 and CCM3 also giving similar EndMT phenotypes it will be of importance to understand at a molecular level if CCM2 and CCM3 are also regulating Notch signaling and whether CCM1 coordinates this interaction. Questions remain as to

whether the EndMT is a driver of lesion formation or if it is a developmental artifact detected during developmental angiogenesis in mice. It will be interesting to determine if this EndMT is driven by RhoA/ROCK signals and whether it is reversible by ROCK inhibition.

CCM2

The second protein responsible for CCM (CCM2) was originally characterized as the Osmosensing Scaffold for MEKK3 (OSM). Sorbitol induced hyperosmotic shock causes dynamic actin polymerization and membrane ruffles that are regulated by Rac1 and MEKK3 mediated activation of p38. MEKK3 was used as a bait to identify potential unknown scaffolding proteins that may be important regulators of the cellular response to hyperosmotic shock [70]. The OSM/CCM2 gene product was identified in this screen and was shown to bind to MEKK3 and Rac1 at sites of active membrane ruffles following sorbitol treatment. Furthermore, OSM/CCM2 co-immunoprecipitated with actin in vitro and was required for activation of p38. Knock down of CCM2 or MEKK3 alone led to decreased p38 activation and the double knock down synergistically decreased p38 activation, suggesting that CCM2 coordinates MEKK3 subcellular localization. This study suggested that the Rac1-OSM-MEKK3-p38 signaling cascade regulates cellular adaptation to osmotic stress similarly to the Hog1 stress signaling pathway in yeast [70]. Interestingly, MEKK3 and p38 knock out animals die in utero from defective vascularization [71, 72]. It is unknown whether p38 signaling contributes to the development of CCM.

Concomitant with this work, OSM was genetically mapped as a novel PTB domain containing protein, which was the second gene responsible for CCM [73].

The establishment of CCM2 as a scaffolding protein closely resembled the function of CCM1. Hilder et al. 2007 utilized nanoelectrospray mass spectrometry and multidimensional protein identification technology (MudPIT) to map out all potential CCM2 interactors in mouse macrophage cells [74]. Importantly, in this unbiased proteomic approach the previously identified CCM interactors CCM1, MEKK3, Rac1, ICAP-1, and PDCD10 (CCM3) was identified as a novel CCM2 interactor (Table 2 and Fig 1.3). Follow up co-immunoprecipitation assays demonstrated that CCM3 binds CCM2 but not CCM1, and the three are found in a complex when overexpressed. Interestingly, a designed CCM2 F217A PTB domain mutant, which mimics CCM2 point mutations found in patients, abrogated the binding of many of the interacting proteins. The PTB domain was not found to be essential for CCM3 binding as the crystal structure of CCM3 and CCM2 demonstrated that binding was between the CCM3 FAT domain and CCM2 C-terminal Karet domain [75]. This concept of the CCM1, -2, and -3 proteins working in complex helps to explain how the loss of three structurally different proteins yields indistinguishable clinical presentation and identical in vitro cell phenotypes. Much work remains to describe how each of the CCM proteins function in this complex to regulate EC homeostasis.

CCM2 knock out mice die mid gestation due to improper heart patterning and branchial arch artery formation, which phenocopies CCM1 knock out animal models [3, 40, 41]. These heart defects were endothelial cell autonomous as excision of the

CCM2 gene by cre recombinase in neurons and smooth muscle had no effect [3]. This loss of CCM2 decreased endothelial tube morphogenesis, increased endothelial cell permeability, and increased F-actin stress fiber formation [3]. However, in contrast to CCM1, the CCM2 knock out model did not affect β-catenin membrane localization, cellular proliferation, or phospho-Erk levels [3]. One of the major regulators of F-actin formation is the small GTPase RhoA. Indeed, it was shown that CCM2 binds to RhoA and Rac1 but not CDC42 and loss of CCM2 only increases the basal activity of RhoA [3]. Importantly, direct inhibition of RhoA prenylation and membrane association by Simvistatin decreased actin stress fibers and membrane permeability. Deregulated RhoA signaling concomitant with F-actin stress fibers and changes in cellular morphogenesis suggests that there is a major cytoskeletal defect component to the pathology of CCM.

In CCM deficient endothelial cells, increased RhoA levels are due to the decreased degradation of RhoA as no changes in message levels have been detected [4, 5]. Crose et al. demonstrated that CCM2 binds to Smurf1 in a PTB and HECT domain dependent fashion, which functions to localize Smurf1 to the cell periphery where it ubiquitinates RhoA, leading to its proteasomal degradation [5]. CCM2 was neither a substrate of Smurf1 nor did CCM2 affect the ability of Smurf1 to ubiquitinate other targets [5]. It was further shown that CCM2 functions to degrade RhoA in a dose dependent fashion, which was specific as the levels of other Smurf1 substrates, such as MEKK2 were unchanged [5]. This role of CCM2 as a molecular shuttle for Smurf1 is analogous to the recruitment of Smurf1 to the membrane of epithelial cells by atypical PKCζ, which results in the ubiquitination and degradation

selectively of the active form of RhoA in the regulation of protrusion formation [76]. It is unknown whether CCM2 functions within the Par6-PKCζ complex. However, it was shown that loss of CCM2 endogenously stabilizes total RhoA protein [4]. Given that loss of CCM2 increases active RhoA, and Smurf1 increases active RhoA in other cell systems we hypothesized that the loss of Smurf1 would also increase active RhoA in endothelial cells through its interaction with CCM2. Furthermore, it is unknown mechanistically how the loss of CCM1 and CCM3 increases RhoA levels, but it is likely that they work in conjunction with CCM2 to regulate Smurf1 dependent RhoA degradation. Thus, degradation, in addition to GEF and GAP regulation of RhoA signaling, is likely a major pathway that underlies the etiology of CCM.

Recently the CCM2 like or CCM2L paralog of CCM2 has been discovered, which developmentally antagonizes CCM2 function [77]. CCM2L is expressed solely in endothelial cells of the developing embryo at sites of active angiogenesis, and mice lacking CCM2L were severely retarded in their ability to form xenografted tumors due to lack of neovascularization [77]. Thus, CCM2L functions as a positive regulator of angiogenesis during development and tumor progression. CCM2L competes with CCM2 for binding with CCM1 [77]. In contrast to CCM2, CCM2L cannot bind CCM3 and decouples the endothelial cell stabilizing effects of the CCM1, -2, and -3 complex [77]. Expression of CCM2L mimics the loss of CCM2 by increasing RhoA activation, and total RhoA protein, while also decreasing lumenogenesis in vitro [77]. These effects on RhoA protein levels could be through competition for Smurf1 binding and provides another example of where the disruption of the CCM complex may promote RhoA signaling. Similar to the HEG

receptor, CCM2L mutations or overexpression have not been described in patients; however, with agreement in the field on the importance of sequencing CCM patient mutations, the identification additional genes involved in CCM pathology, such as HEG and CCM2L may be realized.

In addition to its endothelial cell autonomous functions with CCM1 and CCM3, CCM2 regulates TrkA receptor tyrosine kinase dependent apoptosis [78, 79]. Normally the TrkA receptor is involved in prosurvival signaling; however, in the case of pediatric neuroblastomas it functions as a pro-apoptotic protein [78]. Intriguingly, CCM2 was found to interact with the TrkA receptor with the requirement of both the PTB domain and Karet domain [78]. Loss of CCM2 in TrkA sensitive neuroblastoma cells increased cell survival, where as the overexpression of CCM2 decreased cell survival in a dose dependent fashion in TrkA insensitive cells [78]. Mechanistically, CCM2 functioned as a scaffolding protein, which bound to the germinal center kinase III (GCKIII) Stk25 and to the TrkA receptor [79]. CCM2 also bound to the GCKIII kinases Mst4 and Stk24, but this interaction had no effect on cell survival [79]. The interaction between Stk25 and CCM2 is essential as knock down of Stk25 protected neuroblastoma cells from TrkA- dependent cell death [79]. Furthermore, an intact kinase domain of Stk25 is also essential for TrkA- dependent cell death, as mutations in the active site abrogate its protective functions [79]. Interestingly, CCM2 has numerous phosphorylation sites and was shown to be phosphorylated by Stk25 [79]. The functional consequences of this phosphorylation is still unknown. Previously, CCM3 had been shown to directly bind to Mst4, Stk24, and Stk25 [6]. It will be of interest to determine if CCM2 also directly binds to these kinases and

whether the phosphorylation of CCM2 by Stk25 differentially affects CCM2 function. These studies will be of importance to further understanding the molecular mechanisms of how CCM2 contributes to CCM pathology.

CCM3

CCM3 appears to have more diverse functionality than that of CCM1 or CCM2. The gene product of CCM3 (PDCD10) was discovered as a protein that was up regulated in fibroblasts in response to pro-apoptotic stimuli and was later defined as the third gene responsible for CCM through mutational analysis [13, 80]. CCM3 is a 25 Kd protein with a focal adhesion targeting (FAT) domain that is required for binding to CCM2 and paxillin [75]. Through proteomic analysis it has been shown to interact with the GCKIIIs Stk23, Stk25, Mst4, and the striatin-interacting phosphatase and kinase (STRIPAK) complex [81]. This association with the GCKIIIs Mst4, Stk24, and Stk25 has led to numerous potential functions of CCM3. CCM3 was found to associate in a complex with GCKIII kinases and the GM130 Golgi protein at the cis side of the Golgi apparatus [82]. Functionally CCM3 led to the correct orientation of the Golgi during wound healing [82]. Golgi re-orientation is reflective of the cells ability to polarize correctly. Interestingly, lack of polarization due impart to cytoskeletal defects in endothelial cells is one of the hallmarks of CCM [83]. It will be important to confirm these findings on CCM3 regulation of the Golgi in endothelial cells as CCM proteins are expressed in all cell types and may function differently from cell type to cell type.

Developmentally, the knock out of CCM3 by specific morpholinos in zebrafish results in branchial arch artery defects that are identical to that of CCM1 and CCM2 [6]. Moreover, morpholino knock down of all Stk24 and Stk25 phenocopies the loss of CCM1, -2, or -3 in zebrafish, suggesting that there may be some functional redundancy between these two kinases; independent knock down had no developmental effect [6]. This single knock down effect is in contrast to the knock down of CCM3 alone, which has a profound defect on heart development [6]. In vitro, knock down of Stk25 increases endothelial monolayer permeability and F-actin stress fibers [6]. At a molecular level this interaction with GCKIII kinases promotes the STK24/25 mediated phosphorylation of moesin both in in vitro kinase assays and in vivo cell immunoflourescence [6]. Phospho-moesin negatively regulates RhoA, and promotes cell junction protein interactions and stability [6]. These data strongly link CCM3 both developmentally in vivo and in cell culture to the CCM specific phenotypes observed in CCM1 and CCM2 deficient cells.

Similar to data generated in zebrafish, the murine CCM3 knock out mouse exhibited global primary vascularization defects with no surviving embryos past embryonic day 8.5 [31]. This defect was found to be due to decreased VEGFR2 signaling as both phospho-VEGFR2 and total VEGFR2 levels were decreased as well as the VEGFR2 downstream targets phospho-PLC-γ and phospho-AKT [84]. Similar observations were seen in an independent study, which described CCM3 positively regulates the Notch pathway and subsequent VEGFR2 signaling [85]. CCM3 and downstream VEGFR2 loss decreased endothelial cell proliferation, increased apoptosis, led to disorganized junctional marker expression and

localization, and disrupted VEGF dependent in vitro tubulogenesis [31, 85]. Mechanistically, CCM3 was found to bind to the VEGFR2 protein, which led to its stabilization by preventing receptor endocytosis [31]. This effect was specific to CCM3 as CCM2 overexpression was unable to increase VEGF [31]. These data point to a potential differing role for CCM3 in the generation of CCM3 lesions; however, it is unknown whether loss of CCM1 or CCM2 also decreases VEGFR2 dependent signaling due to the disruption of the CCM1, -2, and -3 complex. While, there are many examples of VEGFR2 activation increasing the activation state of RhoA and promoting aberrant angiogenesis in cancer, it is unknown what the effect of VEGFR2 loss upstream on the RhoA protein is in the CCM signaling environment [86].

There remains some controversy about whether CCM3 functions in the same mechanistic pathway of CCM1 and CCM2 (Table 1). Chan et al. generated a separate CCM3 knock out mouse model, which growth arrests at embryonic day E8.0 before circulation is required and are embryonic lethal at day 13 [87]. This observation is in contrast to the CCM3 mouse model generated by He et al., which was lethal at day 8.5, failed to vascularize properly, and had noticeable cardiac structural defects [31]. In addition, CCM1 or CCM2 knock out mice die because of ineffective circulation and disrupted branchial arch artery development [3, 40]. The Chen et al. CCM3 knock out mouse developed both normal patent branchial arch arteries and cardiac structures but died due to venous rupture. In vitro, loss of CCM3 was shown to not increase actin stress fibers or phospho Myosin Light Chain (pMLC), a common mechanism to CCM1 and CCM2. In contrast to He et al. CCM3

did not bind to VEGFR2, effect VEGFR2 levels, or effect VEGFR2 downstream signaling molecules [87]. These differing in vitro phenotypes could be explained by residual CCM3 present in cell culture.

Further obfuscating the CCM3 mouse model phenotypic consensus, Louvi et al. described neural cell autonomous phenotypes in a third CCM3 knock out mouse model [44]. This study generated tissue conditional knock out mice under the control of the Nestin, GFAP, and Emx1 promoters [44]. All three neural specific knock out mice gave rose to enlarged brains and cerebrovascular defects [44]. These observations are in contrast to the mouse models generated by Chen et al. and He et al, which had no observed neural phenotypes. The developmental time points used to assess these neural effects could account for these conflicts. The first two CCM3 mouse models described differences in vascular development during embryogenesis and assessed that there were no relevant phenotypes because mice were born. These studies failed to examine whether brain tissue abnormalities existed where CCM lesions are the most symptomatic in patients. The neural specific knock out mice generated by Louvi et al. were born but died at P3; tissue examination was restricted to the brain. Thus, the knock out mice from the first two studies does not exclude the possibility of a neural cell autonomous function of CCM3. Importantly, the GFAP CCM3 knock out mouse described by Louvi et al. developed CCM lesions that pathologically are similar but not identical to human lesions. One characteristic of these lesions was an increased proliferation of astrocytes and astrogliosis. Global cytoskeletal deregulation was detected through RNA sequencing from laser microdissected lesions [44]. A gene signature for

proteins in the RhoA signaling pathway were more abundant than in controls [44]. These data suggest that CCM3 may be functioning in neural tissues in a similar way to CCM1 and CCM2 in the endothelium by regulating RhoA signaling. Moreover, the alternative CCM3 mouse models do no exclude CCM3 deficient neural tissues from promoting CCM lesion formation. To establish the clinical relevancy of CCM3 loss in neurons it will be important to determine whether patient CCM3 lesions occur when CCM3 is absent in neural tissues and present in endothelial cells. CCM lesions exhibit astrogliosis and those that exhibit the highest levels may result from mutations in CCM3 in neural tissues. These experiments are now possible with CCM tissue banks and CCM3 antibodies that can be used for immunohistochemistry [87].

Integrated CCM signaling

All signaling work to date has described the three proteins as adapter-like proteins that lack enzymatic activity. Clinically, mutations in the CCM proteins are indistinguishable and are only determined upon genetic sequencing analysis. This finding has given rise to the notion that the CCM proteins function in a similar way. This hypothesis is supported by data from Hilder et al. where all three CCM proteins form a stable ternary complex in the cell [74]. It has also become clear that the CCM proteins have dynamic independent functions. Therefore, it is likely that CCM1, CCM2, and CCM3 have both independent and dependent functions that regulate a common endothelial cell pathway. Clinically, it would be advantageous to find therapeutic targets that could lead to the treatment of CCM 1, -2, and -3 mutations

as a single entity. Currently, the only way to definitively distinguish between CCM1, -2, and -3 mutations is through expensive whole exome illumina DNA sequencing. Thus, there may be numerous independent molecular pathways that can lead to CCM lesion formation in mouse models and cell culture, but establishing the most accepted common pathway that is present in both CCM models and in patient lesions is paramount to establishing the first CCM therapy. This concept would limit the time for drug development and FDA approval, which is both time and cost intensive.

Small GTPase regulation

With this goal in mind, the most phenotypically relevant hallmarks of CCM pathology are increased endothelial cell monolayer permeability with deregulated angiogenesis attributable to global changes in the actin cytoskeleton. Work in the CCM field has conclusively shown that these hallmarks are due principally to deregulated RhoA signaling [83]. The role of deregulated RhoA signaling in CCM was first established from the experiments demonstrating that siRNA mediated loss of CCM1 led to an increase in F-actin stress fiber formation, a major *in vitro* phenotype occurring from overactive RhoA [62]. The Rho GTPases (RhoA, RhoB, and RhoC) are members of the Ras-related super family of small GTPases. They function as molecular switches that regulate many cellular processes including cell cycle progression, migration, gene expression, and cytoskeletal dynamics. This class of proteins cycles between an active GTP-bound state and an inactive GDP-bound state. Guanine nucleotide exchange factors (GEFs) activate GTPases by

exchanging GDP for GTP, and GTPase activating proteins (GAPs) inactivate them by promoting their intrinsic GTPase hydrolysis activity. The third type of regulation is through guanine nucleotide dissociation inhibitors, which block spontaneous GDP to GTP exchange [86].

Small GTPase regulation of endothelial junctions

CCM phenotypes can be effectively narrowed down to the deregulation of important small GTPases in angiogenesis. Part of the CCM protein complex function is to tightly regulate RhoA and Rap1 small GTPases. Therefore it is important to understand how the RhoA, Rap1, CDC42, and Rac1 small GTPases control EC migration, angiogenic patterning, barrier function, and capillary stability. In response to an angiogenic cue such as VEGF, vessels sprout from preexisting vessels and migrate into new tissue through a RhoA, Rac1, and CDC42 mediated up regulation of matrix metallo proteins [88]. The tip cells, which lead this sprout, form lamellipodia and filopodia through activation of Rac1 and Cdc42, respectively [89]. Cdc42 and Rac1 then activate p21 activated kinase (PAK), which activates Lim kinase, which phosphorylates and inactivates the actin de-polymerization factor cofilin [90]. This process leads to F-actin polymerization and protrusion formation. When neighboring endothelial cell lamellipodia and filopodia contact each other they form adherens junction interactions that have been shown to be mediated by nectin proteins [91]. This junction formation results in a positive feed back loop leading to further leading edge activation of Cdc42 and Rac1, which interact with the WASP and WAVE, respectively [91]. This interaction leads to activation of the Arp2/3 actin

polymerizing proteins, leading to actin polymerization, branching, and fortification at sites of interendothelial junctions [91]. During initial migration, RhoA works coordinately with this system by activating several downstream effectors. One is Rho associated kinase (ROCK1/2). One branch of the RhoA Rock pathway results in a similar activation of Lim kinase and phosphorylation of cofilin. This leads to F-actin polymerization and stress fiber formation. Concomitantly, active Rock also directly phosphorylates myosin light chain and myosin light chain phosphatase, which cumulatively promotes the association of actin and myosin II. In addition to ROCK, RhoA activates mDia, which results in actin polymerization and stress fiber formation [92]. Overall, this cascade results in cell contraction along the cell cytoskeleton. When cell contacts are made there is both inactivation and degradation of RhoA [91, 93]. With aberrant spatial and temporal activation of RhoA, the cell experiences aberrant contractile forces that physically separate junctional proteins [94]. These complex cytoskeletal dynamics in angiogenesis is tightly regulated in endothelial cells and recent studies suggest that CCM proteins may function to scaffold these regulators of the cytoskeletal GTPases.

In addition to limiting opposing contractile forces through regulating RhoA degradation and activity, CCM proteins play a direct role in junctional stabilization. CCM1 binds to Rap1 through its FERM domain and recruits it to the membrane [62, 95]. Once at the membrane, Rap1 functions to activate VAV2, a GEF for both CDC42 and Rac1, which promotes the stabilization of adherens junctions through VEcadherin [96]. In endothelial cells, RNAi knock down of CCM1 was able to prevent the Rap1 mediated stabilization of endothelial cell junctions [62].

Concomitantly, cell contraction and junctional instability is inhibited by the inactivation of RhoA through Rac1 mediated activation of p190RhoGAP [97]. Interestingly, CCM1 co-immunoprecipitates with p120CTN, which also has redundant functions with Rac1 in activating p190RhoGAP [98]. This deregulation of the actin cytoskeleton and EC barrier through increased and overactive RhoA likely accounts for CCM pathology of leaky and aberrantly clustered capillaries.

E3 ubiquitin ligase regulation of RhoA levels

An emerging role in small GTPase regulation in addition to GEF, GAP, and GDI regulation, is through the ubiquitin proteasomal system (UPS) protein degradation pathway. This pathway has been recognized as a major regulator of cellular function and has been shown to be an important mechanism for the regulation of the small GTPases Rac1, RhoA, and Rap1 and their respective GEFs and GAPs [99]. The signal for this pathway is carried out through addition of the ubiquitin modifier protein, a small peptide tag that binds covalently to acceptor lysine residues of specific substrates. Following ubiquitination with a string of four or more ubiquitin proteins, the substrate is transported to the 26S proteasome where the substrate protein is degraded to peptide fragments and the ubiquitin protein tags are recycled. This process occurs through three sequential ubiquitin activating enzymes (E1, E2, and E3). A series of biochemical reactions occurs resulting in the recruitment of ubiquitin by E1 and the subsequent passing of ubiquitin from E1 to E2 to E3 and then covalently to the substrate protein. The number of ubiquitin ligases grows from one E1 ligase to several dozen E2 ligases to over 400 E3 ligases. This

drastically increased number of E3 ubiquitin ligases yields an important dynamic range in substrate specificity [99]. The HECT domain family and RING/U-box family are the two families of E3 ligases shown to regulate the small GTPases. RhoA levels are regulated by the SMAD ubiquitin regulatory factor (Smurf) family and the Cullin E3 ubiquitin ligases, HECT domain and RING/U-box family members, respectively [99].

Smurf1 is a widely found E3 ubiquitin ligase, which has important roles in cellular growth, differentiation, and migration. It has a C2 domain, WW1 and 2 domains, and a catalytic HECT domain. Smurf1 originally was discovered as an important regulator of TGF-β signaling during osteogenesis [100-102]. Specifically, it ubiquitinates the SMADs 1 and 5 (receptor SMADs), 4 (common SMAD), and 7 (inhibitory SMAD) [103-105]. It also ubiquitinates type 1 and 2 BMP receptors and the TGF-β receptor 1[106, 107]. When phosphorylated at T306, Smurf1 is induced to ubiquitinate RhoA and has been shown to induce membrane protrusions, reduce actin stress fibers, and decrease cellular mobility in numerous cell systems [108]. Smurf1 ubiquitination is inhibited by the protein synaptopodin and reduces stress fibers [109]. PKCζ localizes Smurf1 to the membrane where it interacts with Par6 and degrades active RhoA at active sites of cellular protrusions. CCM2 also relocates Smurf1 to the membrane at sites of active actin polymerization [5, 70]. It has been shown that CCM1 regulates the membrane localization of PKCζ and mPAR3 for correct establishment of cellular polarity [110].

Cellular polarity is carefully maintained through the coordinate regulation of the cytoskeleton through the small GTPases Rap1, RhoA, and CDC42. CCM1 has

been shown to regulate the function and localization of the small GTPase Rap1A [95]. Similar to RhoA, Rap1A is degraded by the E3 ubiquitin ligase Smurf2. Functionally, this results in the establishment of correct neuronal polarity during development by the selective degradation of Rap1 in retracting neurites [111]. The Par polarity complex is responsible for localizing proteins for the establishment of proper cell polarity. Just as the Smurf1 interaction with PKCζ, Smurf2 interacts with mPar3, which localizes Smurf2 properly [112]. Interestingly, Smurf2 has been shown to ubiquitinate and degrade Smurf1, and these two E3 ligases have opposing functions in development [113]. Thus, it is clear that the localization of the E3 ubiquitin ligases and post translational modifications are paramount to their proper function. Smurf1 and Smurf2 are highly similar; therefore, an outstanding question in the CCM field is whether Smurf2 regulates Rap1A levels in ECs and whether CCM proteins function to localize Smurf2.

The Cullin ring ligase (CRL) family of ubiquitin ligases have broad functions and regulate the ubiquitination of many cell proteins [114]. There are six members of this family (Cul1, Cul2, Cul3, Cul4, Cul5, and Cul7); they function as scaffolds that link RING finger domain containing proteins, which bind to E2 ligases, and specific BTB domain containing substrate adapters that bind target proteins [115]. The cullin 3 family member previously has been shown to ubiquitinate total RhoA protein leading to its degradation [116]. In cell culture, loss of either cullin 3 or the RhoA substrate adapter Bacurd increases RhoA protein, stress fibers, and inhibits cellular migration [116]. This process has been implicated in vascular smooth muscle function, which when deregulated increases blood pressure in a mouse hypertension

model [117]. Currently, there have been no investigations into cullin function in ECs and whether CCM proteins have any roles in modulating cullin regulation

Rho-associated protein kinase (ROCK)

The main effector of RhoA that results in broad cytoskeletal changes that underlies CCM specific phenotypes occurs through ROCK. ROCK was initially identified as a RhoA effector that was involved in stress fiber and focal adhesion formation [118]. Currently, two highly similar isoforms of ROCK have been found (ROCK1 and ROCK2) [119]. Both ROCK1 and ROCK2 are required for normal development as knock out results in death soon after birth and in utero in ROCK1 and ROCK2 knock out mice [119]. Both isoforms of ROCK are up regulated by the cytokines angiotensin II and interleukin-1B. Interestingly, an isoform difference in angiotensin converting enzyme (ACE) in patients with familial CCM has been found [84, 120]. Structurally, ROCKs contain a catalytic kinase domain, coiled coil domain that includes a Rho binding domain, and a pleckstrin-homology domain with a cysteine rich domain [121]. ROCK1 and ROCK2 are inactive until RhoA in its active GTP bound form binds to the Rho binding domain of either Rock1 or Rock2 releasing their autoinhibited state [122]. ROCKs are ubiquitously expressed with ROCK II expression being the highest in the brain and in muscle tissue and ROCK I expression highest in the liver, spleen, lung, kidneys, and testis [118, 123]. ROCK proteins are found principally in the cytosol with a small fraction being membrane localized [118]. This membrane localization only occurs after activation of RhoA and subsequent RhoA and ROCK association [118]. After activation, ROCK

phosphorylates and regulates a myriad of substrates [121]. There is no empirical evidence that ROCK1 and ROCK2 phosphorylate alternate substrates, which is expected based upon their 92% kinase domain similarity [121].

ROCK substrates include, myosin light chain phosphatase, myosin light chain, adducin, ezrin-radixin-moesin (ERM proteins), and LIM kinase [121]. These substrates are directly involved in regulating actin filament polymerization and actin cytoskeletal dynamics. ROCKs provide a mechanism for smooth muscle contraction independently of calcium. ROCK2 dependent phosphorylates myosin light chain on serine 19, which results in the association of actin and myosin [124]. In addition to phosphorylating MLC directly, ROCKs phosphorylate myosin light chain phosphatase, which increases the stoichiometry of phosphorylated myosin to non-phosphorylated myosin [125]. This association results in the ATP dependent myosin cross bridge cycle of contraction. ROCK1 is involved in phosphorylating LIM kinase (LIMK) leading to subsequent actin stabilization through LIMK mediated phosphorylation and in activation of the actin severing protein cofilin [126-128].

Aberrant RhoA signaling through its effector ROCK is a major driver behind CCM and numerous aspects of human disease, including multiple aspects of cardiovascular disease, tumor metastasis, vasospasm, edema, glaucoma, and CNS neurological disorders [129]. The important role of ROCKs in the pathogenesis of CCM lesions is just now being realized to be the underlying molecular basis to the pathology of CCM. To this extent, positive pMLC2 staining has been reported in patient lesion samples that lack CCM1 or CCM2 expression but not in the normal flanking brain regions [7]. Furthermore, tight junction marker staining is decreased

in CCM patient lesion samples, consistent with the role of ROCKs in antagonizing junction stability [130, 131]. *In vitro*, positive pMLC2 immunoflourescent staining and immunoblotting has been shown in primary cell lines isolated from CCM1 and CCM2 haplo-insufficient mice and in shRNA knock down endothelial cells for CCM1, CCM2, and CCM3 [7] [4]. These high levels of pMLC2 result in F-actin stress fiber formation indicating that ROCK activity is a physiological readout for CCM both in vivo and in vitro. In addition, ROCK down regulates eNOS expression in endothelial cells through destabilization of eNOS mRNA, which leads to the activation of pro-inflammatory pathways and reactive oxygen species (ROS) generation [132]. Changes in redox state has been implicated in multiple facets of cardiovascular disease, including atherosclerosis, aortic aneurysm, and vascular stenosis [133]. In patient CCM lesions it has been shown that macrophages and lymphocytes enter into lesion sites and contribute to local inflammation around the lesion [134]. ROCKs are known to activate the expression of pro-inflammatory cytokines, such as NF-κB that lead to the infiltration of inflammatory cells [135]. Thus, it will be important to determine if the inflammation found in CCM lesions is due directly to overactive ROCK or secondarily because of the decreased barrier protection, which allows for immune cell extravasation.

In vitro assays that have been used to mimic *in vivo* phenotypes include permeability assays, tube formation assays, and migration assays. Loss of the CCM proteins and the subsequent increase in ROCK activity results in decreased endothelial barrier that has been reproduced by both transwell permeability assay and trans endothelial resistance [8]. Interestingly, reduction in endothelial barrier

and stress fiber formation could also be obtained by overexpressing a mutant form of CCM2 (CCM2 F217A) that is unable to bind to CCM1, suggesting that CCM proteins must work in a complex to regulate RhoA and ROCK [7]. In addition to decreased barrier, high ROCK activity due to the loss of CCM proteins results in deregulated endothelial cell morphogenesis, cell shape programs, and migration [4, 7]. With the loss of CCM proteins, endothelial cells are unable to properly form capillary like tube structures in both Matrigel and a 3D collagen matrix [4]. This phenotype has been replicated in two separate studies utilizing time-lapse microscopy and is thought to be due to an inability of the cell to form proper shape by sending out filopodial protrusions of the proper length or number [4, 7]. Endothelial cell migration is also effected with the loss of CCM proteins, which is in line with the important role of RhoA and ROCK signaling in cell migration [4]. In a wound healing assay, CCM2 deficient cells are unable to migrate and reform a monolayer, and CCM1, CCM2, and CCM3 deficient ECs demonstrate a decreased invasive ability in Matrigel invasion assays [4, 5]. However, the distance of haptotactic migration towards fibronectin is increased in an active RhoA dependent manner as simvastatin was able to rescue this increased migration [3]. These differences could be assay and substrate dependent effects, and more experiments are needed to elucidate the effects of CCM protein loss on ROCK mediated endothelial cell migration that may play roles in the dysangiogenesis and vascular remodeling of early in vivo lesion formation.

Therapeutic avenues for CCM

Simvastatin

A promising avenue for the pharmacological treatment of CCM is through statins. Statins are safe, effective, and have been used in treating hypercholesterolemia since 1987 [136]. Their efficacy comes from inhibiting 3-hydroxy-3-methyl-glutaryl-CoA reductase (HMG-CoA Reductase), which is an enzyme that controls the rate-limiting step in cholesterol biosynthesis [136]. Statins have been shown to decrease endothelial cell tone, reduce hypertension, and decrease arteriosclerosis [137]. Some of these "pleiotropic effects" come through the inhibition of RhoA localization through preventing its posttranslational prenylation. This inhibition has been shown in vitro to affect endothelial cell angiogenesis [138]. Relevant to CCM, Whitehead et al. demonstrated that Simvistatin could rescue CCM phenotypes in vitro and in vivo. The physiologically relevant EC50 Simvistatin to inhibit RhoA function, and whether this would be safe in patients needs to be determined. Therefore, while feasibly challenging, it would be very interesting to initiate a retrospective clinical study on CCM patients that take statins and whether the overall outcome of these patients is improved.

A phase 0 clinical trial was recently initiated for the use of statins in CCM titled, "Permeability MRI in Cerebral Cavernous Malformations Type 1 in New Mexico: Effects of Statins" (NCT01764451). The study will follow CCM patients by MRI who were treated with placebo vs. Simvastatin. Because statins are already FDA approved, the repurposing of this class of drugs for a new indication in the treatment of CCM will have minimal regulatory hurdles. This is the first clinical trial

initiated for CCM, and it highlights the importance of how understanding the basic biology of CCM over the past decade has led to a potential therapeutic avenue.

ROCK inhibitors in CCM

Inhibition of ROCK is able to rescue in vitro and in vivo CCM phenotypes and constitutes a promising avenue for the pharmacological treatment of CCM. Inhibition of RhoA and the activation of ROCKs by simvastatin rescues VEGF stimulated vascular leak in CCM2 deficient heterozygous mice [7]. This rescue was shown to be ROCK dependent as the ROCK selective inhibitor Y27632 was able to decrease stress fiber formation in CCM2 knock down cells [7]. Importantly, shRNA mediated ablation of ROCK2 was able to lower pMLC levels by immunoblotting in CCM1, CCM2, and CCM3 deficient endothelial cells [4]. Phenotypically, both knock down of ROCK2 and inhibition with Y27632 rescued Matrigel tube formation [4]. This effect is likely do to the rescue of cell shape by normalizing actin cystoskeleton dynamics as cells treated with Y27632 or ROCK2 stable knock down cells were able to extend multiple protrusions [4]. In addition to tube formation, ROCK inhibition by two structurally distinct inhibitors, H-1152 and Fasudil, reversed permeability and stress fiber defects *in vitro* in CCM1 and CCM2 knock down cells and decreased in vivo vascular leak stimulated by LPS in CCM1 and CCM2 heterozygous mice, respectively [7].

Recently, two mouse models for CCM1 and CCM2 were generated that model the two hit hypothesis for loss of heterozygosity that lack either the mismatch repair gene 2 (Msh2) or p53 [8]. These mice randomly incur mutations that result in

the loss of the remaining CCM allele because of heightened genomic instability. These loss of function mutations result in CCM lesion generation, which pathologically mimics human CCM lesion development. Importantly, when treated with a median dosage of Fasudil, these mice demonstrate a decrease in both lesion burden and severity as well as decreased hemosiderin deposition, a principle factor behind the seizures in CCM patients [8]. Due to phenotypes unrelated to CCM in the Msh2 deficient strain, namely lymphoma, mice were sacrificed at 5 months of age; therefore, no long term morbidity studies following Fasudil treatment can be done with these mice [8]. Regardless, the in vitro and in vivo completed at this point points to ROCK inhibition as a promising therapeutic option for CCM.

ROCK inhibition represents and important avenue for the treatment of CCM. In Japan, the ATP competitive inhibitor, Fasudil has been successfully used for the treatment of cerebral vasospasm after subarachnoid hemorrhage since 1995, and displays positive outcomes with little to no adverse side effects [139]. Therefore, Fasudil has been used successfully in small-scale clinical trials for the treatment of multiple cardiovascular diseases, including hypertension, coronary artery disease, coronary vasospasm, ischemia, and infarction [140]. The principal effect of Fasudil has been to inhibit ROCK, resulting in decreased smooth muscle contraction, increased eNOS expression, and reduced inflammation [140]. However, first generation ROCK inhibitors such as Fasudil, Y-27632, and H1152 have been shown to have off target effects and inhibit other kinases as well [140]. Thus, the success in these trials has led to the development of isoform specific and more selective ROCK inhibitors by pharmaceutical companies.

Rationale for an iPS cell disease model for CCM

The work from current models has allowed for the understanding of many complex phenotypes; however, it is unknown how these findings will translate to patients. Thus, most cell culture models of CCM entail the use of finite endothelial cells, which have limited usefulness in fully understanding the development of CCM lesions. Mouse models are now beginning to be utilized; however, generating an accurate animal model of spontaneous CCM, which encompasses the genetic diversity of human patients, is not possible. This basic disconnect underlines the importance of generating new patient specific models of CCM. Thus, understanding CCM in the context of patient cells will verify current disease mechanisms, allow for the discovery of new deregulated pathways in CCM, and test therapeutics for efficacy and toxicity (Fig 1.2).

Recent advances in cell biology have made the study of patient cells from rare or hard to study diseases possible. This importance of studying diseased cells from patients has been fully recognized for many years. However, the isolation and propagation procedures are often complicated by access, purity after isolation and slow cellular growth rates. Seminal work from the laboratory of Shinya Yamanaka demonstrated that fully differentiated fibroblasts can be induced to a pluripotent state or become induced pluripotent stem cells (iPS) through the ectopic introduction of transcription factors, which officially initiated the “reprogramming” era in cell biology [141, 142].

This establishment of reprogramming was built upon the initial work of James Thomson, who elucidated the growth conditions for pluripotent human embryonic stem cells (hESCs), and the reprogramming work in the field of somatic cell nuclear transfer (SCNT) [143, 144]. The molecular mechanisms driving the pluripotency machinery was mapped out, which led to the initial screen that identified Oct4, Sox2, KLF4, and cMyc as reprogramming factors known as the classical “Yamanaka cocktail” [142, 145]. Since the initial reprogramming experiments, new techniques, which avoid viral integration have been established, and there has been significant progress in elucidating the molecular mechanisms governing reprogramming [146]. These new methods reduce the chance that transgenes will be reactivated and inherently generate more homogenous iPS cell lines albeit at a cost of reprogramming efficiency.

The importance of hESCs cannot be understated, as they are the gold standard for determining how to differentiate pluripotent stem cells to relevant terminally differentiated daughter cell types. hESCs are normally occurring developmental cells, which are isolated from a pre-implantation embryo [144]. These cells are in contrast to iPS cells, which are forcibly derived from somatic cells through forced gene overexpression or chemical means [146]. On a superficial level these cells morphologically look the same and express the core pluripotency regulators at similar levels. However, the ability of these cells to differentiate into different daughter cell types is highly variable and is dependent upon the starting cell of origin. In fact, it has been shown that depending on the starting somatic cell being reprogrammed there is an “epigenetic memory” effect, where by the reprogrammed

cell has left over epigenetic markers, which pushes the iPS cell preferentially back into the original somatic cell type [147, 148]. For example, iPS cells generated from pancreatic islet beta-cells retained open chromatin marks for beta-cell related genes and retained a higher efficiency to differentiate to beta-cells [149]. This epigenetic memory effect typically becomes less pronounced with time in culture or with treatment with epigenetic modifying drugs such as, trichostatin A and 5-azacytidine [150]. In situations where directed differentiation is challenging this epigenetic memory can be exploited by selecting the same cell of origin that the iPS cells will be in re-differentiated back into for study or therapy. Therefore, the somatic cell type of choice for initiating reprogramming becomes important when considering differentiation potential and kinetics.

The proper differentiation of pluripotent stem cells to a desired daughter cell type has been a major hurdle for researchers. Knowledge obtained from in vivo mammalian and chick development has been in valuable in establishing the conditions for differentiating pluripotent stem cells, which involves recapitulating many signaling aspects of normal development (Fig 1.3). Accordingly, different cytokines or small molecules that are agonists or antagonists for major signaling pathways are utilized to commit pluripotent stem cells to the ectoderm, mesoderm, or endoderm germ layers with further cytokines or small molecules added to specify more specific lineage commitments. The results of these experiments typically produce immature somatic cells, which are heterogeneous in respect to cellular subtype. The limitation to obtaining an exact cell type needed for study is limited by the knowledge of developmental pathways and signaling molecules that normally

result in the in vivo development of that cell. Purifying the target cell is typically accomplished by cell surface marker analysis either by flow cytometry or micro bead purification strategies. To date, neurons, myocardiocytes, haematopoietic cells, endothelial cells, hepatocytes, pancreatic cells, smooth muscle cells, and numerous other cell types have been generated from first hESCs followed by hiPS cells. Importantly, the field has begun to establish protocols for generating specific subtypes of each type of these cells. For example, specific dopaminergic neurons found only in the striatum have been developed for the in vitro study of Parkinson's disease and cortical neurons. Many cell types require more substantial functional development, meaning these cell types such as cardiomyocytes must contract in a directed manor to fully develop into a differentiated cell type, which are now being defined [151].

The generation of patient specific cell therapy has been a major focus for stem cell researchers. Thus, the establishment of hESCs and hiPS cells that can differentiate into a myriad of cell types was thought to be a major break through in the regenerative medicine field. These cells represented a unique and transient developmental cell type with the ability to differentiate along the three germ layers, mimicking in vivo gastrulation to any and all cells that constitute the human body. Furthermore, they expressed telomerase and were immortal until properly differentiated [152]. Therefore, it was initially thought that these cells would generate a plethora of regenerative cells for the treatment of diseases ranging from neurodegenerative disorders, heart disease, and spinal cord injury.

Along these lines, two breakthrough studies by the Jaenisch group at MIT demonstrated the powerful regenerative potential of iPS cells in the mouse. Hanna et al. set out to demonstrate that iPS cells could ameliorate sickle cell anemia [153]. To accomplish this goal, they generated disease miPS cells from a humanized sickle cell anemia mouse, which had the murine α and β globin genes replaced with the human sickle cell globin genes. With homologous recombindation, they were able to correct the gene mutations and re-transplant in vitro differentiated bone marrow precursor cells back into an irradiated mouse. These genetically corrected miPS cell derived precursor cells were able to reconstitute a healthy bone marrow and drastically increase erythrocyte function. The second study by Wernig et al. used iPS cells to correct Parkinson's disease phenotypes following administration of 6-hydroxy dopamine [154]. They established that iPS cells differentiated in vitro to dopamine neurons were able to functionally integrate into the mid brain, express tyrosine hydroxylase, and reverse the behavioral phenotypes associated with Parkinson's disease.

Despite these promising results, the regenerative medicine applications of hESCs and hiPS cells have yet to be realized with the only study receiving FDA approval for clinical trials in the treatment of retinal degeneration being recently abandoned by Geron Corporation [155]. hESCs have been limited from the beginning by host vs. graft rejection issues and careful HLA evaluation of the hESC line is required, and immunosuppressive agents may be needed [156-158]. Principally, concerns remain with the possibility of hIPS cells forming aberrant tumors. This possibility of tumor formation is especially of concern in iPS cells

generated with integrating retro or lenti viruses that encode oncogenes, such as cMyc, which have the possibility of aberrant transgene re-activation [159]. Furthermore, if residual pluripotent stem cells remain in the transplanted culture there is a possibility for teratoma formation. Most of the preclinical iPS cell therapy studies have been done in immune suppressed mice, and the level of aberrant teratoma formation is directly correlated to the level of immunosuppression [160]. Interestingly, a recent study demonstrated that mice were immunogenic to syngeneic iPS cell teratomas and not to ES cells teratomas due to aberrant gene expression [161]. Therefore more work needs to be done to establish whether iPS cells truly will not elicit an immune response, differentiate and integrate into the host properly, and not be tumorgenic.

The use of iPS cells in the immediate term has been repurposed from cell therapy to in vitro diagnostics. In this context, iPS cells represent a unique patient-specific disease modeling and drug screening platform technology [162]. The best diseases to model with iPS cells are monogenetic with cell autonomous disease presentation [163]. iPS cells are grown and differentiated in an in vitro environment that is much different than the in vivo environment of the patient; therefore, the phenotypes need to be inherent to the cell rather than environmentally induced. One of the most impressive examples of iPS based disease modeling comes from the modeling of familial dysautonomia (FD) [164]. This disease is caused by a single mutation in the IKBKAP gene, which leads to gene silencing and peripheral neuropathy. Using lineage differentiation, it was found that the loss of this gene solely occurred in neural crest progenitor cells. Furthermore, upon screening small

molecules, the plant protein kinetin was found to rescue the in vitro phenotypes. This avenue of patient specific in vitro research has become highly fruitful with patient iPS cells being generated from over 24 different diseases [163]. Importantly CCM has these similar characteristics in that it is cell autonomous and monogenetic with distinct phenotypic assays.

Another facet of disease modeling with iPS cells or hESCs cells comes following the advent of next generation genome editing technologies. Gene targeting of mouse embryonic stem cells (mESCs) through homologous recombination has been realized as one of the great breakthroughs in biomedical science allowing for the generation of animal models of human genetic disease [165]. This technique has been hard to employ with hESCs with low rates of recombination. To address this issue, researchers have generated zinc finger mediated Fok1 fusion protein nucleases, Talens and Crispr [166]. Each of these methods increase the efficiency of gene recombination by using a rationally designed DNA binding domain, fused to an endonuclease domain [167]. The specificity of zinc fingers and Talens is established by two anti-parallel engineered DNA binding domains bound to the Fok1 endonuclease, which cuts each respective strand that generates a double strand break (DSB) [77]. Crispr technology uses guide RNA and the Cas9 endonuclease ribonucleoprotein complex to align and generate a DSB. The template DNA is then recombined into the host genome through non-homologous end joining (NHEJ). When modeling patient diseases, these technologies are invaluable because they will allow the generation of diseased control iPS cell lines by knocking out the gene that is implicated in the onset of the disease. These cells will be invaluable for

establishing if patient cell phenotypes are monogenic or polygenic. Furthermore, these cells will help establish important phenotypes from those that occur simply from iPS line to iPS line clonal variance.

CCM is an autosomal dominant disease with incomplete penetrance, which requires LOH. The phenotypic severity and number of lesions during life varies widely among patients Therefore, CCM is a disease that would benefit greatly from an iPS disease model. With this model it will be possible to obtain cells from patients and reprogram these cells to iPS cells. With established differentiation paradigms and the ability to take advantage of cellular epigenetic memory mechanisms in iPS cells, we will be able to establish the cell autonomous disease phenotypes from CCM mutant cells. Furthermore, we will be able to use genome-editing technologies to simulate disease progression by removing the healthy allele from CCM patients. One of the most exciting avenues will be to utilize genome editing to knock in fluorescent tags to CCM proteins to visualize their endogenous functions across a myriad of cell types including endothelial cells. These modified cells will allow for an unprecedented ability to determine the endothelial cell functions of CCM proteins from the functions of CCM proteins in other cells. More clinically relevant, these iPS cells will allow for the validation of CCM phenotypes from patients and also present the possibility of patient-specific small molecule drug screening, while also addressing some of the controversies in the CCM field.

Objectives

In recent years there has been much progress into establishing the mechanisms behind CCM pathophysiology. This process started with the molecular cloning of the three CCM genes and has progressed to the point of initiating the first clinical trail in CCM. In lieu of these milestones, much work is needed to fully understand the complex CCM protein-signaling network in cells from actual CCM patients. There is little known about the involvement of kinases as drivers of CCM phenotypes either up or downstream of RhoA. Kinases are important signaling molecules that translate extracellular cues to cell changes, of which many are targetable and have FDA approved inhibitors currently available. **Therefore, an objective of this project is to profile the kinome in an unbiased way to discover important regulators of the endothelium that are deregulated in CCM protein deficient ECs.** This objective was accomplished through multiplexed kinase inhibitor beads coupled with quantitative mass spectrometry. We found many conserved kinases that were deregulated in both CCM protein deficient ECs from mouse and human. We validated previously identified kinases described in CCM biology and expanded this list with many more kinases that directly regulate the actin cytoskeleton and the previously described RhoA signaling node. Further validation of these data will provide additional kinase-mediated drivers of CCM phenotypes.

Our laboratory has previously established that the loss of any one of the CCM proteins increases both the active and total pools of RhoA without any increase in message level. Overall, these elevated levels of RhoA increase F-actin stress fibers and EC permeability (Fig 1.0). Thus, we posit that that the central function of the

CCM proteins in ECs is to regulate RhoA and the actin cytoskeleton. **However, an outstanding question in the CCM field is how RhoA levels are increased following CCM protein loss. Thus, we seek to further define how RhoA is regulated in ECs.** Specifically, we focused on how the degradation of RhoA is a molecular mechanism contributing to an increase in RhoA signaling. To this extent we show that the ubiquitinated status of GTP bound RhoA is decreased in CCM or Smurf1 protein deficient ECs. We further hypothesize that the CCM protein ternary complex coordinates Smurf1 function or localization and facilitates the Smurf1 mediated degradation of GTP bound RhoA.

CCM is a multifactorial disease, which varies greatly in the severity of lesions from patient to patient. Despite this known facet of CCM, there has been little study of the phenotypes in cells from CCM patients. Most all of the studies from CCM patients have been from surgically resected lesions, which can only provide retrospective information about CCM lesion genesis. Thus, the further understanding of the molecular pathways driving defects in ECs and how individual patient genetic backgrounds influence this process is greatly needed. Furthermore, it is unknown whether heterozygous CCM patients have defects in EC function. **Therefore, the final objective of this thesis is to establish a feasible model for studying diseased patient endothelial cells**. We undertook this objective by establishing endothelial progenitor derived ECs (EPC-ECs) and hESCs as valid models for the study of CCM phenotypes. We further were able to generate iPS cells from these EPC-ECs as a novel cell source for iPS cell generation. The relevance of this approach is two-fold; EPC-ECs allow for immediate study of CCM

phenotypes from patients, and iPS cells allow for the generation of an immortalized CCM patient cell bank. The proof of concept studies provided here will allow for the generation of iPS cells for the study of patient ECs and potentially uncover novel mechanisms driving CCM phenotypes, which can only be realized in CCM patient cells.

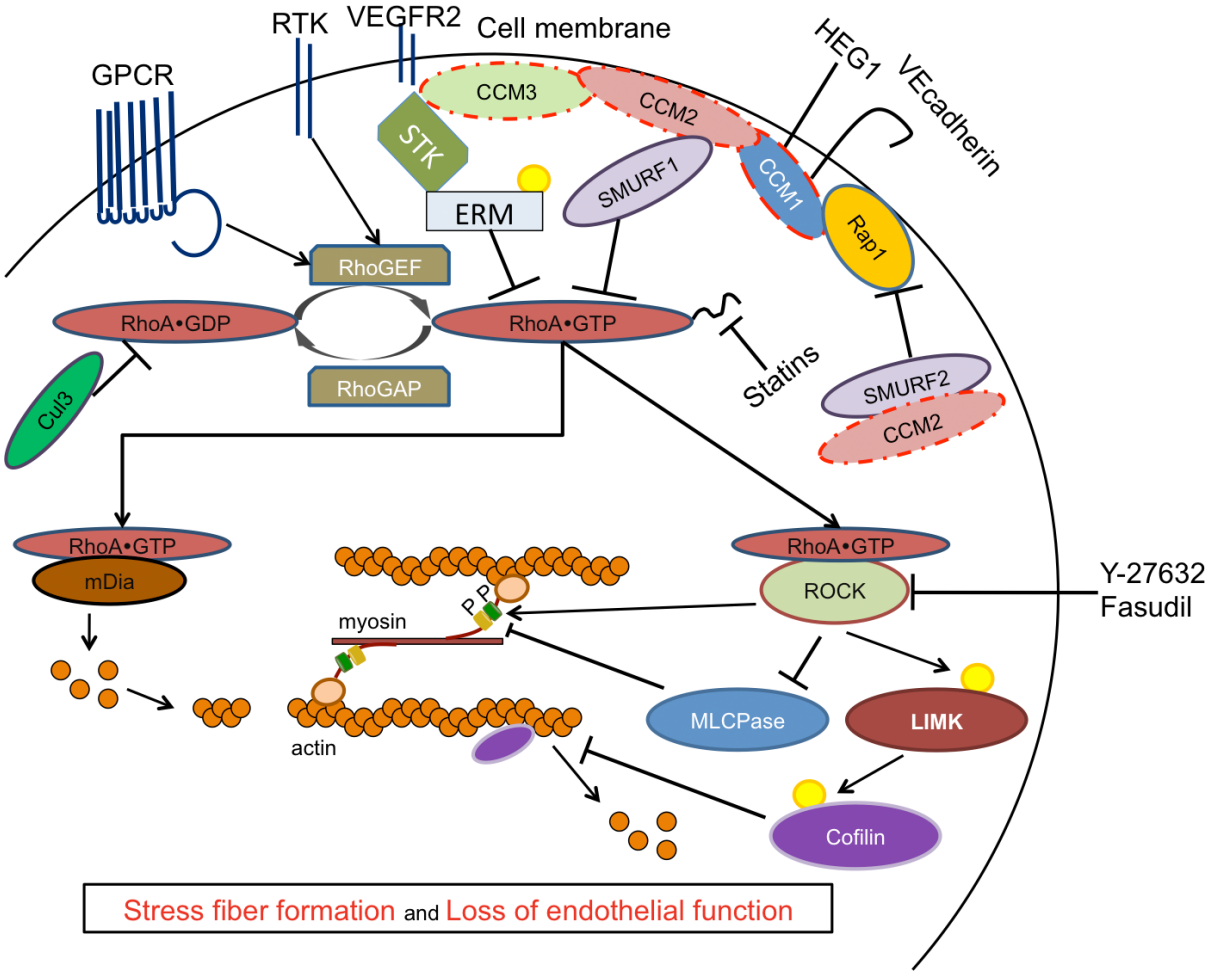

Figure 1.0. Core CCM signaling circuitry in endothelial cells. Activated GTP bound RhoA is at the core of driving CCM phenotypes. RhoA GTP activates ROCK and mDia, leading to actin polymerization, stabilization, and cross linking with myosin. In normal cells CCM1, -2, and -3 are in complex with each other and regulate the levels of active RhoA. In this complex, CCM1 binds HEG1 and CDH5 (vecadherin), which stabilizes vecadherin juntions while also regulating Rap1 function. CCM3 binds to the GCKIII steril kinases (STK), which phosphorylate ezrin radixin moeisin proteins that antagonize GTP bound RhoA. CCM2 interacts with Smurf1 at sites of actin polymerization at the cell membrane to ubiquitinate and degrade active GTP bound RhoA. Smurf2 and Cullin3 ubiquitinate and degrade Rap1 and GDP bound RhoA, respectively.

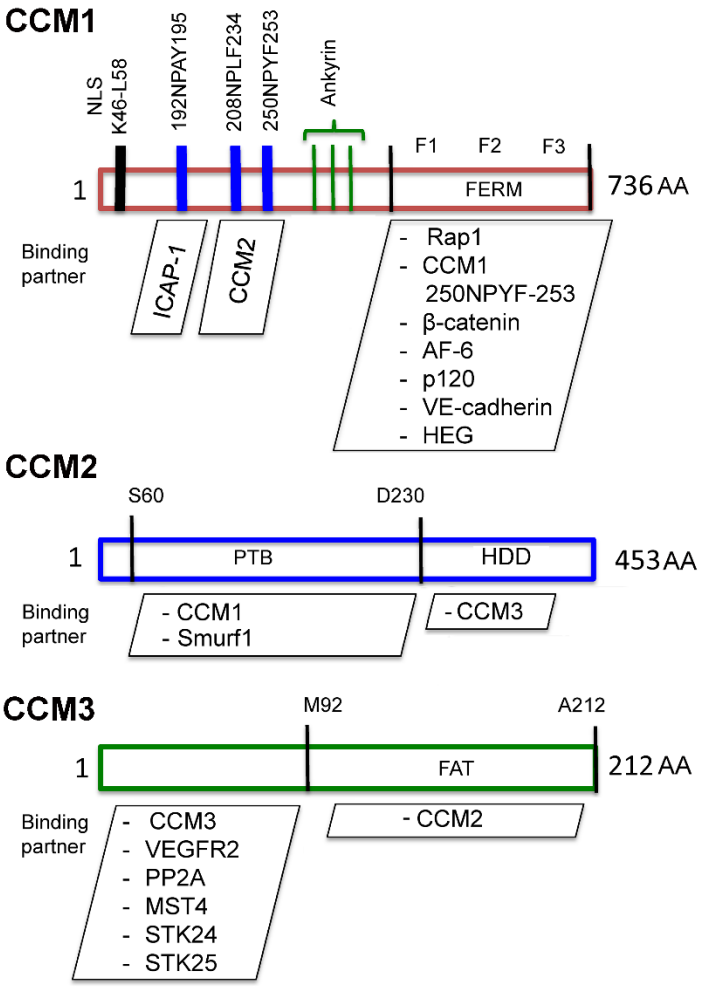

Figure 1.1. Defined structural domains and interacting proteins for CCM1, -2, and -3. Interactions were defined using multiple techniques, including co-immunoprecipitation coupled with mass spectroscopy and/or immunoblotting and yeast 2-hybrid screens. The CCM1 FERM (Four-point-one, Ezrin, Radixin, Moesin) domain binds multiple proteins. The NPAY, NPLF and NPYF sequences in CCM1 bind to phosphotyrosine-binding (PTB) domains. CCM1 also encodes a nuclear localization (NLS) sequence. CCM2 encodes a PTB domain and Karet domain. CCM3 has a FRAP-ATM-TRAP (FAT) domain that binds MST4, STK24 and STK25 serine/threonine protein kinases.

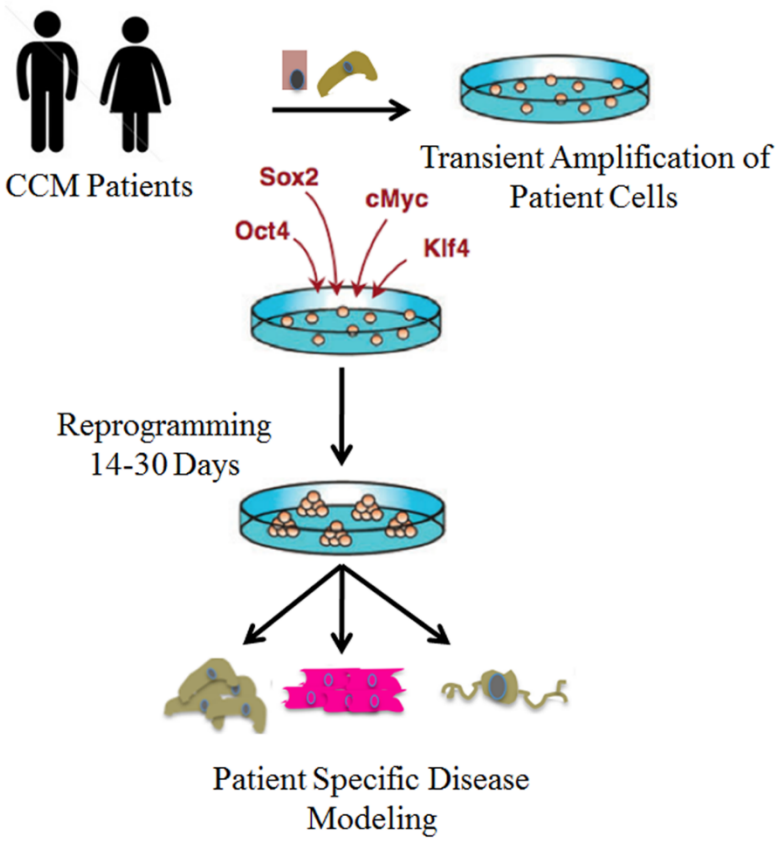

Figure 1.2. Strategy for developing and utilizing a CCM patient specifc iPS disease library. iPS technology allows for the development of a normal immortalized library of CCM patient cells. Blood cells can be obtained from CCM patients and transiently amplified. Either traditional retroviral (integrating) or newer sendai viral (non-integrating) approaches can be used to infect these primary patient cells. After two weeks to one month, immortalized normal iPS colonies appear for expansion. These cells can then be differentiated to all cell types of the body. Disease specific phenotypes can be studied and new pharmacologic therapies can be validated in the context of the CCM patient genetic background. Next generation genomic targeting approaches will allow for the knock-in of fluorescent tags to study endogenous CCM protein function in real time.

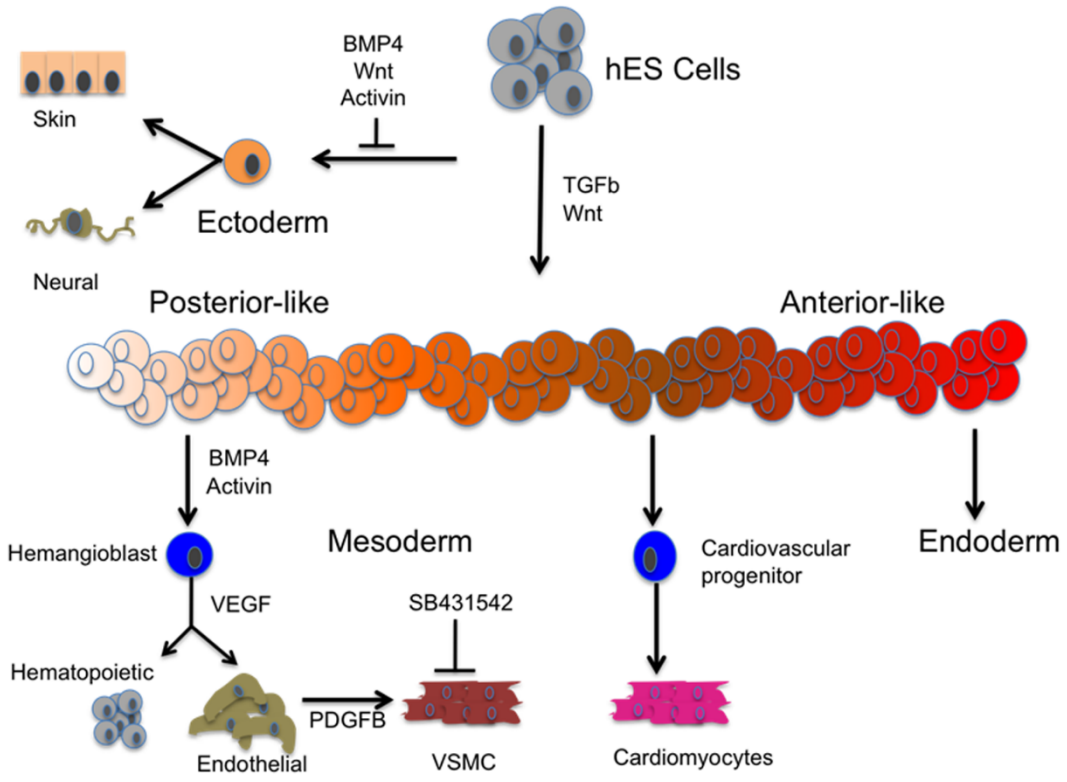

Figure 1.3. Differentiation strategy of pluripotent stem cells to endothelium. Pluripotent cells must be differentiated through a posterior-like primitive streak intermediate. This process is initiated through TGF-β and Wnt cytokine addition. Hemangioblast-like cells are obtained by the addition of Activin A. These cells are then driven to the vasculature by addition of VEGF. Endothelial characteristics are maintained by TGF-β inhibition.

Table 1. Phenotypes associated with CCM1, -2, and -3 protein loss.

Phenotype	CCM1	CCM2	CCM3
Activates p38		Uhlik et al. (2003)	
Anti-oxidant function	Goitre et al. (2010)		Fidalgo et al. (2012)
Branchial arch artery defects	Whitehead et al. (2004)	Boulday et al. (2009)	
Endothelial cell autonomous	Whitehead et al. (2004); Guzeloglu-Kayisli et al. (2004); Plummer et al. (2004); McDonald et al. (2010)	Boulday et al. (2009); Boulday et al. (2011); Cunningham et al. (2011); McDonald et al. (2010)	Chan et al. (2010)
Increases EndMT markers	Maddaluno et al. (2013)	Maddaluno et al. (2013)	Maddaluno et al. (2013)
Increases Phospho Moesin			Zhen et al. (2010)
Loss elevates active RhoA	Borikova et al. (2010); Stockton et al. (2010)	Whitehead et al. (2009);Borikova et al. (2010); Stockton et al. (2010); Zheng et al. (2012)	Borikova et al. (2010); Zheng et al. (2010)
Loss elevates F-actin stress fibers	Glading et al. (2007); Stockton et al. (2010)	Crose et al. (2009); Whitehead et al. (2009); Zheng et al. (2010)	Zheng et al. (2010)
Loss elevates phospho MLC2	Borikova et al. (2010); Stockton et al. (2010)	Borikova et al. (2010); Stockton et al. (2010)	Borikova et al. (2010)
Loss elevates total RhoA	Borikova et al. (2010)	Crose et al. (2009);Borikova et al. (2010); Zheng et al .(2012)	Borikova et al. (2010)
Membrane Localized	Zawistowski et al. (2005); Glading et al. (2007);	Uhlik et al. (2003); Zawistowski et al. (2005); Crose et al. (2009)	Zheng et al. (2010)
Neural cell autonomous			Louvi et al. (2011)
Nuclear Localized	Zawistowski et al. (2005)	Zawistowski et al. (2005)	
Prevents Cell proliferation	Whitehead et al. (2004); Wustehube et al. (2010); McDonald et al. (2010)	McDonald et al. (2010), Boulday et al. (2011)	Zhu et al. (2010)
Prevents endothelial cell sprouting	Wustehube et al. (2010)		
Prevents endothelial cell migration	Wustehube et al. (2010)		
Promotes Cell proliferation			Ma et al. (2007)
Promotes endothelial cell migration	Borikova et al. (2010)	Crose et al. (2009); Borikova et al. (2010)	Borikova et al. (2010)
Promotes endothelial cell sprouting	Borikova et al. (2010)	Borikova et al. (2010)	Borikova et al. (2010)
Promotes Lumenogenesis	Borikova et al. (2010); Lampugnani et al. (2010)	Kleaveland et al. (2009); Whiteheat et al. (2009); Borikova et al. (2010)	Borikova et al. (2010)
Regulates Apoptosis		Harel et al. (2009)	Chen et al. (2009)
Regulates the Notch Pathway	Whitehead et al. (2004);Wustenhube et al. (2010); Maddaluno et al. (2013)		He et al. (2010); You et al. (2013)
Regulates Tumor Formation		Haerl et al. (2009)	
Stabilizes VEGFR2 signalling			He et al. (2010);

Table 2. Proteins that have been shown in the literature to interact with CCM1, -2, and -3.

Interactor	CCM1	CCM2	CCM3
Binds ICAP	Zawistowski et al. (2002); Liu and Boggon (2013); Liu et al. (2013)		
Binds with GCKIIIs		Costa et al. (2012).	Ma et al. (2007); Fidalgo et al. (2010); Zheng et al. (2010); Ceccarelli et al. (2011);
Binds PP2A	Goudreault et al. 2007		
Binds Microtubules	Gunel et al. (2002)		
Binds Actin		Uhlik et al. (2003); Hilder et al. (2007)	
Binds HEG1 receptor	Kleaveland et al. (2009)		
Binds to Rap1	Serebriiskii et al. (1997); Liu et al. (2012); Li et al. (2012)		
Binds RhoA		Whitehead et al. (2009)	
Binds Rac1		Uhlik et al. (2003); Whitehead et al. (2009)	
Binds MEKK3		Uhlik et al. (2003); Hilder et al. (2007)	
Binds CCM1		Zawistowski et al. (2005); Hilder et al. (2007);	
Binds CCM2	Hilder et al. (2007)		Hilder et al. (2007); Li et al. (2010)
Binds to Paxillin			Li et al. (2011)
Binds CCM3		Hilder et al. (2003)	
Binds Smurf1		Crose et al. (2009)	
Binds to the Golgi apparatus			Fidalgo et al. (2010)
Binds to Vecadherin/b-catenin		Glading et al. (2007)	

II. Materials and Methods

Chapter III

Cell culture

Huvecs (Lonza) were maintained in EGM-2 media (Lonza) and passaged every 3 to 4 days for up to 5 passages at a 1:5 sub-culturing ratio with media renewal every other day. MEECs (gift from Dr. Leslie Parise) and BEND.3 (ATCC) were maintained in DMEM (Gibco) supplemented with 3% fetal bovine serum (FBS; Atlantis Biologicals) and 1% penicillin/streptomycin (Gibco) at a 1:10 sub-culturing ratio with media renewal every other day. HEK 293T (ATCC) cells were maintained in DMEM (Gibco) supplemented with 10% FBS (Atlantis Biologicals) passaged every 3 days at a 1:10 sub-culturing ratio with media renewal every 3 days.

Establishment of CCM1, -2, and -3 knockdown cell lines

PLKO.1 specific lentiviral gene shRNAs for human CCM1, -2, and -3 were acquired from the UNCCH Lentiviral Core Facility. Lentivirus was generated by the transient transfection of 293T packaging cells with Lipofectamine 2000 and Plus Reagent (Invitrogen). Virus was subsequently purified by ultracentrifugation and suspended in PBS. Subconfluent cultures of cells were infected at a ratio of 1:4 viral producing cells seeded to host cells (i.e. $1/4^{th}$ volume of virus generated from a 293T producing plate was incubated on the same size host cell plate). Viral particles were

incubated on cells for 48 hours in 8 μg/mL polybrene; cells were then placed in 2.5 μg/mL puromycin to select for transduced cells. Five shRNAs for each gene were initially validated for knock down efficiency. Two shRNAs for each gene were found to have similar phenotypes and knock down efficiency, and were used to control for off target shRNA effects. Knockdown efficiency was quantitative real time PCR (qRT-PCR) with primers specific for each *CCM* gene. Phenotypic experiments were conducted between 7 and 14 days after infection to ensure stable protein knockdown.

Immunofluorescence

Glass coverslips were placed in 24 well plates coated with Matrigel (BD Biosciences) diluted 1:50 in DMEM for 1 hr at 37°C. $8.5x10^4$ bEND.3 or Huvec cells were plated in each cover slipped well of a 24-well cell culture dish and incubated overnight. Seeded cells were fixed in a 3% paraformaldehyde/sucrose/PBS solution, permeabilized with .1% Triton X-100/PBS, and the Actin cytoskeleton was stained with Alexafluor 488-Phalloidin (or 595-Phalloidin). Phospho-cofilin imaging was obtained after cells were fixed in 4% paraformaldehyde/PBS solution, and permeabilized with .1% Triton X-100/PBS. Anti-phospho-cofilin (Cell Signalling) and anti-rabbit Alexafluor 595 secondary antibodies (Invitrogen) were incubated at room temperature for 2 hours and 1 hour in the dark, respectively. Hoechst dye (Sigma) was used to visualize nuclei. Images were taken in oil at a magnification of 40x (Zeiss Axiovert 200) with atleast 5 fields of view. Stress fibers and phospho-cofilin levels were quantitated using a Nikon 80i Research Upright Microscope (Nikon,

Tokyo, Japan) equipped with Surveyor Software with TurboScan (Objective Imaging, Kansasville, WI). Image montages were acquired with a Qimaging Retiga-EXi camera (Qimaging, Surrey, BC, Canada). Cell area was determined by cropping images and manually masking each cell with ImageJ software (NIH). Geometric features of the cells were automatically extracted with Cellprofiler software (Broad Institute of Harvard and MIT, Cambridge, MA).

Immunohistochemistry

Dr. Nana Feinberg of the UNC Translational Pathology Laboratory performed Immunohistochemistry. Briefly, antigen retrieval was performed with Bond-Epitope Retrieval solution (Leica) for 30 min at 100°. Slides were next incubated in either rabbit anti-phospho-cofilin 1:300 (Cell Signaling Technology) or mouse monoclonal anti-CD31 1:200 (Leica Microsystems) primary antibodies for 1 hr. Rabbit or mouse secondary antibodies were then applied for 1 hr and detected by the Bond Polymer Refined Detection System. Tissue immunofluorescence was carried out after incubation with an antibody against CD31 (1:200), which generated an endothelial cell mask. CD31 was then detected by a HRP linked to Bond Polymer. Following CD31 staining, an anti-phospho-cofilin antibody (1:300) was added. A goat anti-mouse-HRP (Envision+) secondary antibody was then added to the samples and Cy5-tyramide (PerkinElmer) was used for the fluorescence. Slides were then cover slipped and preserved with ProLong gold antifade reagent (Molecular Probes) with DAPI for nuclear staining. Slides were then quantified through AQUA image analysis. Briefly, an Aperio FL microscope (Aperio) integrated with HistoRx AQUA scan

technology (HistoRx) made a 20x scan of each slide for the DAPI, CY3, and CY5 channels. These spectrum of these scanned images were then analyzed using the AQUA algorithm following provided instructions (AQUAnalysisTM Aperio Edition Rev. 1.0, CDN0044, HistoRx).

Image densitometry analysis

Densitometry for western blotting was obtained using ImageJ (NIH) normalized to Erk1/2 loading control pixel density.

Multiplexed inhibitor beads coupled with mass spectrometry

MIB/MS experiments were performed as described previously by Duncan *et al.* Briefly, cells were lysed in low salt buffer (LSB) comprising 0.5% Triton X-100, 50 mM HEPES, 1 mM EGTA, 1 mM EDTA, 150 mM NaCl, 10mM sodium fluoride, 2.5 mM sodium orthovanadate, 1X protease inhibitor cocktail (Roche), and 1% of the phosphatase inhibitor cocktails 2 and 3 (Sigma). Protein kinases were isolated by flowing lysates over columns containing the following kinase inhibitors that were covalently conjugated to sepharose beads: Bisindoylmaleimide-X, SB203580, Lapatinib, Dasatinib, Purvalanol B, VI16832, PP58, AKT inhibitor, and Shokat. Inhibitors were synthesized by Dr. Jian Jin (UNC) and covalently attached to sepharose beads by Deborah Grangier (UNC). Kinases bound to the inhibitor beads were washed with LSB followed by high salt buffer (HSB) containing 50 mM HEPES, 0.5% Triton X-100, 1 mM EGTA, 1 mM EDTA, 1 M NaCl and then washed with 0.1% SDS, and eluted in 0.5% SDS after boiling for 5 minutes. Standard

methanol/chloroform extraction methodlogy was utilized for the purification of proteins, followed by resuspension in 50 mM HEPES and overnight trypsin (Roche) digestion at 37 °C. Samples were then iTRAQ labeled for two hours at room temperature and cleaned with PepClean columns (Pierce). Peptides were subjected to liquid chromatography and spotted based on hydrophobicity with a Tempo LC/MALDI (Applied Biosystems). Spotted plates were loaded on a MALDI TOF/TOF 5800 (ABSCIEX) and MS/MS spectral data were acquired. Peptides were identified by the Protein Pilot Software (ABSCIEX), which links to the UniProtKB/Swiss-Prot online database. The Pro Group algorithm was utilized for specific peptide quantitation and the subsequent ratios were corrected for bias. Individual peptide spectral mass accuracy was verified manually. The MIB/MS experiments were performed in collaboration with Dr. Christopher Dibble and Rachel Reuther.

Sequence analysis of human CCM samples

CCM lesions were obtained from the Angioma Alliance CCM DNA and Tissue Bank (www.angiomaalliance.org). Surgically resected familial patient lesions were confirmed by radiographic analysis by clinicians. The mutation of each CCM lesion was determined by screening patient peripheral blood mononucleocyte DNA with specific CCM PCR probes, which is standard methodology for for genetic diagnosis of CCM patient mutations.

Statistical significance

Statistical significance was determined through a paired Student's *t*-test (two-

tailed) and the data represent the average of at least 2 independent biological experiments.

Tube formation assays

Tube formation assays were conducted by seeding 8.5×10^5 cells on 310 μl of Matrigel (BD Biosciences) for at least 15 hours. Tube-like structures were fixed in 4% para-formaldehyde for 15 min permeabilized with .1% Triton X100/PBS for 10 min. Actin was stained with rhodamine-phalloidin (Invitrogen), and nuclei were stained with Hoechst dye (Sigma). Quantitative image analysis was performed using a Cellomics ArrayScan (Thermo Scientific) or the BD Pathway (BD Biosciences). The mean tube area was automatically quantified utilizing Cellomics Arrayscan software.

Western blotting

Total cell lysates were prepared by washing cell cultures twice with ice cold PBS and incubating the dishes with lysis buffer containing 50 mM Tris (pH 8.0), 150 mM NaCl, 1% Triton X-100, .5% sodium deoxycholate and .1% SDS supplemented with 1x protease inhibitor tablets (Roche) on ice for 10 min followed by aggressive scrapping. 30 μg of total protein lysate was separated by SDS-PAGE and transferred to nitrocellulose membranes. Membranes were probed with anti-Erk2, anti-RhoA sc-22, anti-BMX (Santa Cruz), anti-cofilin, anti-phospho-cofilin, anti-LIMK1, anti-phospho- LIMK1/2, and anti-Tie2 (Cell Signaling Technology) antibodies. All mouse or rabbit secondaries were from Jackson ImmunoResearch. Cells were

incubated with the indicated with the Rock inhibitors Fasudil or Y-27632 (CellBiochem) pharmacological agents at indicated concentrations for 1 hr before lysis.

Chapter IV

Cell culture

MEECs or Huvecs were subcultured and CCM1, -2, -3, Smurf1, Smurf2, and Cullin3 knock down cells were generated exactly as described for Chapter III.

Immunoprecipitation assays

GFP tagged CCM1, CCM2, and CCM2 F217A, HA tagged CCM2 and Flag tagged Smurf1 or Flag tagged Smurf2 were co-expressed in HEK 293T cells for 16 hrs using lipofectamine and reagent plus transfection following manufacturer instructions (Invitrogen). Cells were lysed in lysis buffer containing 50 mM Tris (pH 8.0), 150 mM NaCl, 1% Triton X-100, 5 mM MgCl2 supplemented with 1x protease inhibitor tablets (Roche) on ice for 10 min followed by aggressive scrapping. Insoluble membrane fractions were spun down for 5 minutes at 4°C. Approximately 500 μg of cell lysate was used for immunoprecipitation with 1 μg of anti-Flag M5 antibody (Sigma) for 1 hour with gently rotation at 4°C. A total of 25 μl of a 50% slurry of Protein G sepharose beads were then added to each of the samples for 1hr with gentle rotation at 4°C. Protein antibody immunoprecipates were eluted by boiling in SDS sample buffer for 5 minutes at 100°C.

Rhotekin-RBD active pull down assays:

Recombinant GST tagged RBD (gift from Dr. Keith Burridge) was used for the assessment of activated GTP bound RhoA. GST-RBD was purified using glutathione sepharose resin from 1 L cultures of BL-21 Gold E. coli bacteria transformed with pGEX GST-RBD. Cell cultures were washed twice with ice cold PBS and lysed on ice in a cold room with a lysis buffer containing 50 mM Tris (pH 8.0), 150 mM NaCl, 1% Triton X-100, .5% sodium deoxycholate, .1% SDS, 10mM MgCl2 and supplemented with 1x protease inhibitor (Roche). Lysates were incubated with either control glutathione sepharose beads or GST-RBD beads for 25 minutes with gentle rotation at 4°C. GTP Bound RhoA beads were washed 3x with 1 mL of wash buffer containing 50 mM Tris (pH 8.0), 150 mM NaCl, 1% Triton X-100, 5mM MgCl2 supplemented with 1x protease inhibitor (Roche). GTP RhoA bound to GST RBD was eluted from the glutathione beads by boiling in SDS sample buffer for 5 minutes. Input total cell lysate and pull down samples were then separated by SDS PAGE, transferred to nitrocellulose membranes, and blotted using anti-RhoA, anti-Erk2, or anti-Ubiquitin antibodies (Santa Cruz) with the corresponding secondary antibody.

Statistical significance

Statistical significance was calculated using a paired two-tailed Student's *t*-test. Data represented the mean of at least 2 biologically independent experiments.

Densitometry, Immunofluorescence, Tube formation assays, and Western blotting.

These methods were carried out exactly as described for chapter III.

Chapter V

Cellular proliferation assays

Cells were seeded in triplicate in 96 well tissue culture plates. The CellTiter-Glo reagent was incubated on cells per manufacturer instructions (Promega). Luminescence was read and quantified on a PHERAstar plate reader (BMG Labtech).

Endothelial differentiation

Confluent hESC cultures were scored and lifted for the generation of EBs (D-1). EBs were generated in EB generation media constituting the following ingredients: DMEM/F12 (Gibco) supplemented with knock out serum replacement (Gibco), .1 mM β-mercaptoethanol, 1X non-essential amino acids, 1X penicillin/streptomycin, and 1X L-Glutamine. Media was changed and only formed EBs were kept. BMP4 (D0), Activin A (D1), and bFGF (D2) were added sequentially each day (D0-D2). On Day 4 the EBs were spun and resuspended in fresh EB generation media supplemented with VEGF-A, bFGF, and BMP4; EBs were plated out on a regular tissue culture plate coated with 1:120 diluted matrigel. From days 7 to 14, cells were cultured in EB generation media supplemented with VEGF-A, bFGF, and SB431542 with media renewal every 48hours. On day 14, $CD31^+$ endothelial cells were separated from differentiating cultures. Cells were trypsinized and

incubated with CD31 specific magnetic microbeads and isolated over two MS or LS columns per manufacturer instructions (Miltenyi Biotec). Isolated ECs were maintained in this media with renewal every 48 hours. BMP4 (Peprotech), VEGF-A (Shenandoah Biotechnology), bFGF (Peprotech), Activin A (Peprotech), and SB431542 (Tocris) were used at 20 ng/mL, 50 ng/mL, 10 ng/mL, 10 ng/mL, and 10 μM, respectively.

Establishing and passaging EPC-ECs

Six well plates were coated with 50 μg/mL of rat type I collagen suspended in .02N acetic acid 1 hr prior to plating PBMCs. This solution was washed 2x from the plates with HBSS and PBMCs (approximately 20x 10^6) were plated in EGM-2C at 37°C. Media was renewed every 72 hrs for 7 days, after which it was renewed every 48 hours until colonies were visualized. Typically colonies of ECs appeared after 4 weeks and were passaged when covering between 30 and 50% of the dish. These EP-ECs were passaged at 95% confluency and were cultured at low split ratios to maintain a high confluency.

Flow cytometry

All flow cytometry was done in the UNC Flow Cytometry Core Facility using Beckman CyAn instruments. At least 1e^4 cells were analyzed after being stained with isotype specific control antibodies or epitope specific antibodies conjugated to either PE, APC, or FITC; all flow cytometry antibodies were purchased from BD biosciences.

Human embryonic stem cell culture and CCM protein knock down

The H1, H7, and H9 hESC lines were grown in the UNC Human Embryonic Stem Cell core facility under supervision from the University Embryonic Stem Cell Research Oversight Committee (ESCRO). hESCs were maintained as colonies grown on standard tissue culture dishes coated with 1:120 diluted hESC-qualified matrigel (BD biosciences) in mTeSR1 growth media (Stem Cell Technologies). hESCs were fed daily and split every 3-5 days once proper density was reached. CCM proteins were knocked down using the shRNAs described in chapter 3. Briefly, cells 48 hours following the previous passage were infected with viral particles at a ratio of 1:1, 2:1, and 3:1 viral producing cells seeded to host cells (i.e. 1, 2, or 3 volumes of virus generated from a 293T producing plate was incubated on the same size host cell plate). Clones were passaged after puromycin selection, and knock down efficiency was determined by qRT-PCR.

iPS cell derivation and culture

Retrovirus encoding Oct4, Sox2, KLF4, and cMyc was packaged as previously described utilizing PMX vectors purchased from Addgene (Yamanaka ref). Infected EPC ECs, Huvecs, or MRC5 fibroblasts were seeded on MEFs in iPS cell induction media constituting the following ingredients: DMEM/F12 (Gibco) supplemented with knock out serum replacement (Gibco), .1 mM β-mercaptoethanol, 1X non-essential amino acids, 1X penicillin/streptomycin, 1X L-Glutamine, and 10

ng/mL bFGF. Colonies were picked based upon similar morphology to hESCs, expanded on MEF feeders and then cultured on matrigel as described for hESCs.

Neural differentiation

EBs were formed as described for endothelial differentiation in EB generation media for 4 days. EBs were then placed in a new petri dish in neural induction media constituting the following ingredients: DMEM-F12, 1X N2 supplement (Gibco), 1X penicillin/streptomycin (Gibco), 1x non-essential amino acids (Gibco), 10 μg/mL heparin (Sigma), 10 ng/mL bFGF (Peprotech). EBs were seeded on fibronectin coated cell culture dishes and neural induction media was changed every day. Neural rosette-like structures were observed on day 14 and used for pan-neural marker stanings.

PBMC isolation

The UNC Institutional Review Board approved the blood draws and the use of human blood (IRB# 10-1595). Normal patient peripheral blood was obtained using standard phlebotomy techniques the anti-coagulant sodium citrate. PBMCs were obtained by diluting 80 mL of peripheral blood in half with HBSS (Gibco) containing .5% BSA/1 mM EDTA. This blood solution was then quickly but gently layered on an equal volume of Histopaque-1077 (Sigma) in 50 mL polypropylene tubes. Before separation occurred, the tubes were spun at room temperature (RT) for 30 min at 400 x G. Following centrifugation, the plasma layer was removed and the white/opaque layer containing PBMCs was collected in new tubes and total

volume was brought to 50 mL with 12% FBS EGM-2 (Lonza) containing 12% FBS (Atlantic Biologicals) and an additional 1x antibiotic/antimycotic solution (Gibco) (denoted as EGM-2EP). The tubes containing the PBMCs were centrifugated at RT 15 minutes at 400 x G. Pellets were combined, washed twice to remove residual platelets, and counted for plating.

Statistical significance

Statistical significance was calculated using a paired two-tailed Student's *t*-test. Data represented the mean of at least 2 biologically independent experiments.

Teratoma Formation

Mouse teratoma studies were completed under approved IACUC protocols. Pluripotent cells were disassociated into a single cell suspension with .03% EDTA (Sigma). BALB/c nude mice were injected on both flanks with 1e^6 cells suspended in a 50% matrigel/PBS solution containing 10 μM ROCK inhibitor (Tocris). Mice were carefully monitored, and tumors were removed before they reached 1 cm^3. Tumors were formalin fixed and prepared for hematoxylin and eosin histological staining by the UNC Animal Histopathology Core Facility.

Densitometry, immunoflourescence, tube formation assays, and Western blotting.

These methods were carried out exactly as described for Chapter III.

III. Global kinome profiling of deregulated kinases in CCM

Introduction:

The signaling mechanisms driving CCM lesion development remain incompletely characterized. It is likely that deregulated signaling cascades are driving the common biochemical and phenotypic abnormalities observed after the loss of any of the three CCM proteins. Current studies have indicated that the CCM protein complex regulates the actin cytoskeleton, which helps maintain vascular homeostasis [4, 39, 168]. The CCM proteins form a ternary complex, and shRNA knock down of CCM1, -2 or -3 increases active and total RhoA levels in ECs [4, 74]. Therefore, a major focus in CCM research has been to elucidate potential mechanisms driving deregulated RhoA signaling.

RhoA regulates the actin cytoskeleton by activating its downstream effectors mammalian diaphanous (mDia) and Rho kinase (ROCK) [118]. Recent studies have demonstrated that loss of CCM proteins increases ROCK activity and phospho-MLC2, which negatively effects tube forming ability, invasion, and monolayer stability [4, 7]. Importantly, small molecule inhibition of RhoA or ROCK rescues both the biochemical and cellular phenotypes. These data suggest that increased ROCK activity downstream of RhoA stabilizes the actin cytoskeleton and drives CCM phenotypes. As a therapeutic strategy, targeting RhoA and ROCK signaling is promising as several ROCK inhibitors are being actively developed, and the ROCK

inhibitor Fasudil has been used to treat cerebral vasospasm in Japan for two decades [169, 170].

In lieu of this progress, the deregulation of additional kinases in CCM remains largely unknown. There are at least 130 kinase inhibitors currently in clinical trials, and the kinome as a whole is understudied in CCM signaling biology. Thus, the discovery of additional kinases that can be targeted may be a useful therapeutic avenue for the treatment of CCM. Examining the expression or activity of kinases typically requires an enrichment procedure, such as antibody-mediated immunoprecipitation followed by western blotting or mass spectrometry. This strategy is only useful for those kinases for which good antibodies are available, and the assessment of activation status requires the availability of phosphorylation state specific antibodies. Thus, an approach that allows for the identification of many kinases across all families of the kinome would represent an important method for obtaining a profile of deregulated kinase networks that may drive the CCM phenotype. To address this need, kinase inhibitors immobilized on bead resin technologies have been developed [171, 172]. These inhibitors selectively bind to the activated form of the kinase, and can be used to pull down active kinases, which then can be identified by quantitative mass spectrometry. This type of approach has been used to identify differentially phosphorylated kinases and novel protein phosphorylation sites during cell cycle regulation with great precision [171]. Our lab expanded on this approach with multiplexed kinase inhibitor beads coupled with quantitative mass spectrometry (MIB/MS) to elucidate the kinome reprogramming following Mek inhibition in triple negative breast cancer. These inhibitors are both

selective (Bisindoylmaleimide-X, SB203580, Dasatinib, Lapatinib, AKT, and Shokat) and broad (PP58, VI16832, and Purvalanol B). This proteomic kinome approach led to the discovery of kinases that were over activated upon Mek inhibition and the rational design of a new combinatorial therapeutic for Mek resistant cells and tumors [173]. Therefore, understanding the kinome signaling mechanisms involved in driving CCM lesion formation could be instrumental in designing a single agent or combinatorial agent therapy in CCM.

In this study, we utilized MIB/MS technology to discover potential novel kinase signaling networks involved in CCM. For these experiments, we used both Huvec and MEEC cell culture systems with stable shRNA knock down of the CCM proteins. We detected LIMK downstream of RhoA that was hyperactivated in CCM deficient ECs. We demonstrated that LIMK1 was both phosphorylated and overactive in CCM1, -2, and -3 deficient endothelial cells from both mouse and human and surgically resected patient lesions. These data have validated LIMK as a therapeutic target and show for the first time that LIMK signaling resulting in the inactivation of the actin depolymerizing factor (ADF) cofilin gives rise to CCM phenotypes. We further show that endothelial regulators such as, Tie2, TGF-β receptor, and BMX/ETK kinases are deregulated following loss of CCM proteins.

This work was done in collaboration with Dr. Christopher Dibble who validated in vitro LIMK signaling and Rachel Reuther who assisted in MIB/MS assay development.

Results

Kinome profiling of CCM deficient human and mouse endothelial cells.

There is relatively little known about the CCM protein specific kinome regulation and how that contributes to the pathology of CCM. To address this problem, we utilized MIB/MS technology to discover novel kinases that are over or under represented in CCM2 protein deficient cells. For a typical experiment, cells were grown following knock down for a period of 10 to 14 days to obtain the later and more stable changes following CCM protein loss. Knock down was validated by q-RT-PCR and the CCM phenotype was validated by cellular stress formation assays (Fig 3.0). Knock down data for all cell lines is provided (Fig 3.20 A-D). The knock down cells were then lysed, and the whole cell protein fraction was flowed over multiplexed kinase inhibitor beads, purified, and peptides were quantified (Fig 3.1). We identified 169 kinases covering approximately 32% of the known human kinome that were either over represented or under represented in CCM2 deficient endothelial cells (Fig 3.2 A).

We were able to validate this approach by detecting kinases previously implicated in the signaling biology of CCM, such as ROCK1, ROCK2, STK24, STK25, Tie2, MEKK3, MKK3, and TGF beta (Fig 3.2 B). As a proof of concept, we found that ROCK1, which is a widely accepted driver of the CCM phenotype, was also over represented. TGFR1 (TGF-β receptor 1) was found to be over represented consistently across experiments. This result is inline with a recent study that demonstrated that elevated TGF-β signaling is involved in promoting EndMT in CCM1 deficient cells, suggesting that CCM2 deficient cells may be undergoing a

similar process [69]. We also observed over representation of the Tie2 receptor, which is a specific endothelial receptor tyrosine kinase, which has been shown to be overexpressed in CCM patient lesions and in cells isolated from patient lesions [174]. Lastly, our laboratory reported that CCM2 (OSM) functions to increase the activity of M3K3 leading to increased MP2K3 phosphorylation and p38 activation [70]. Consistent with this result, we observed a decrease in M3K3 binding to the inhibitor beads following the loss of CCM2 protein (Fig 3.2 B). In addition, approximately 1/3rd of the quantified kinases were found to regulate the actin cytoskeleton after Ingenuity Pathway Analysis. This result is in line with the field as there is a general consensus among all studies that CCM proteins regulate endothelial cell cytoskeletal stability (Fig 3.3). Overall, these data suggest that MIB/MS technology can be used as a consistent method for probing novel kinase networks in CCM.

Our results showed that approximately 30% of the detected kinases were conserved across mouse and human (Fig 3.4). CCM phenotypes are rescued with the inhibition of ROCK; therefore, we treated MEEC CCM2 stable knock down cells with the Y-27632 ROCK inhibitor for 48 hours. After proteomic analysis, we discovered that only a few of the kinases other than ROCK itself were oppositely affected either negatively or positively by Y-27632 (highlighted in red boxes). This finding suggests that the majority of kinases were not greatly affected by ROCK inhibition, and these kinases maybe some how acting upstream or independently of ROCK in CCM2 deficient ECs (Fig 3.4).

We next wanted to determine if CCM1 and CCM3 deficient ECs had similar kinase profiles to that of CCM2 deficient ECs. After completing MIB/MS analysis

over multiple experiments with CCM1 and CCM3 deficient Huvecs, we similarly achieved 30% coverage of the human kinome with all kinase families represented (Fig 3.5 and 3.6). Clustering kinases based upon shared kinases that were either over or under represented revealed differences in the conserved kinases between CCM1/CCM2, CCM1/CCM3, or CCM2/CCM3 (Fig. 3.7, 3.8, and 3.9). The number of deregulated kinases was similar both in total number of changed kinases and in the number of under and over represented kinases with more under represented kinases detected than over represented kinases (Fig. 3.10). The total number of conserved kinases between CCM1, -2, and -3 deficient Huvecs was significantly lower with 62 similarly represented kinases. Some of these overlapping kinases for CCM1, -2, and -3 deficient ECs are important mediators of RhoA signaling or regulate endothelial function (Fig 3.11). We detected ROCK1 and ROCK2 in all Huvec samples with CCM2 cells having a strong increase in ROCK1 representation and CCM3 cells having a lesser increase in ROCK2 representation. ROCK2 is thought to be more brain endothelial cell specific; however, the two isoforms are highly conserved and specific isoform studies involved in endothelial function have not been carried out. Surprisingly, CCM1 deficient cells had decreased levels of both ROCK1 and ROCK2. This finding is unexpected because CCM1 deficient cells have a strong induction of stress fibers upon CCM protein loss and those stress fibers can be rescued following ROCK inhibition (Fig 3.0). Furthermore, loss of human CCM proteins consistently increases total and activated RhoA levels. It is possible that the loss of CCM1 potentiates other RhoA mediated drivers for the CCM phenotype, such as mDia1 and ROCK inhibition is sufficient to overcome these

parallel events. In addition to the RhoA effector ROCK, we were able to detect the RhoA effector PKN1, which was under represented in CCM1, -2, and -3 deficient Huvecs (Fig 3.10). PKN1 binds to and is activated by RhoA and has further been shown to perpetuate RhoA signaling by preventing the endogenous GAP activity of RhoA [175]. A closely related family member PKN3 has been shown attenuate F-actin stress fiber formation and alters VEcadherin localization following TNF-α stimulation in Huvecs; it is unclear whether these results were dependent upon RhoA/ROCK signaling [176]. Therefore the interplay of the PKN family members and RhoA signaling could represent an unknown mechanism behind CCM phenotypes.

The most relevant kinase that we discovered, which was both over represented and intrinsically linked to F-actin formation, downstream of RhoA was LIM kinase 1 (LIMK1). LIMK could represent an important targetable kinase in CCM, as LIMK inhibitors are being developed and have shown promising results in pre-clinical mouse breast cancer models [177, 178]. Interestingly, only LIMK1 and not LIMK2 was over represented in CCM2 deficient endothelial cells from both mouse and human, which was decreased after ROCK inhibition (Fig 3.4). Therefore, we focused our validation studies on LIMK1. The activation state and not the expression of LIMK1 was effected in CCM1, -2, and -3 knock down ECs as only the phosphorylated form of LIMK1 was increased (Fig 3.12A). Furthermore, the activation of LIMK1 was placed downstream of RhoA/ROCK signaling because ROCK inhibition by Fasudil decreased the activity of LIMK (Fig 3.12B).

LIMK and cofilin phosphorylation decreases tube formation rescuable by LIMK1 knockdown

The role of LIMK as a driver of CCM phenotypes was interrogated by generating stable LIMK and CCM protein double knock down ECs. The ability of these cells to form tube-like structures was compared to Plko.1 control and CCM single knock down ECs. Knock down of LIMK1 with two independent shRNAs resulted in a large decrease in the phosphorylation levels of LIMK and cofilin (Fig 3.13A and B). CCM2/LIMK double knock down cells had normal levels of pMLC2 when compared to controls, which indicates that LIMK is selectively inhibiting cofilin (Fig 3.13C). We have previously published that tube formation defects can be rescued by CCM protein knock down in ECs through the inhibition of ROCK (Fig 3.14A) [4, 5]. Importantly, we now show that the knock down of LIMK1 in CCM protein deficient ECs is sufficient to rescue tube-like structures similar to ROCK inhibition. Examining the tube formation process across time points reveals that CCM2 knock down cells that have been treated with either Y27632 or LIMK1 knock down begin forming tubes after 4 hours, which is identical to control Plko.1 cells. These morphological changes are in contrast to untreated CCM2 knock down cells, which maintain a rounded and immobile phenotype, indicating defects in the actin cytoskeleton consistent with the observed increases in pMLC2 and pCofilin. These data suggest that the LIMK1 activation and subsequent phosphorylation of cofilin is important for CCM pathophysiology. Taken together, decreasing actin depolymerization increases total F-actin, which is required for the cross linking of MLC and actin. When LIMK1 is knocked down in the absence of CCM proteins, the

amount of phospho-cofilin decreases and actin is again severed. The levels of pMLC2 remain high; however, there is no functional effect because there is not any F-actin for MLC2 to cross-link. Thus, targeting LIMK may represent a more specific therapeutic avenue than inhibiting ROCK with several non-toxic LIMK inhibitors that decrease pCofilin levels [177, 179].

Phospho-cofilin levels are increased in surgically resected human CCM lesions

Previously, it has been shown that pMLC2 levels are increased in human CCM lesions [7]. Therefore, we sought to determine if pCofilin might also be active in human surgically resected CCM lesions. We first validated a monoclonal antibody specific to pCofilin through an immunohistological quantitation methodology known as Advanced QUantitative Analysis (AQUA), which scores immunoflourescent protein expression from tissues slides [180]. This validation was accomplished by placing stable CCM knock down MEECs in paraffin and processing them identically to tissue sections. After staining, we observed a significant increase in pCofilin staining levels in CCM protein deficient MEECs, consistent with our immunoblotting data (Fig. 3.15A and B). Phospho-cofilin levels were then analyzed in surgically resected lesions from CCM patients that have confirmed gene mutations in *ccm1*, *-2*, or *-3* (Fig. 3.15F). Immunohistochemical analysis shows a dark brown staining only in CCM lesions and not in normal brain capillaries from non-CCM patients (Fig 3.15C). CCM phenotypes are thought to be endothelial cell autonomous; therefore, we utilized an endothelial specific CD31 (Pecam1) mask to assess whether the elevated pCofilin levels were restricted to the endothelium by immunoflourescence

[181]. Accordingly, we observed a high overlay of pCofilin signal in the endothelial cell monolayer, which was not observed in normal brain tissues. The levels of this staining were between 4 and 10 fold higher in CCM patients after AQUA analysis (Fig 3.15 E). These results are similar to previous immunohistochemical studies on pMLC2 expression in CCM lesions and provide additional evidence of aberrant ROCK signaling in the ECs from CCM lesions [7]. Overall, these data show for the first time that pCofilin is a unique biomarker for CCM patient samples and suggest that LIMK is a physiologically relevant kinase involved in CCM pathophysiology.

CCM proteins regulate the expression of Tie2 and BMX upstream of ROCK

We next validated some of the other kinases that we identified by MIB/MS profiling that have important functions in either regulating RhoA or endothelial cell function that were conserved among CCM1, -2, and -3 knock down cells. (Fig 3.11). The Tie2 angiopoietin receptor is specifically expressed in the endothelium and is an important regulator of endothelial activation, quiescence, and is activated by either angiopoietin 1 or 2 (Ang1/2). These two ligands compete with each other for binding to Tie2. Ang1 promotes vascular quiescence through the strong agonist activity of Tie2, which increases Notch1 signaling, where as Ang2 acts as a competitive antagonist of Ang1 leading to decreased Notch1 signals [182-184]. The net result is Ang1 and Ang2 promote a stable impermeable vasculature or a hyperpermeable activated vasculature, respectively. Furthermore, high levels of Ang2 decrease pericyte recruitment to endothelial cells [185]. The effects of altered vascular quiescence, permeability, and mural cell recruitment that also occurs through altered

Tie2 and Notch signaling are all shared phenotypes with CCM1 -2, or -3 deficient ECs. Currently, there are not any reliable activation state specific phospho-tyrosine antibodies for Tie-2. Therefore, we first assessed Tie2 expression. We find that both Tie2 protein levels and message levels are increased significantly after CCM1, -2, and -3 protein loss (3.16 A and B). This increased expression appears to be upstream of ROCK signaling as ROCK inhibition did not attenuate the expression of Tie2 (Fig 3.17). Tie2 through Ang1 binding is thought to promote endothelial cell quiescence; therefore, a more detailed study into whether Tie2 is being activated by either Ang1 or Ang2 is needed.

In contrast to Tie2, we observed a conserved under representation of the BMX/TEC non-receptor tyrosine protein kinase (Fig 3.16 C). This kinase is directly activated by Tie2 and is essential for proper in vitro tube formation and hind-limb ischemia recovery in mice through its functions in regulating RhoA activity [186, 187]. BMX may be relevant to CCM biology through its ability to activate RhoA and localize RhoA to the membrane by disrupting the interaction of RhoA and Rho GDIs [188]. Similarly to Tie2, we noted a marked decrease in protein and mRNA levels in CCM deficient ECs (Fig 3.16 D). The expression defects were not significantly rescued with ROCK inhibition (Fig 3.17). These results are somewhat obfuscating in that CCM deficient cells have greatly increased RhoA activity levels. It would be expected that if BMX were a driver of the CCM phenotype, it would also be strongly activated. However, our data by MIB/MS, qRT-PCR, and western blotting show a strong decrease in BMX expression (Fig 3.10, 3.16 C and D). These data suggest that CCM deficient endothelial cells maybe employing some form of compensation

mechanisms to overcome the increased RhoA activation. This hypothesis is in agreement with the over representation of Tie2 binding to our inhibitor beads, which should promote endothelial cell quiescence. Therefore, a comprehensive mechanism that includes Tie2 and BMX may exist to carefully regulate RhoA activity in vascular homeostasis, which is insufficient to overcome the RhoA overactivation in CCM protein deficient cells. Identifying additional RhoA regulatory mechanisms that are changed in CCM protein deficient cells will determine whether additional pharmacologically relevant targets exist that can be exploited to restore proper RhoA levels.

Discussion

This study has uncovered a plethora of kinases that are deregulated after the loss of CCM proteins in a non-biased way. Because there are many kinase inhibitors that are FDA approved or are in clinical trials, this information will be a valuable resource for the scientific community to establish new potential targetable kinases. To this extent, we have both provided an independent validation of kinases already shown to be involved in CCM and added to this list of validated kinases. We show that the LIMK/cofilin arm of the RhoA/ROCK signaling pathway is involved in CCM phenotypes. The over activation of LIMK leads to increased phosphorylated coflin and increased actin stability [189, 190]. This LIMK/cofilin pathway may represent the dominant acting portion of the RhoA/ROCK pathway. Previously, pMLC2 has been thought to be the only functional surrogate marker for CCM. However, increased cofilin function through shRNA mediated knock down of LIMK is

sufficient to restore endothelial cell functionality in CCM protein deficient ECs even with elevated pMLC2 levels. This result suggests that LIMK/cofilin maybe dominant over just pMLC alone in causing CCM phenotypes. Inhibition of MLC phosphatase (MLCP) has been shown to increase actin stress fibers [191, 192]. Therefore, it would be interesting to use a MLCP inhibitor, such as Ruthenium Red, to determine if increasing pMLC2 levels is sufficient to generate CCM phenotypes [193]. These data raise important observations on the relative contributions of actin stabilization through LIMK activation and actin myosin contractility promoted by increased ROCK activation. Relevant to in vivo pathology, this study further shows that CCM patient lesions have elevated phospho-cofilin. This finding in conjunction with prior work establishing increased pMLC2 in patient lesions corroborates how the RhoA/ROCK signaling pathway is physiologically relevant. Thus, through an unbiased approach our work has established that LIMK is a physiologically relevant kinase for therapeutic intervention. This basic discovery could be translated to the clinic relatively rapidly with pre-clinical LIMK inhibitors being developed for the treatment of breast cancer.

Our MIB/MS proteomic data further identified kinases that are known to be important in endothelial function. The Tie2 receptor has been shown to be elevated in certain CCM patient lesions and cells isolated from those lesions and have been implicated in other vascular malformations [174, 194, 195]. Furthermore the opposing function of Ang2 to Ang1 results in an increased expression of the Tie2 receptor [196]. This result is consistent with our increased Tie2 expression data. Therefore, it will be of interest to determine the relative contributions of Ang1 and

Ang2 on Tie2 in CCM protein deficient ECs. Inflammatory cytokine expression has been reported to increase Tie2 expression and is characteristic of CCM lesions [134, 197]. Indeed, by MIB/MS we have detected a large decrease in both IKKA and IKKB representation, which regulate the important inflammatory regulator NF-κB (Fig 3.10). The elucidation of these signaling nodes could provide a mechanistic insight into the Tie2 expression changes we observe. BMX and TGF-β receptors were further shown to be deregulated by MIB/MS profiling. These kinases have well documented important functions in regulating the activation state of the endothelium and RhoA. Thus, future work will elucidate how these kinases are regulated and how they contribute to the CCM phenotypes. Overall, our data gathered by MIB/MS profiling represents the first broad scale examination of the kinome in CCM, and future work will reveal additional therapeutically relevant kinases for disease intervention

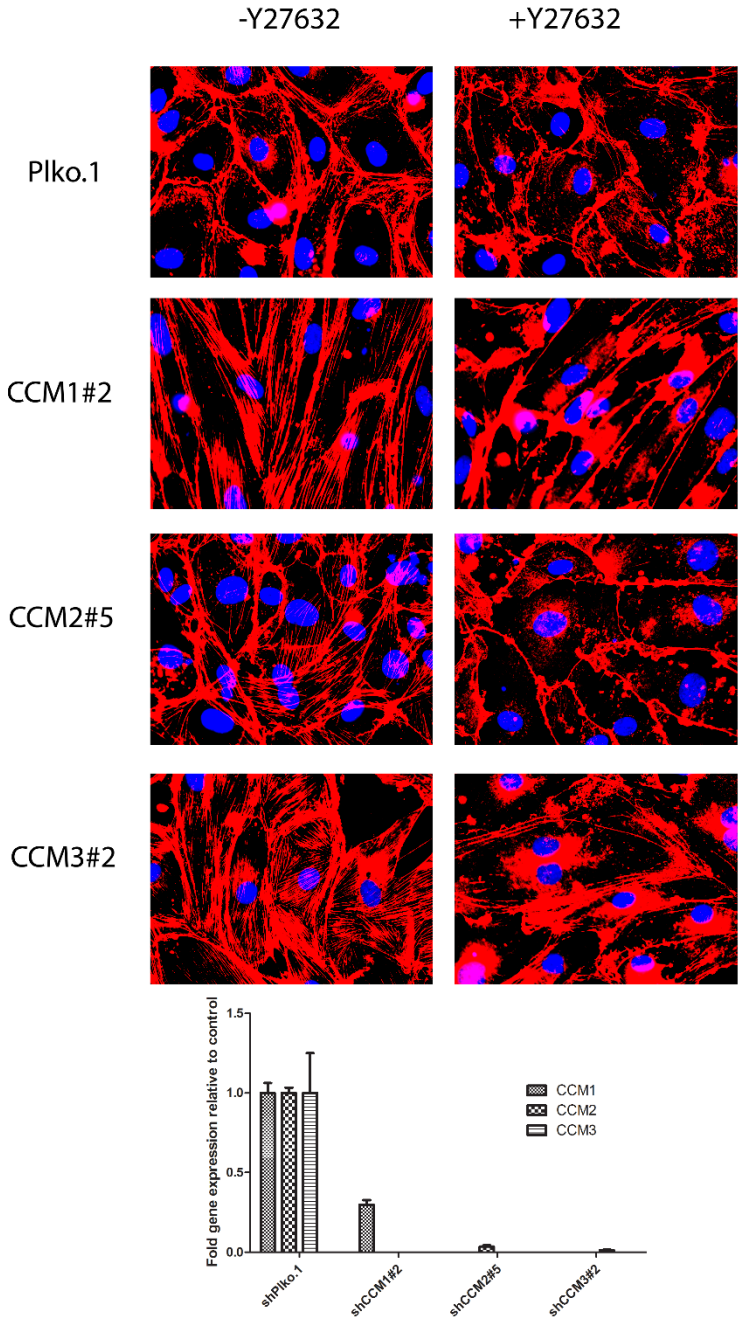

Figure 3.0: CCM protein deficient Huvecs have increased stress fiber formation. Example validation of the known stress fiber CCM phenotype following loss of CCM1, -2, or -3. Stress fibers were rescued by ROCK inhibition by Y-27632 (images taken at 40x magnification). Bottom panel shows shRNA knock down efficiency (N=3 CCM1 and CCM3; N=4 CCM2 and Plko.1).

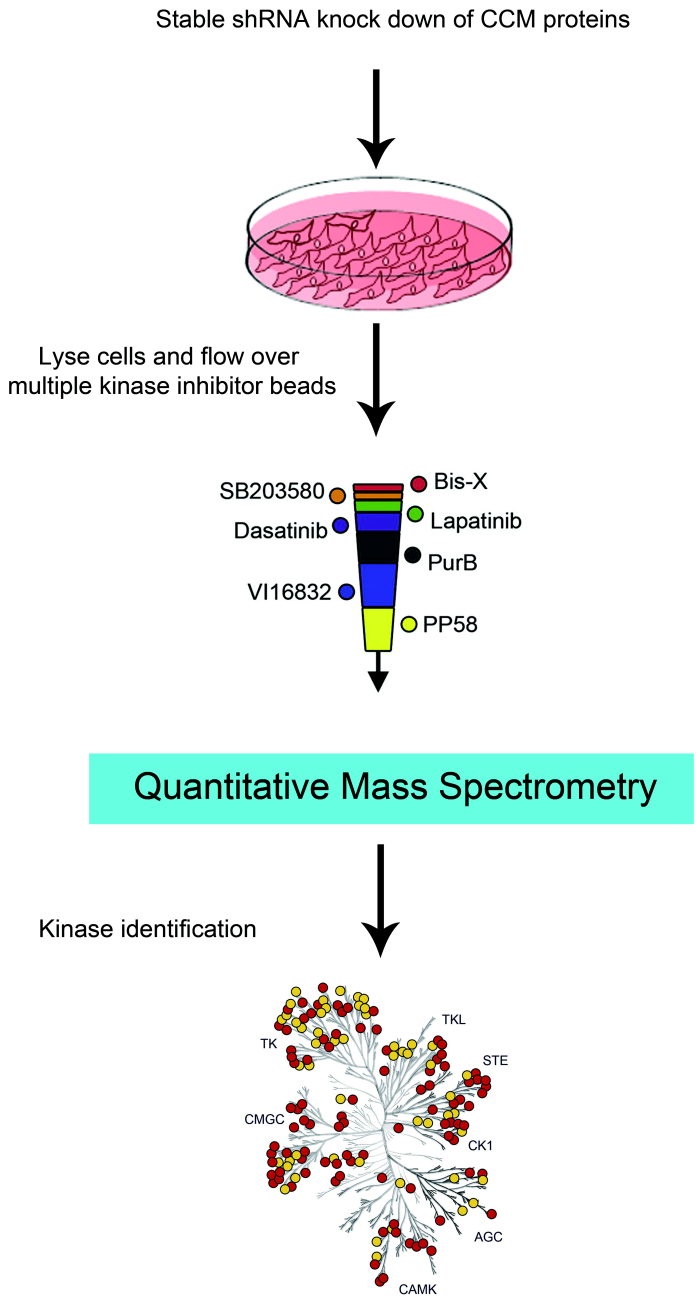

Figure 3.1: Strategy for assessing global kinome activation status in CCM protein deficient cell culture. Viral particles are generated in 293T producing cells and incubated on normal healthy endothelial cells. Stable knock down cultures are verified by qRT-PCR and maintained for at least 10-14 days. Cell cultures are lysed, proteins extracted, and flowed over multiplexed kinase inhibitor bead columns. The MS/MS spectra corresponding to peptides are quantified after running on a MALDI TOF/TOF 5800.

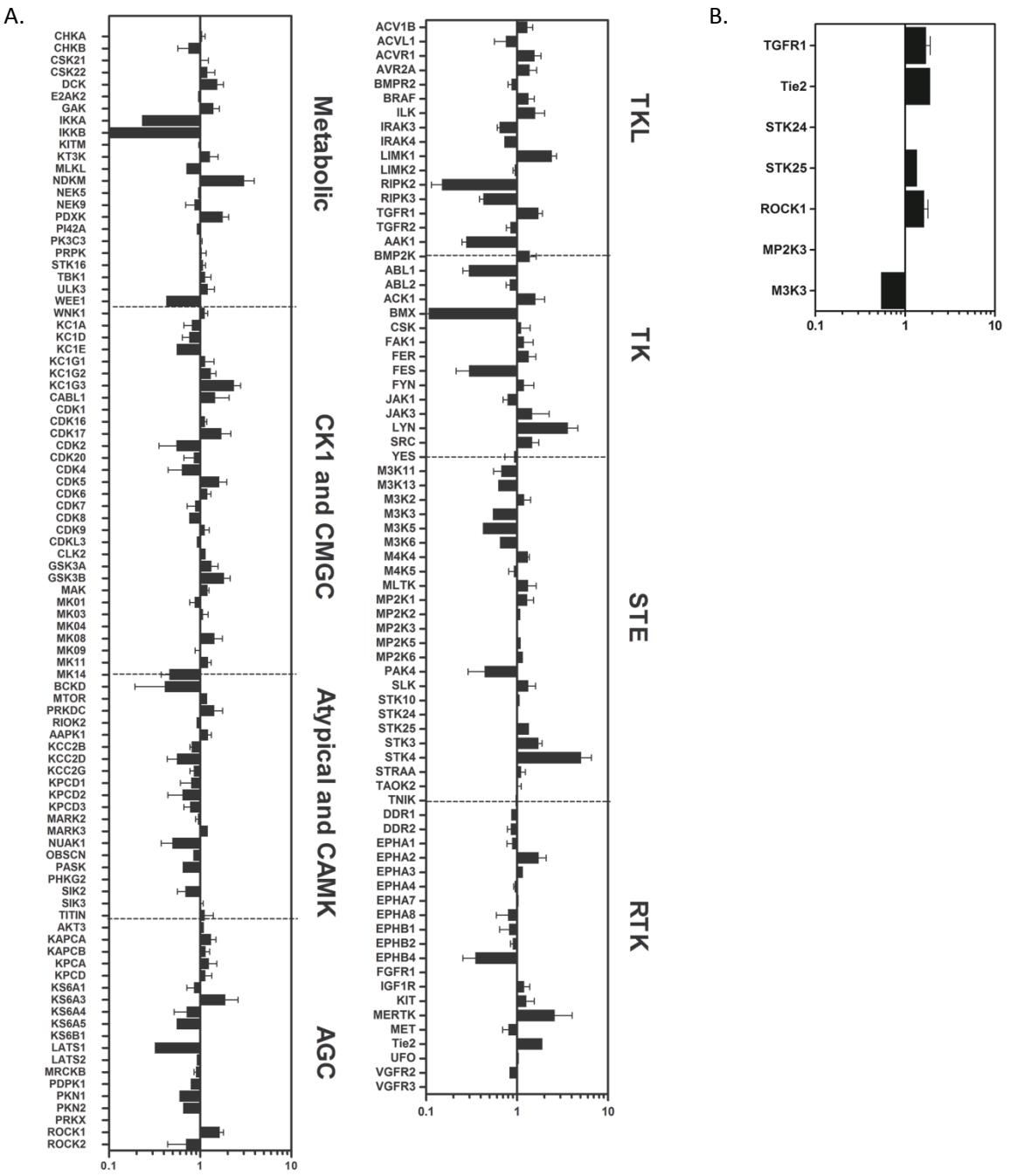

Figure 3.2: CCM2 protein loss affects the kinome. Stable shRNA knock down was achieved in Huvecs and the kinome was profiled. **A).** Altered kinase activation or expression was detected across all major kinase families. **B).** Previously identified kinases in CCM were also detected. Bars to the right of center and left of center indicate kinases over or under represented when compared to control, respectively. No bar indicates a kinase detected but unchanged compared to control. Error bars represent the average of at least two experiments where a kinase was quantified; four independent experiments were conducted.

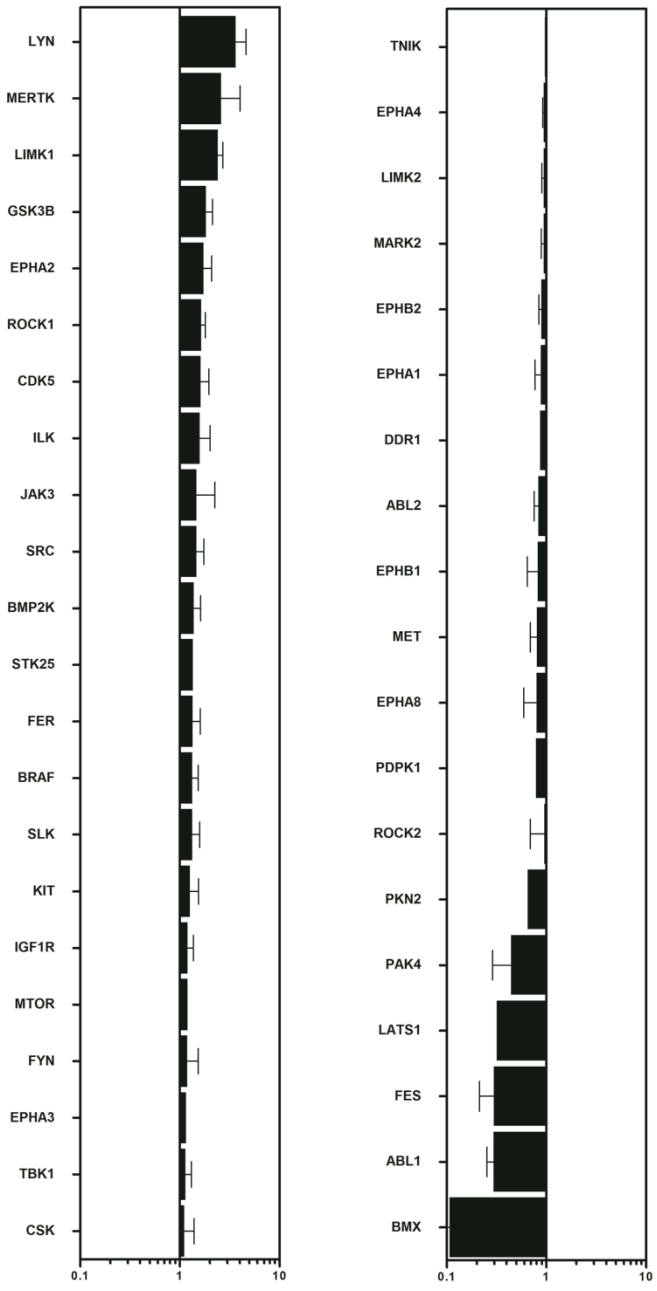

Figure 3.3: Cytoskeletal regulating kinases are both over and under represented. Ingenuity pathway analysis was used to determine, which quantified kinases had direct effects in modulating the actin cytoskeleton. Importantly, the kinases LIMK1 and ROCK1, which function downstream of RhoA, were among the highest. Error bars represent the average of at least two experiments where a kinase was quantified; four independent experiments were conducted

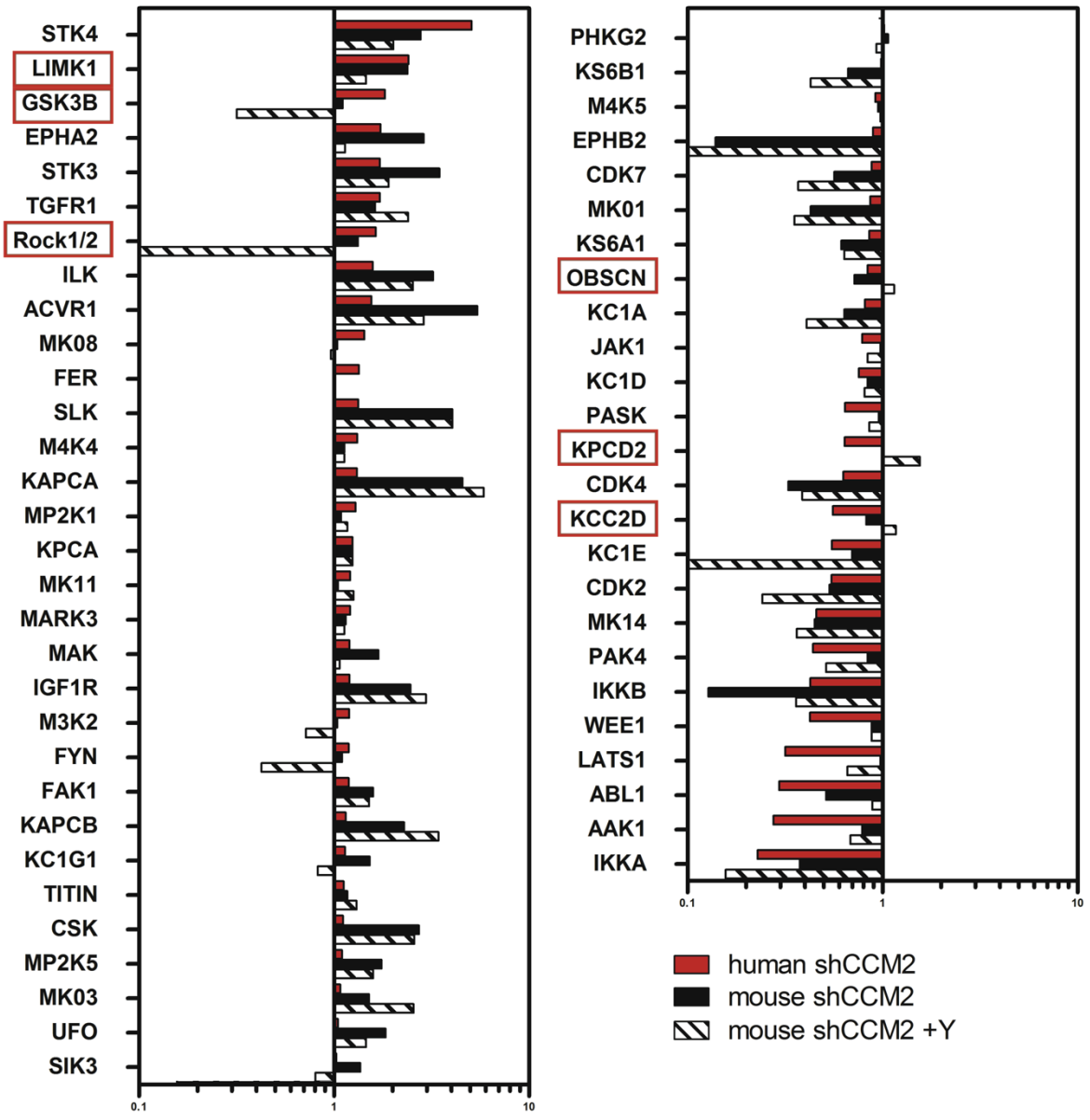

Figure 3.4: Subset of over or under represented kinases are conserved across mouse and human cells. The kinome from Stable CCM2 shRNA knock down Huvecs and MEECs were compared with many kinases showing conserved changes. Red boxes highlight the kinases changed in opposite direction after pharmacological inhibition of ROCK with 10 μM Y27632 for 48 hours.

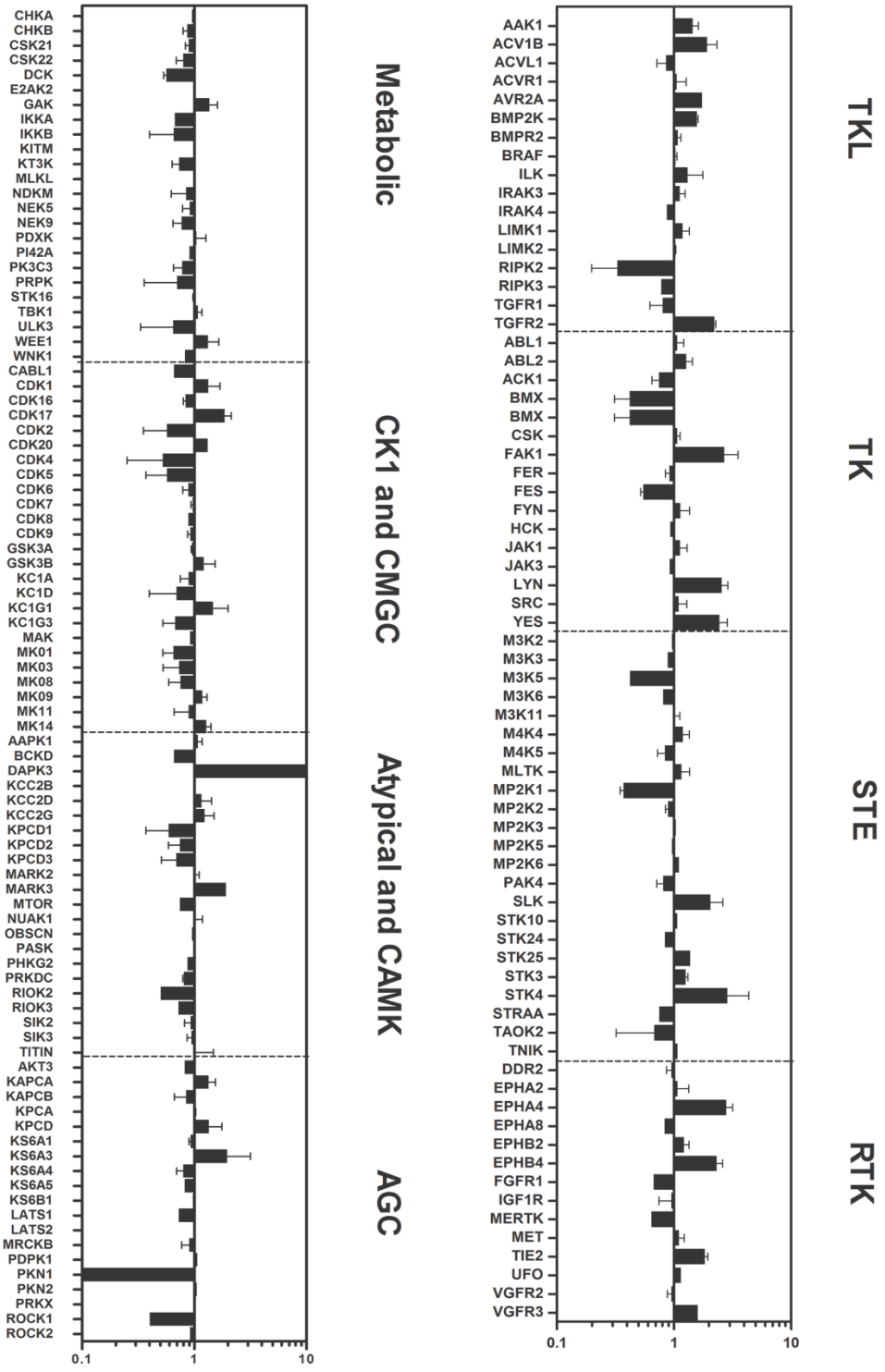

Figure 3.5: CCM1 protein loss affects the kinome. Stable shRNA knock down was achieved in Huvecs and the kinome was profiled. Error bars represent the average of at least two experiments where a kinase was quantified; three independent experiments were conducted.

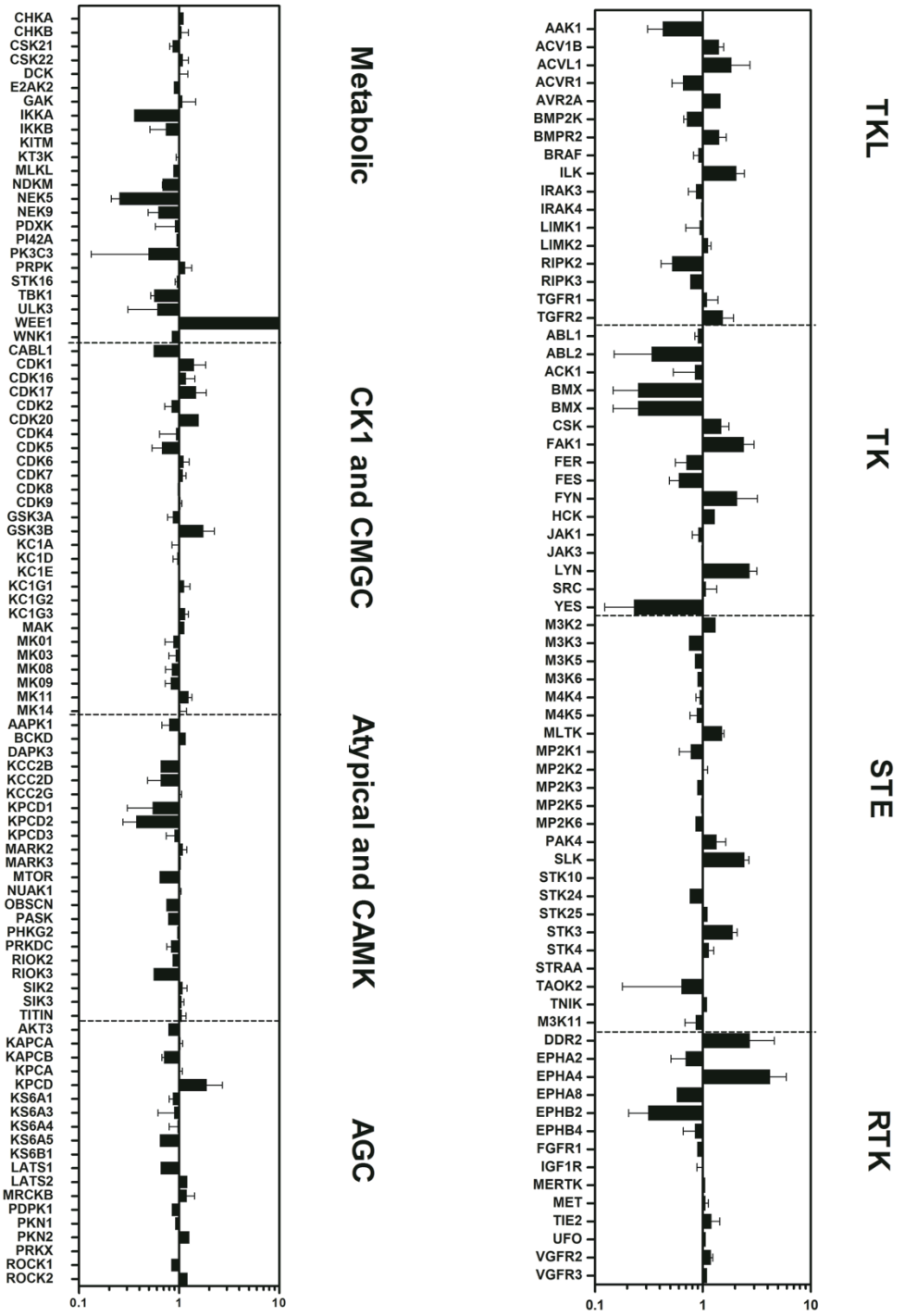

Figure 3.6: CCM3 protein loss affects the kinome. Stable shRNA knock down was achieved in Huvecs and the kinome was profiled. Error bars represent the average of at least two experiments where a kinase was quantified; three independent experiments were conducted.

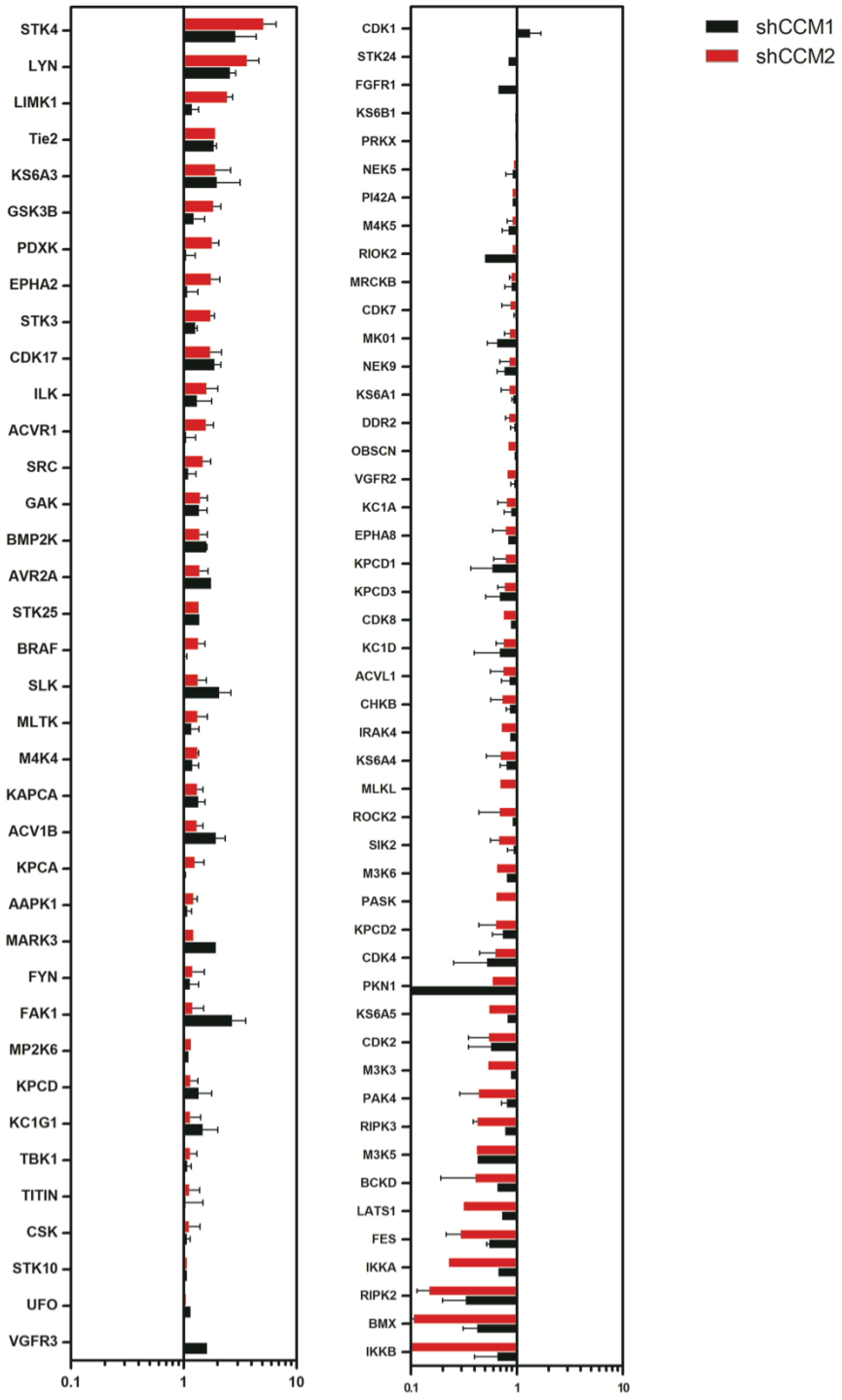

Figure 3.7: A subset of over or under represented kinases are conserved across CCM1 and CCM2 deficient Huvecs. Error bars represent the average of at least two experiments where a kinase was quantified; three independent experiments were conducted

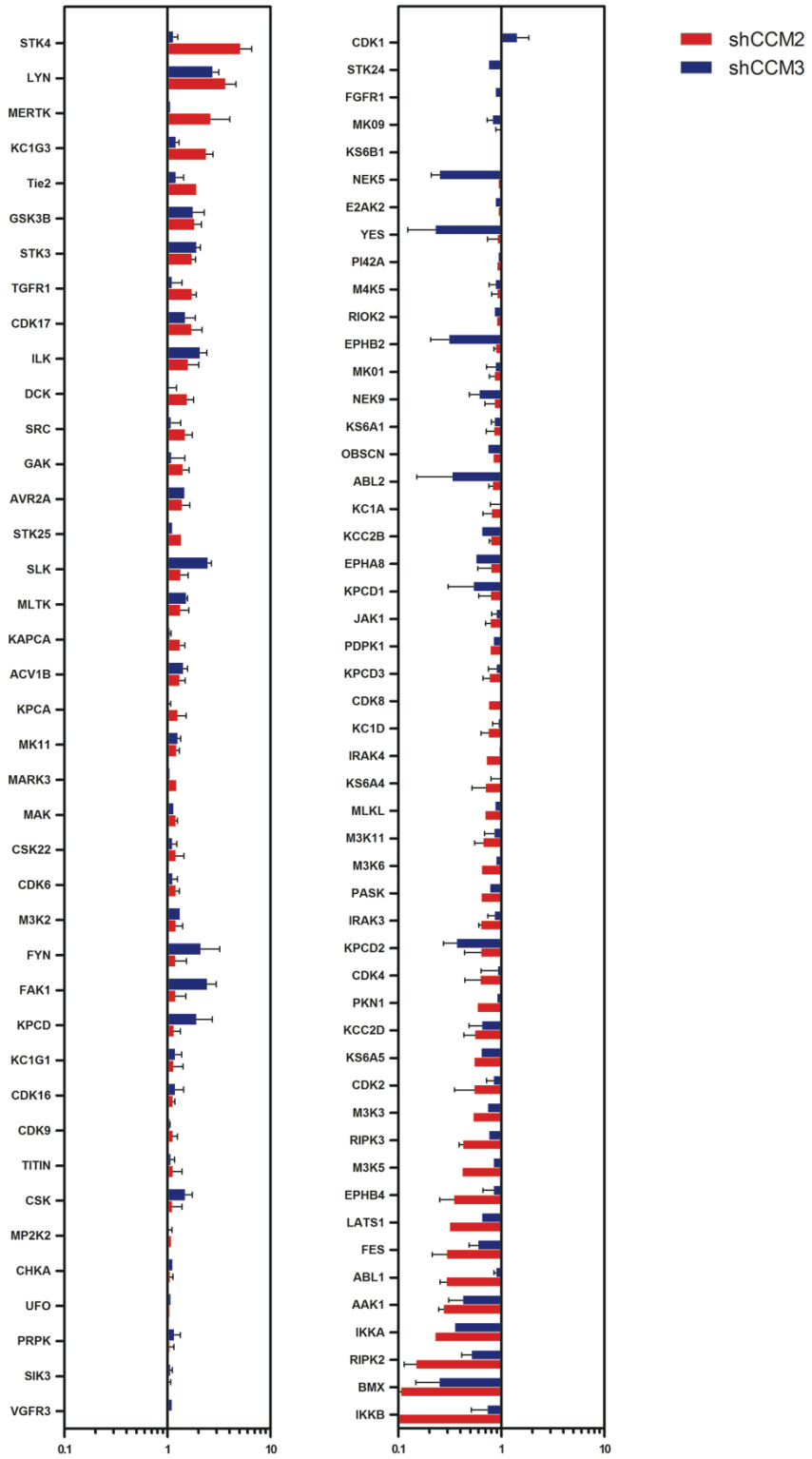

Figure 3.8: A subset of over or under represented kinases are conserved across CCM2 and CCM3 deficient Huvecs. Error bars represent the average of at least two experiments where a kinase was quantified; three independent experiments were conducted

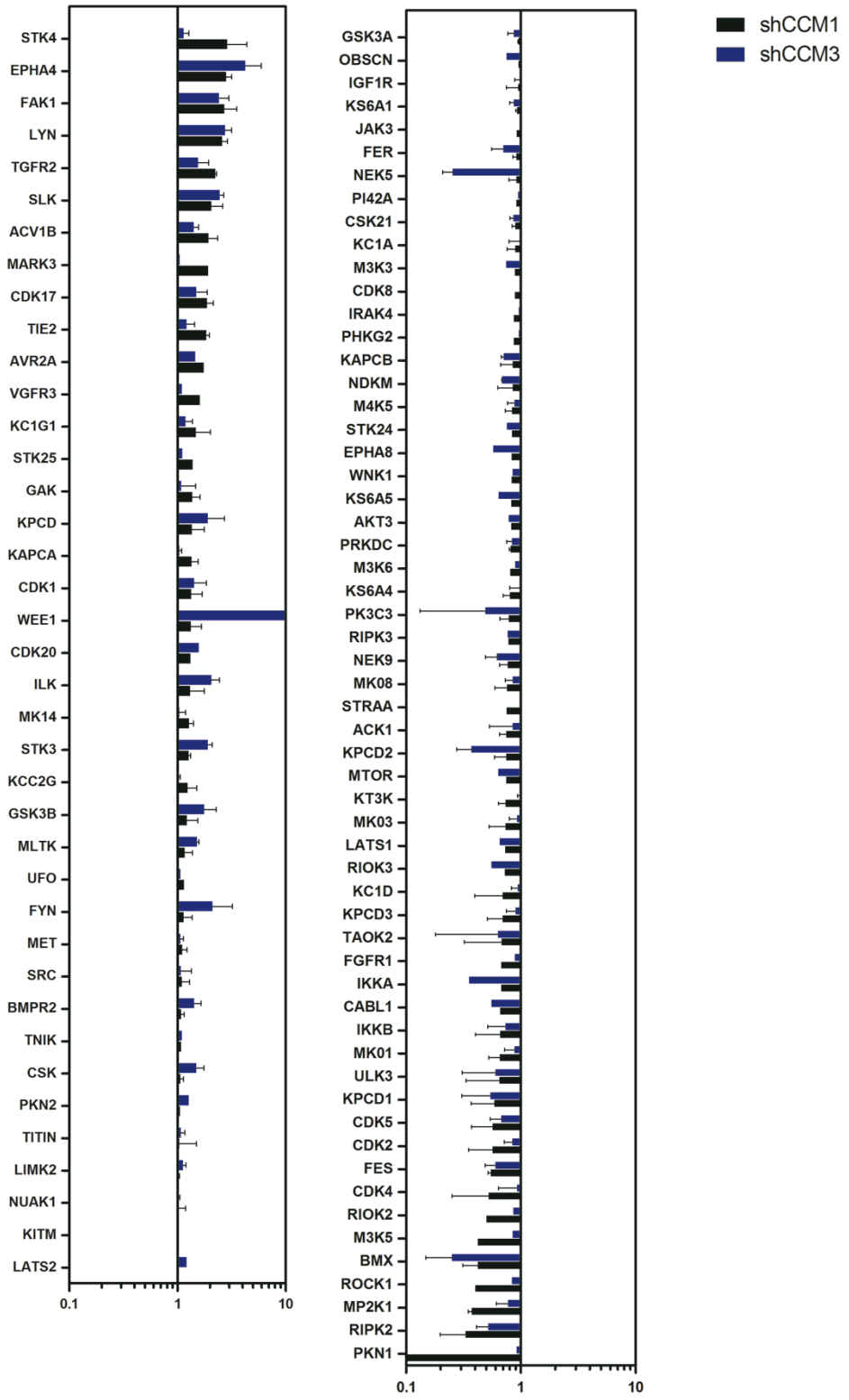

Figure 3.9: A subset of over or under represented kinases are conserved across CCM1 and CCM3 deficient Huvecs. Error bars represent the average of at least two experiments where a kinase was quantified; three independent experiments were conducted

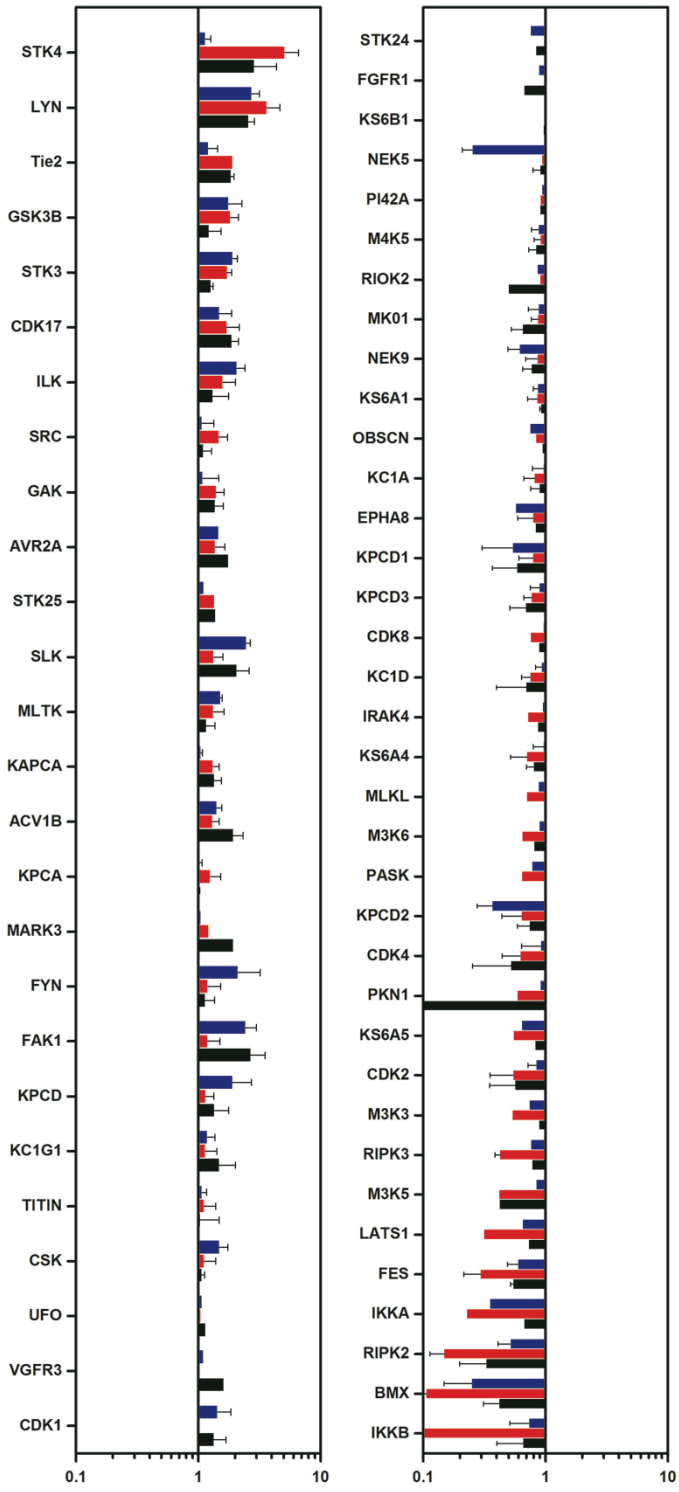

	Down	Up	Total
CCM1/CCM2	48	37	85
CCM2/CCM3	51	40	91
CCM1/CCM3	58	39	97
CCM1/2/3	36	26	62

Figure 3.10: A subset of over or under represented kinases are conserved across CCM1, CCM2, and CCM3 deficient Huvecs. Error bars represent the average of at least two experiments where a kinase was quantified; three independent experiments were conducted

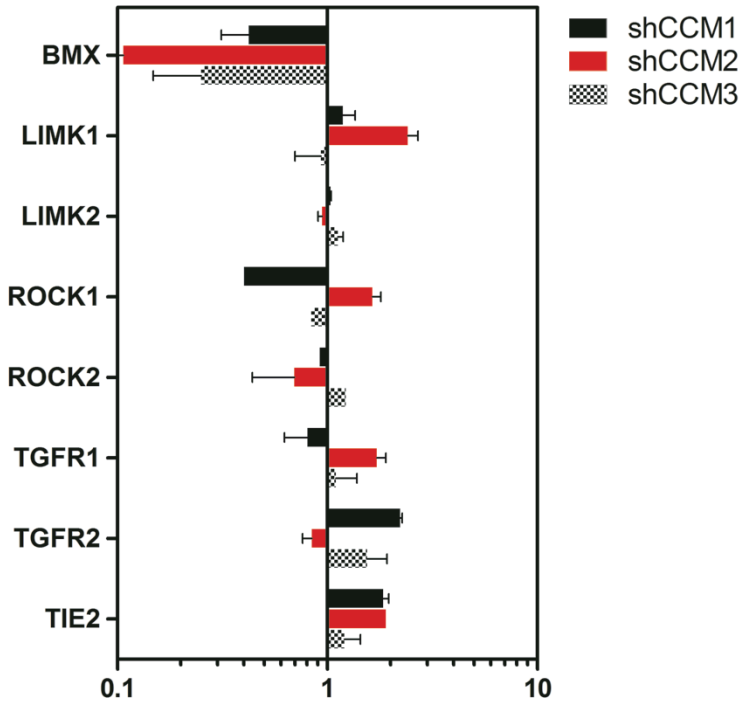

Figure 3.11: Kinases important for endothelial function are deregulated in CCM1, -2, and -3 deficient Huvecs. TGF-βR1, TGF-βR2, and Tie2 are strongly overrepresented, whereas BMX is strongly underrepresented. LIMK signaling also is overrepresented with CCM1 and CCM2 deficient cells having increased LIMK1 and CCM3 deficient ECs having increased LIMK2. ROCK1 and ROCK2 are differentially regulated in CCM2 and CCM3 deficient ECs, and CCM1 unexpectedly has decreased ROCK1/2 levels. Error bars represent the average of at least two experiments where a kinase was quantified; three independent experiments were conducted

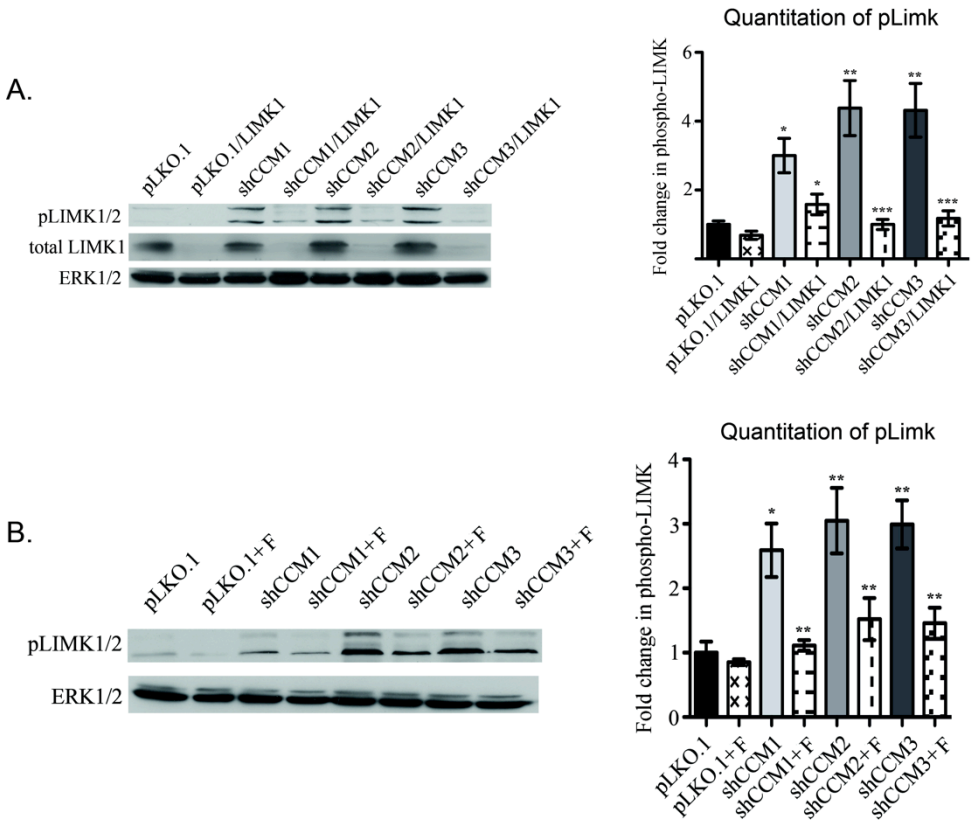

Figure 3.12: pLIMK1 is increased in stable CCM1, -2, or -3 knock down MEECs. A). Loss of CCM proteins increases pLIMK1/2 but not total LIMK1, suggesting that LIMK activation is effected. shRNAs against LIMK1 by in large decrease this signal, suggesting that most of the signal is from LIMK1 and not LIMK2. **B).** The activation of LIMK1 is downstream of ROCK as inhibition of ROCK activity by Fasudil decreases pLIMK1. (*P <.05 from independent experiments) (*Courtesy of Dr. Christopher Dibble).

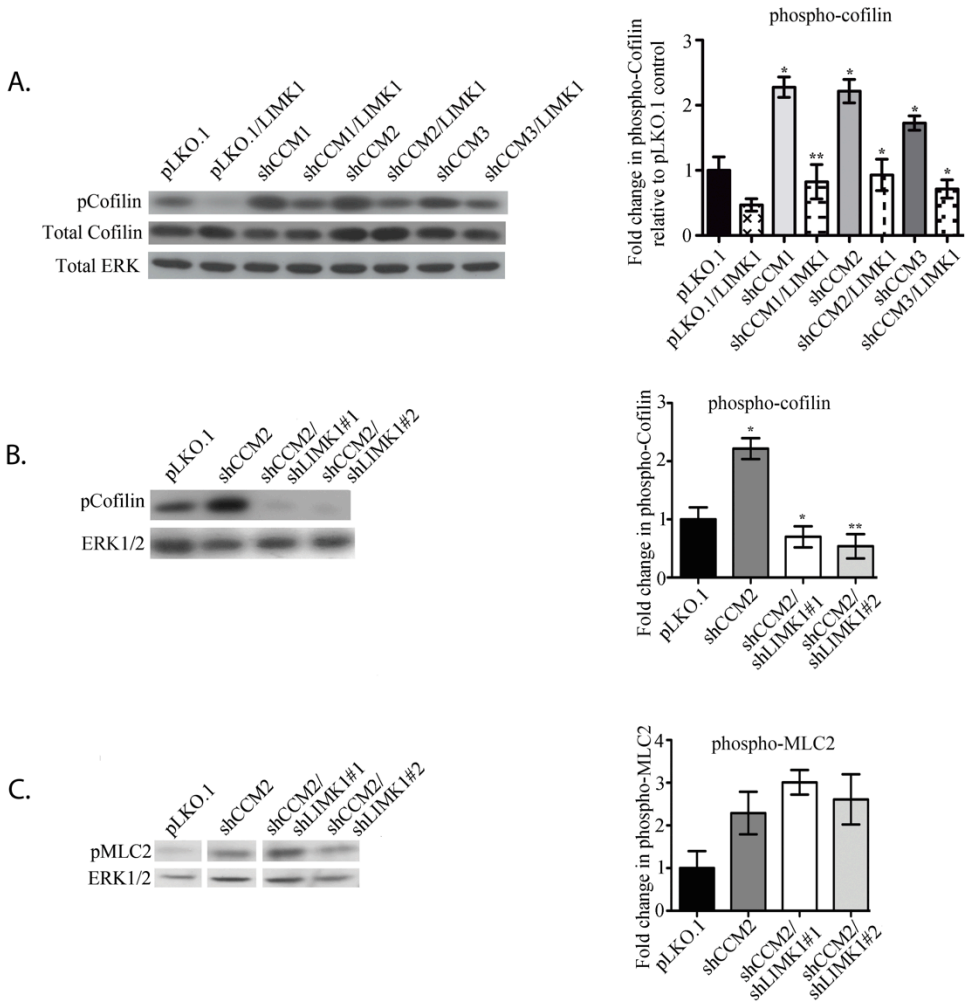

Figure 3.13: pCofilin levels are increased by LIMK1 following CCM protein loss A). Loss of CCM proteins increases pCofilin levels, and double stable knockdowns for CCM1, -2, or -3 with LIMK1 rescue these elevated pCofilin levels. **B).** Two independent shRNAs for LIMK1 decrease pCofilin in CCM2 knock down cells. **C).** pMLC2 is elevated in CCM2 knock down cells but LIMK knock down is unable to decrease these elevated levels suggesting that LIMK1 is only effecting the pCofilin arm of the RhoA/ROCK pathway. (*P <.05 from independent experiments) (*Courtesy of Dr. Christopher Dibble).

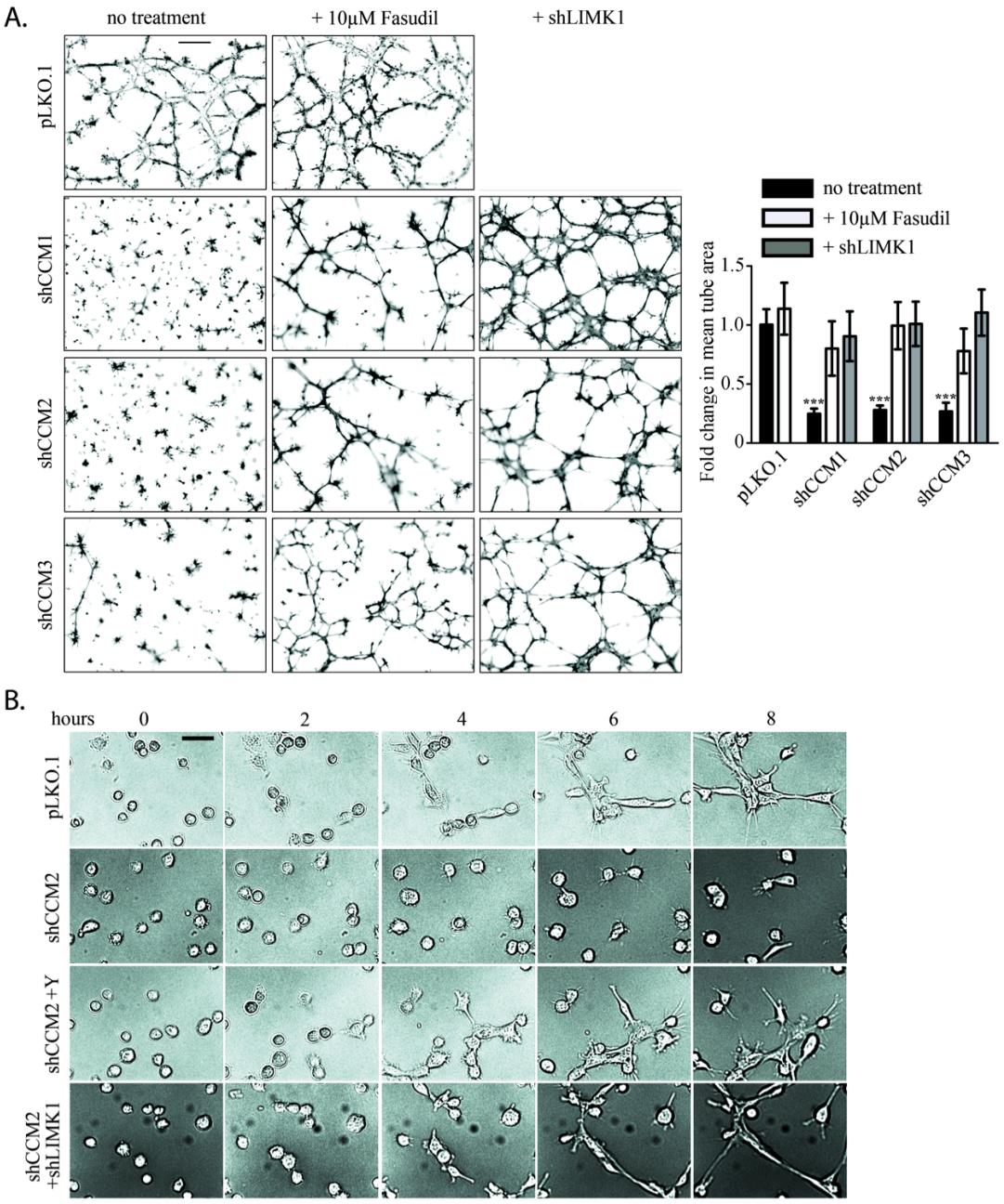

Figure 3.14: Knock down of LIMK1 is sufficient to rescue CCM phenotypes in vitro A). Loss of CCM proteins decreases endothelial tube forming ability that is rescuable with ROCK inhibition (10 μM Y27632) or stable knock down of LIMK1. **B).** Time course analysis of endothelial tube formation shows that CCM2 deficient ECs are unable to make cell contacts and elongate into tube structures, where as cells treated with ROCK inhibitor or LIMK1 knock down are able to start forming cell-cell contacts and elongate similar to control cells after 4-6 hours. Images were taken at 10X magnification (*P <.05 from independent experiments) (*Courtesy of Dr. Christopher Dibble).

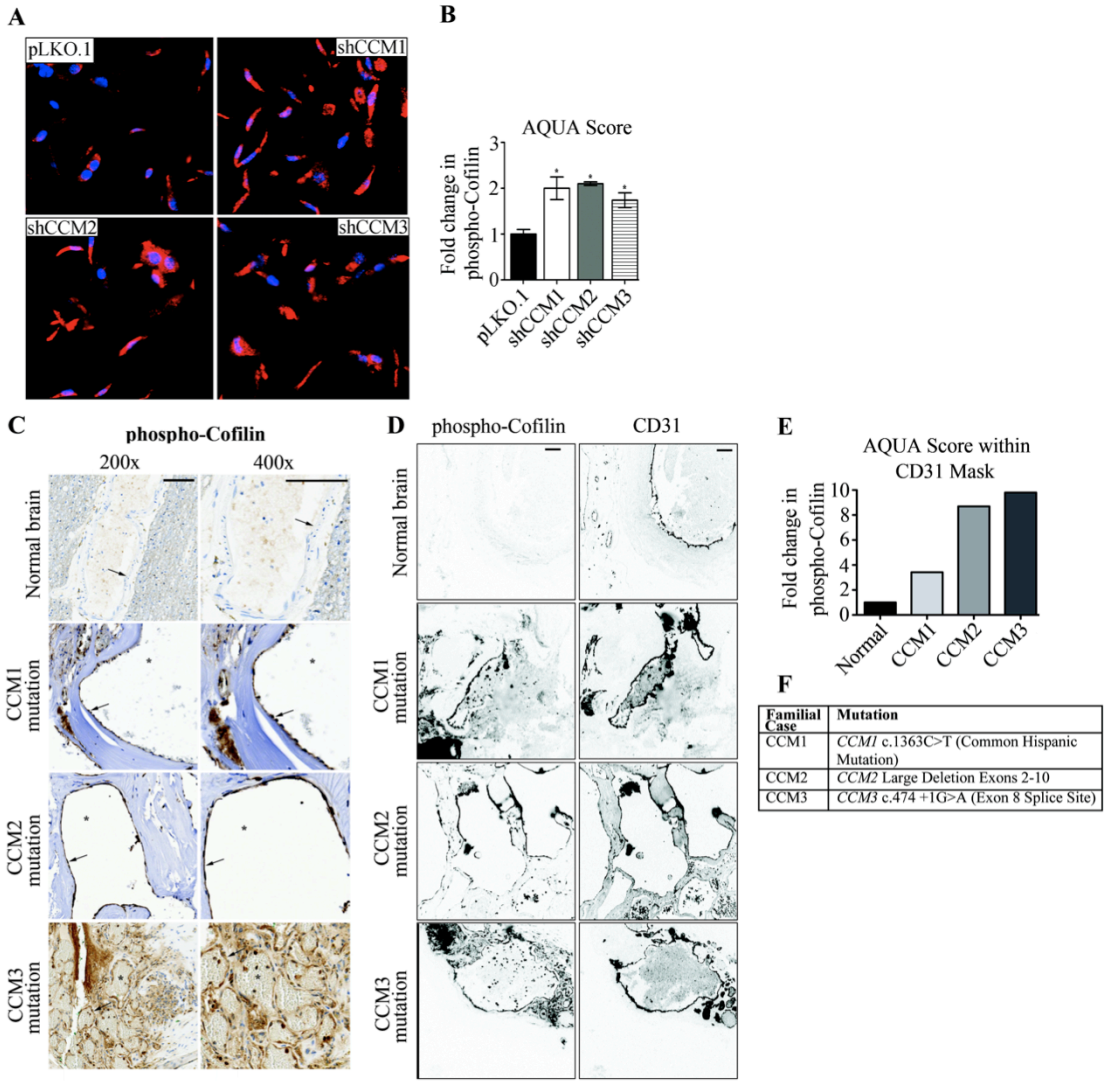

Figure 3.15: Elevated pCofilin staining is observed in surgically resected human CCM1, -2, and -3 lesions A). pCofilin antibody was validated by showing to elevated pCofilin levels in paraffin embedded MEECs with stable CCM1, -2, or -3 knock down. **B).** Advanced QUantitative Analysis (AQUA) was used to quantitate pCofilin levels by immunoflourescence. **C).** Human lesions with sequence verified CCM1, -2, or -3 mutations but not adjacent normal brain endothelial tissue display elevated pCofilin staining in the endothelium by immunohistochemistry. **D).** pCofilin is elevated by immunoflourescence of human CCM lesions and overlays perfectly with a CD31 (endothelial specific mask), indicating that pCofilin is elevated only in the endothelium (right panel). **E).** AQUA of immunoflourescence shows between a 4 and 10 fold increase in pCofilin signal when compared to normal brain tissue. **F).** Table listing the CCM1, -2, and -3 patient mutations from the stained lesions. (*P <.05 from independent experiments).

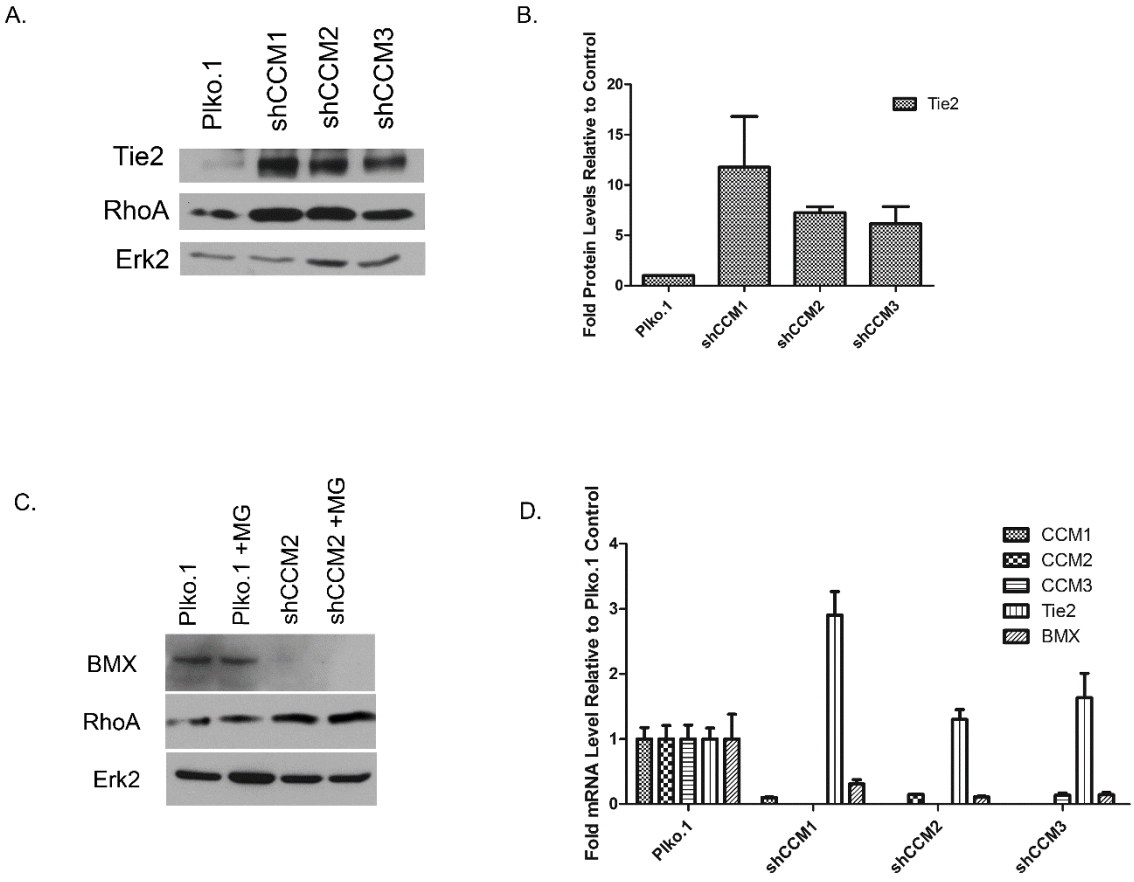

Figure 3.16: Tie2 and BMX are increased both at protein and mRNA levels in Huvecs after CCM1, -2, or -3 loss. A). Tie2 and RhoA protein expression is increased after CCM1, -2, or 3 knock down in Huvecs. **B).** Densitometry quantification of three separate experiments on Tie2 levels normalized to Erk2. **C).** BMX protein is down regulated and RhoA protein levels are increased after loss of CCM2. Proteasome inhibition by MG132 is insufficient to rescue BMX. **D).** Tie2 message levels are increased and BMX message levels are decreased by qRT-PCR.

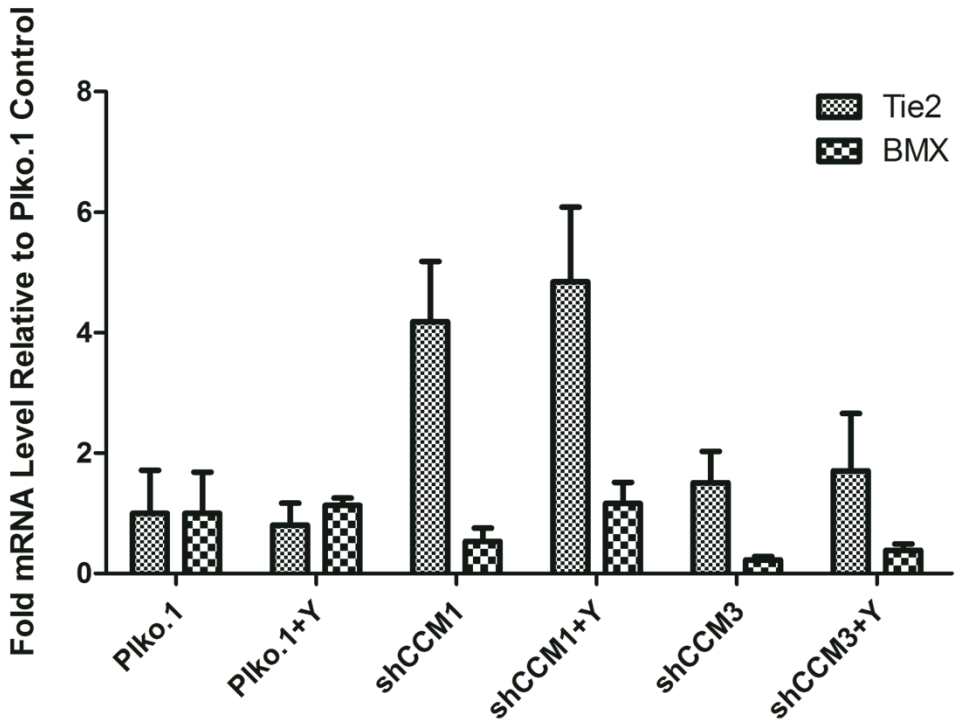

Figure 3.17: Tie2 and BMX message levels are not significantly affected by ROCK inhibition. Huvec cells with stable knock down of CCM1 or CCM3 were treated with 10 μM ROCK for 48 hours. No significant changes in message levels of Tie2 or BMX were detected (N=2 separate experiments).

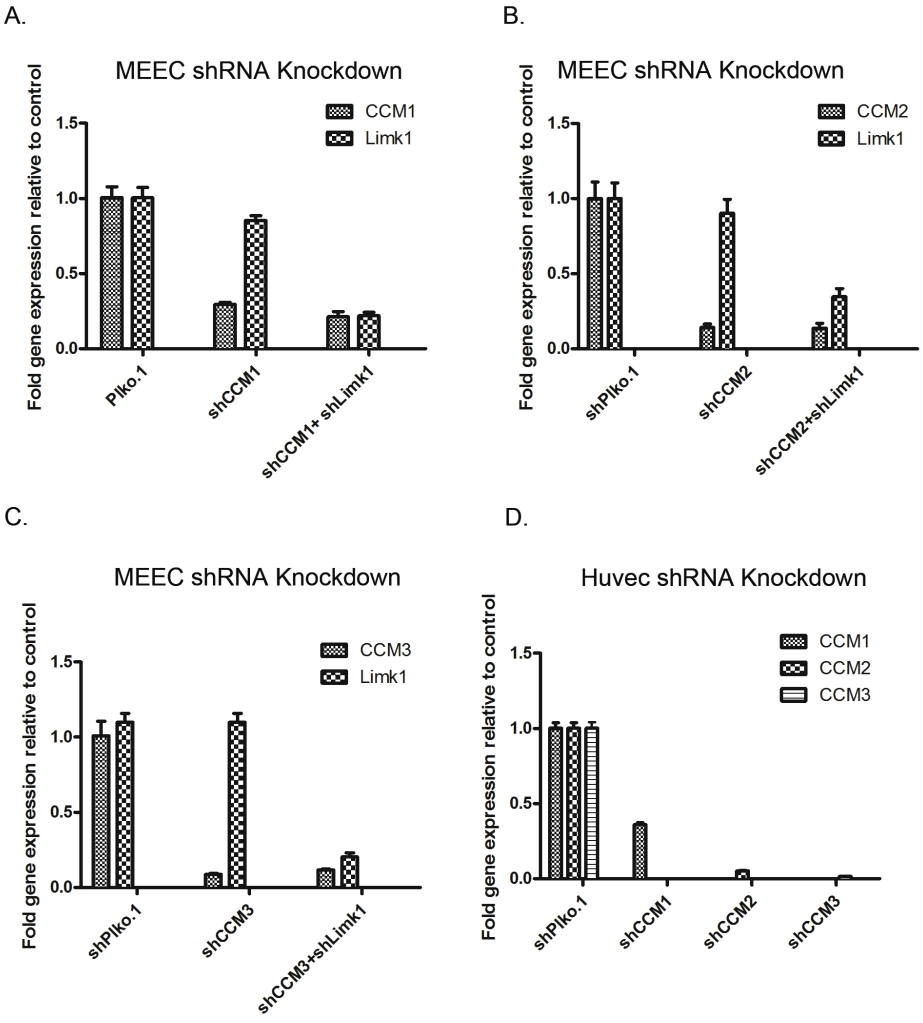

Figure 3.18: qRT-PCR analysis of knock down lines used for chapter III. A). Stable double knock down of CCM1 and Limk1 in MEECs. **B).** Stable double knock down of CCM2 and Limk1 in MEECs. **C).** Stable knock down of CCM3 and Limk1 in MEECs. **D).** Stable knock down of CCM1, -2, and -3 in Huvecs

IV. Ubiquitin ligase mediated degradation of RhoA as a molecular mechanism deregulated in CCM protein deficient ECs.

Introduction

Recent studies have increased our understanding of how CCM protein loss contributes to endothelial cell dysfunction and lesion generation. It has become apparent that elevated RhoA/ROCK signaling leads to CCM pathogenesis. Currently, it is unknown how RhoA becomes over activated in CCM. There have been no published studies examining canonical GEF or GAP regulation of RhoA, and we have led unsuccessful attempts in uncovering known RhoA GEF or GAPs that function downstream of the CCM proteins. However, we have consistently observed increases in total RhoA protein without subsequent increases in RhoA message levels following knock down of CCM proteins [4, 5]**.** This information suggests that the degradation of RhoA is being affected by CCM protein loss.

There have been numerous findings that suggest degradation is an important mechanism behind the regulation of small GTPase function [198]. The degradation of RhoA was observed after stimulation of CNF1 led to increased activation of RhoA [199, 200]. Currently, only the Smurf1 and cullin 3 E3 ubiquitin ligases have been found to degrade RhoA with Smurf1 selectively degrading active RhoA and cullin 3 targeting total RhoA [76, 116]. We have previously established that Smurf1 binds to CCM2 in a PTB dependent manner, which is in line with degradation as a potential molecular mechanism regulating RhoA levels. This interaction in Cos7 cells results

recruits Smurf1 to the cell membrane resulting in a cell spreading effect. CCM2 overexpression along with Smurf1 led to a CCM2 dose dependent decrease in RhoA levels. CCM2 is neither a substrate of Smurf1 nor does it affect Smurf1 catalytic function [5]. Thus, deregulated Smurf1 is an attractive candidate driver of the increased RhoA signaling observed in CCM. In addition to RhoA, Rap1 is also degraded by a structurally similar E3 ubiquitin ligase Smurf2. This degradation results in selective degradation of Rap1 in retracting neurites after correct membrane localization by mPar3 [111, 112]. Based on the ability of CCM2 to bind Smurf1 and regulate its localization, we sought to investigate the ability of the CCM proteins to bind the other E3 ubiquitin ligases Smurf2 and cullin 3 and how that affects EC phenotypes.

In this study, we demonstrate that Smurf1, Smurf2, and cullin 3 phenocopy the loss of CCM proteins through the differential regulation of RhoA and Rap1. CCM2 but not CCM1 or CCM3 bind to Smurf1, and this interaction occurs endogenously. We further show that CCM2 is able to interact with Smurf2, which provides a potential link for Smurf2 in regulating Rap1 levels in CCM. Lastly, we demonstrate that RhoA protein levels are elevated following CCM protein loss through decreased ubiquitination of the GTP bound form of RhoA and a steady accumulation of RhoA protein.

Results

CCM2 but not CCM1 or CCM3 bind to Smurf1, promoting the degradation of GTP bound RhoA

Smurf1 has been shown to selectively degrade GTP bound RhoA, and the CCM disease state occurs from over active RhoA. Therefore, we focused our attention to whether Smurf1 was affecting the poly ubiquitin levels of GTP bound RhoA. We first began by interrogating the CCM ternary complex to determine whether Smurf1 binds to CCM1 or CCM3. Using transfected proteins, we only detected co-immunoprecipitated Smurf1 with CCM2 and not CCM1 or CCM3, which was abrogated with a single point mutation in the PTB domain of CCM2 (Fig 4.0 A and B). We also detected this interaction between endogenous CCM2 and Smurf1, indicating this interaction is physiological at a cellular level (Fig 4.0 C). This result suggests that CCM2 interacts with Smurf1, where as CCM1 and CCM3 may have an indirect role in regulating Smurf1 activity or are required for further localization of the complex through their respective independent interactions with CCM2.

We sought to detect the levels of endogenously ubiquitinated GTP RhoA by utilizing the Rho binding domain from Rhotekin to pull down GTP bound RhoA followed by ubiquitin immunoblotting [201]. We treated all cells with the proteasome inhibitor MG132 for 6 hours to stabilize poly ubiquitinated proteins**.** To determine the specificity of this assay for GTP bound RhoA, we knocked down total RhoA protein by shRNA and blotted for ubiquitin. We detected a complete loss in both total RhoA and GTP bound RhoA with a nearly complete loss in ubiquitin signal when quantified and compared to Plko.1 control cells from independent experiments (Fig 4.1A and B).

This result indicates that we are preferentially detecting ubiquitinated GTP bound RhoA with little to no RhoB or RhoC background. This finding is likely because the other Rho members are degraded through the lysosomal protein degradation pathway and do not utilize the ubiquitin proteasome system (UPS) [202].

Therefore, we sought to determine whether the loss of CCM proteins also affects ubiquitinated GTP bound RhoA. We were able to generate stable knock down CCM1, -2, or -3 in ECs and observed large increase in both activated GTP bound RhoA and total RhoA protein (Fig 4.1A and 4.8 A-E). These increases were followed by a significant decrease in ubiquitinated GTP bound RhoA, and after quantification of multiple experiments, ubiquitinated GTP bound RhoA was decreased to baseline levels (Fig 4.1A and B). Similarly, the loss of Smurf1 increased total and active GTP bound RhoA with a concomitant decrease in ubiquitinated GTP bound RhoA (Fig 4.1 A and B). This decrease in ubiquitinated GTP bound RhoA signal is detected even though there is far more GTP bound RhoA in the pull down from CCM1, -2, 3, or Smurf1 deficient cells. These data indicate that the CCM protein complex first defined in Hilder et al. functions, in part, to regulate the ubiquitination status of GTP bound RhoA with CCM2 directly coordinating Smurf1. Other groups have observed increases in activated RhoA without increases in total RhoA. We hypothesize that the loss of Smurf1 leads to the steady accumulation of GTP bound RhoA, which over time may contribute to increases in total RhoA protein [76, 93]. This observation may not be realized with the use of transient siRNA approaches that have been used previously. To

definitively prove this hypothesis, additional studies into the spatial temporal degradation of activated RhoA versus total RhoA are required.

Forskolin stimulates longer term RhoA degradation and Mst3/4 kinases phosphorylate Smurf1

The mechanism behind how the CCM protein complex regulates total and active RhoA levels is unknown. Phosphorylation of RhoA upon Serine 188 protects RhoA from UPS mediated degradation in vascular smooth muscle cells [203]. This phosphorylation event functionally promotes the association of RhoA with RhoGDI and extracts RhoA from the membrane [204]. Therefore, we wanted to interrogate whether this system is conserved in ECs. Forskolin is an agonist of adenylyl cyclase and functions to produce the cyclic adenosine monophosphate (cAMP) second messenger, which is critical to the activation of protein kinase A (PKA). Therefore, we sought to determine if RhoA levels are sensitive to elevated cAMP/PKA signaling in ECs. We observed that active RhoA levels decrease, and there is a spike in total RhoA levels within several hours following the administration of Forskolin. These levels remain high after 26 hours of treatment (Fig 4.2 A and B). The total RhoA levels are decreased below WT levels after 36 hours, which is in contrast to the more rapid turnover of RhoA following treatment with cycloheximide (CHX) (Fig 4.2 C and D). These data are consistent with previous studies demonstrating that the half-life of a Ser188 phospho-mimetic RhoA is increased after 6 hour treatment [203]. However, the decrease in RhoA with longer treatment of Forskolin is unknown and may indicate a more dynamic regulation of RhoA turn over. Proteasome inhibition

with MG132 was able to rescue the total RhoA levels after prolonged forskolin treatment, suggesting that RhoA is being degraded through the UPS, potentially through Smurf1 (Fig 4.2 C and D). We further have observed decreased PKA-β (KAPCB) subunit activity following loss of CCM1 and CCM3 by MIB/MS profiling (Fig 3.9). Therefore, additional studies are needed to determine if the CCM protein complex is regulating PKA mediated phosphorylation and subsequent degradation kinetics of RhoA. Overall, these data indicate that a component of adenylyl cyclase/PKA signaling functions to regulate RhoA stability in ECs.

CCM3 interacts with several of the sterile kinases, including Mst3 and Mst4, which phosphorylated the ERM proteins among other proteins directly on serine/threonine residues, which leads to decreased RhoA activity [205]. This regulation of phosphorylation activity by CCM3 could provide a link for CCM3 and Smurf1 regulation. Smurf1 substrate switching specificity from the SMADs to RhoA is determined by increased phosphorylation of Smurf1 at T306 downstream of PKA [108]. Therefore, we wanted to determine if either Mst3 or Mst4 phosphorylates Smurf1. Using an in vitro kinase assay, we detected the phosphorylation of GST purified Smurf1 at approximately 20% of Mst3 and 4 autophosphorylation (Fig 4.2 E). Mst3 and 4 autophosphorylation is required for their proper activation and Mst3 autophosphorylation is decreased after Smurf1 substrate addition (Fig 4.2 E). While this hypothesis is speculative, it is possible that CCM3 binding to Mst3 and 4 contributes to the CCM ternary complex regulation of RhoA degradation through PKA or STE family kinases, which may mediate Smurf1 substrate switching.

In vitro loss of Smurf1 and cullin E3 ligases increase F-actin stress fibers and decrease endothelial cell tube formation ability

We next determined the functional consequences of Smurf1 loss in stably transduced ECs and whether that loss phenocopies CCM protein loss. Stable shRNA mediated knock down of Smurf1 by two different shRNAs led to a significant increases in actin stress fibers (Fig 4.3A and C). This result is consistent with the loss of CCM1, -2, or -3 and increases in active RhoA following Smurf1 knock down. These actin stress fibers were decreased following treatment with the ROCK inhibitor Y27632, indicating that Smurf1 is affecting RhoA-ROCK signaling (Fig 4.3A and C). This increase in cellular F-actin also decreased tube formation ability, which was partially rescued by ROCK inhibition (Fig 4.3 B and D). Together these data further suggest that Smurf1 functions alongside CCM proteins to directly regulate activated RhoA.

The cullin E3 ring ligases are purported to affect the ubiquitination status of total RhoA protein. Cullins function similarly to the Smurf proteins through an E1, E2, E3 enzyme ubiquitin transfer cascade which increases substrate specificity [115]. Importantly, the loss of the cullin 3 E3 ligase has been shown to increase RhoA protein levels and stress fiber formation [116, 117]. This effect results from the decreased ubiquitination of total RhoA protein, which leads to a steady accumulation of activated RhoA protein. This process is in reverse for Smurf1, which degrades activated RhoA protein followed by a concomitant increase in total RhoA protein [93, 109]. We, thus sought to understand if the cullin E3 ligases are directly changing total RhoA protein levels. To address this question, we used a commercially

available cullin ligase inhibitor MLN 4924. This inhibitor blocks the neddylation activating enzyme (NAE) [206]. Total protein degradation inhibition by MG132 or bortezomib is over 50% where as MLN 4924 only blocks 9% of total protein turn over [207]. For cullin E3 ligases to function properly, the neddylation factor NEDD8 is transferred sequentially to the E1, E2, and E3 enzymes in an ATP dependent fashion. This final NEDD8 conjugation to the cullin family of ligases is required for recruitment of E2 conjugating enzymes, release of the negative regulator Cand1, and overall activation of the ubiquitinating complex [207]. Tube-like structures were significantly ablated when cells were plated in a Matrigel tube formation assay after treatment with MLN 4924 (Fig 4.4A). Stress fibers and total RhoA protein levels were also increased, which is consistent with the role of cullin ligases in regulating RhoA (Fig 4.4 B, C, and D). Importantly, stress fibers and tube forming ability were significantly rescued when ROCK was inhibited by Y27632 (Fig 4.4 A, C, and D). This result indicates that blocking neddylation by MLN 4924 increases total RhoA protein.

The magnitude of RhoA protein increase and relative short timing of this increase indicates that total RhoA protein degradation is being affected. This result is expected because the estimated total amount of GTP bound RhoA in cell culture is quite low at only 5% [208]. To examine this process, we immunopreciptated total RhoA proteins and then immunoblotted for ubiquitin in wild type cells and in cells treated with MLN 4924 for 24 hours. MLN 4924 treatment significantly increased RhoA total levels while decreasing ubiquitinated RhoA (Fig 4.5A). This decrease in ubiquitinated total RhoA was more than the decrease observed in Smurf1 knock

down cells (Fig 4.5B). Thus, these data suggest that Smurf1 is ubiquitinating the activated form of RhoA more selectively, and cullin ligases are ubiquitinating the total form of RhoA in ECs. We next wanted to ascertain if the cullin 3 ligase was influencing RhoA signaling as has been previously reported. After stable knock down of cullin3 in ECs we noted an increase in F-actin stress fibers and concomitant loss in tube forming ability, which were rescued by ROCK inhibition with Y-27632. (Fig. 4.6A and B). A large increase in pMLC2 levels were observed after Smurf1 knock down and a lesser extent in cullin 3 knock down cells, suggesting that the levels of activated RhoA are higher in Smurf1 deficient cells (Fig 4.6 C). This finding is consistent with previous studies and our hypothesis of Smurf1 degrading activated RhoA and the cullin ligases degrading total RhoA.

Smurf2 binds CCM2 and is required for proper endothelial tube formation through regulation of Rap1.

Rap1 regulation is central to endothelial junction stability and is regulated by CCM1 [62, 95]. Smurf2 also degrades Rap1A in neurons and based upon its similarity to Smurf1, we investigated the effects of Smurf2 loss in ECs. Accordingly, after stable shRNA knock down of Smurf2 we noted a large decrease in tube formation ability (Fig 4.7 A and B). In contrast to Smurf1 knock down ECs, this phenotype was not rescued by ROCK inhibition, suggesting that Smurf2 degrades Rap1 with no effect on RhoA (Fig 4.7 A and B). Accordingly, we noted that Rap1 but not RhoA levels were increased by western blotting after Smurf2 knock down (Fig 4.7 C). This finding further suggests that the selectivity of Smurf1 and Smurf2

between RhoA and Rap1, which has been noted in other cell models, is conserved in ECs. Smurf2 is highly similar to Smurf1 and contains a HECT domain. CCM2 and Smurf1 interact selectively through this HECT domain [5]. We found that Smurf2 was able to co-immunoprecipitate CCM2 using overexpressed proteins (Fig 4.7 D). Stable knock down ECs for CCM-1, -2, and -3 increased Rap1 protein levels, which further links Rap1, Smurf2, and the CCM proteins in the same pathway (Fig 4.7 E). These data indicate a novel interaction between CCM2 and Smurf2, which may function to regulate the overall stability of Rap1 protein. Furthermore, deregulated Smurf2 activity, likely due to the loss of CCM2, aberrantly affects tube formation ability.

Discussion

In this study, we have demonstrated that three different E3 ubiquitin ligases function to regulate RhoA and Rap1 in ECs. The phenotypes associated with loss of either Smurf1, Smurf2, or the cullin family of ligases are highly related. Smurf1 function is the most elucidated and binds CCM2 directly and not CCM1 or CCM3; CCM2 recruits it to membrane at areas of active cellular protrusions. CCM1 and CCM3 do not bind directly to Smurf1, yet they yield virtually the same phenotypes and demonstrate deregulated active RhoA ubiquitination. Thus, we posit that the integrated functions of CCM1, -2, -3 as a ternary complex are required for the proper degradation of RhoA in ECs. CCM2 functions to recruit Smurf1 and CCM1 to the membrane where CCM1 has been shown to selectively bind to the VEcadherin junction protein [62, 209]. CCM1 is required for the proper localization of PKCζ at

the membrane, which is required for Smurf1 ubiquitination of RhoA at sites of active cellular protrusions [76, 209]. These functions of CCM1 may shed light into how the loss of CCM1 is identical to the loss of CCM2. Furthermore, CCM3 interacts with several of the sterile kinases, including Mst3 and Mst4, which phosphorylated ERM proteins directly [205]. This regulation of phosphorylation activity by CCM3 could provide a link for CCM3 and Smurf1 regulation. We observe that increased adenylyl cyclase stimulation results in immediate GTP bound RhoA turn over followed by total RhoA. Furthermore, the CCM3 interactors Mst3 and Mst4 phosphorylate Smurf1 in vitro. More study is needed to determine if adenylyl cyclase regulates RhoA phosphorylation and turn over and how relevant our in vitro phosphorylation data is in Smurf1 substrate selection in ECs. While highly speculative at this point, the ability for CCM1 to regulate PKCζ membrane localization and a putative function for CCM3 protein mediated Smurf1 phosphorylation substrate switching could explain how CCM1 and CCM3 function as a complex with CCM2 in regulating Smurf1 function.

The cullin E3 ligases are instrumental regulators of RhoA degradation. We show for the first time that this system is conserved in endothelial cells with phenotypes that mimic the loss of any of the CCM proteins. We have further shown the cullin ligases preferentially regulate total RhoA levels where as Smurf1 degrades the active form of RhoA. Furthermore, this effect seems to be mediated through the cullin 3 ligase as has been previously established in other cell systems. We have been unsuccessful in demonstrating a binding interaction between the CCM proteins

and cullin 3 (data not shown). Therefore, these phenotypes need a further link to the CCM proteins.

Among many targets, the Smurf2 E3 ligase degrades Rap1 [111]. Previous studies have demonstrated the importance of proper Rap1 function in maintaining junction stability with CCM1 central to its regulation in ECs [62, 95]. We show that loss of Smurf2 decreases the tube forming ability of ECs, which phenocopies loss of the CCM1, -2, or -3. This effect is likely not due to RhoA/ROCK signaling as CCM1, -2, and -3 loss increased Rap1 protein but not RhoA, and no rescue was achieved with ROCK inhibition. We cannot exclude the possibility that the tube formation defects are due to the deregulation of other Smurf2 targets without a proper rescue experiment. In addition, the effects on Rap1 turnover need to be further examined to determine whether active or total Rap1 is being affected in a manner similar to RhoA regulation. We establish a novel interaction between CCM2 and Smurf2, suggesting that the CCM protein complex may be involved in regulating Smurf2 function. The interaction mapping needs to be determined if this interaction occurs through a PTB and HECT domain dependent fashion. Rap1 and RhoA have opposing functions on EC junctions; therefore, it is interesting that both are increased following the loss of CCM proteins. This dual increase could differ depending on the activation status of the endothelium in states of active angiogenesis vs. endothelial quiescence. Thus, further spatial/temporal study is needed to elucidate when the CCM proteins degrade RhoA compared to Rap1 during angiogenesis and if this correlates to when the CCM complex is bound to either Smurf1 or Smurf2.

As the small GTPase field has progressed over the past two decades, the role of small GTPase degradation has become more and more relevant to many cellular processes. Our data suggest that selective RhoA degradation coordinated by the CCM proteins is an important portion of RhoA regulation in ECs. We have provided novel data, which suggests that the cullin E3 ubiquitin ligases and Smurf2 function to regulate total RhoA and Rap1 stability down stream of the CCM proteins, respectively. Thus, deregulated degradation of small GTPase proteins is at least one potential molecular mechanism driving CCM phenotypes.

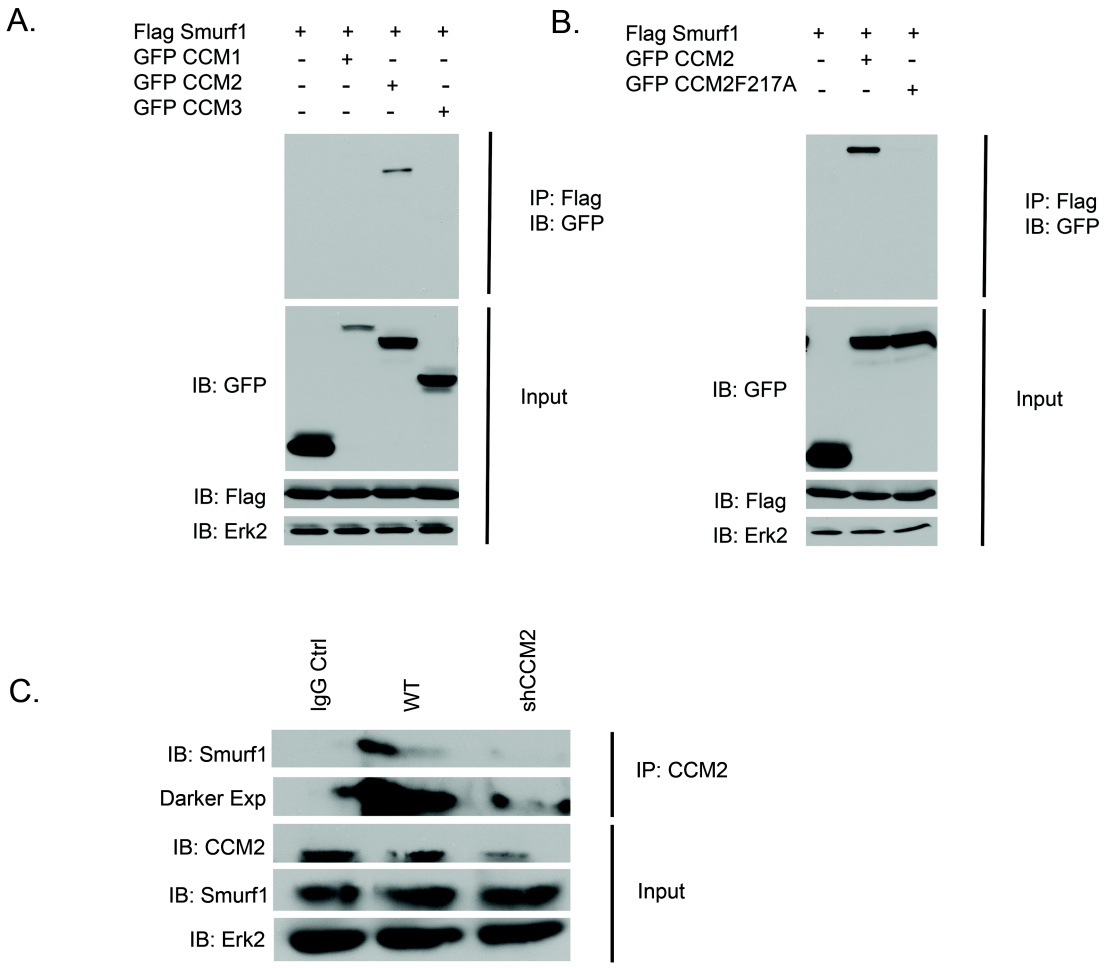

Figure 4.0: Smurf1 binds to CCM2 and not CCM1 or CCM3. A). HEK293T cells were transfected for 12 hours with Flag Smurf1 and GFP tagged CCM1, -2, or -3. Flag immunoprecipitants were then blotted with a GFP antibody, demonstrating that Smurf1 interacts with CCM2 and not CCM1 or CCM3 (IP top panel; Input lower panel). **B).** HEK293T cells were transfected with Flag Smurf1 or GFP tagged CCM2 WT or CCM2F217A. Flag immunoprecipitants were blotted with a GFP antibody, demonstrating CCM2 but not the F217A PTB domain mutant binds to Smurf1 (IP top panel; Input lower panel). **C).** Endogenous Smurf1 was immunoprecipitated from wild type huvec lysates or shCCM2 lysates, demonstrating that CCM2 interacts with Smurf1 endogenously.

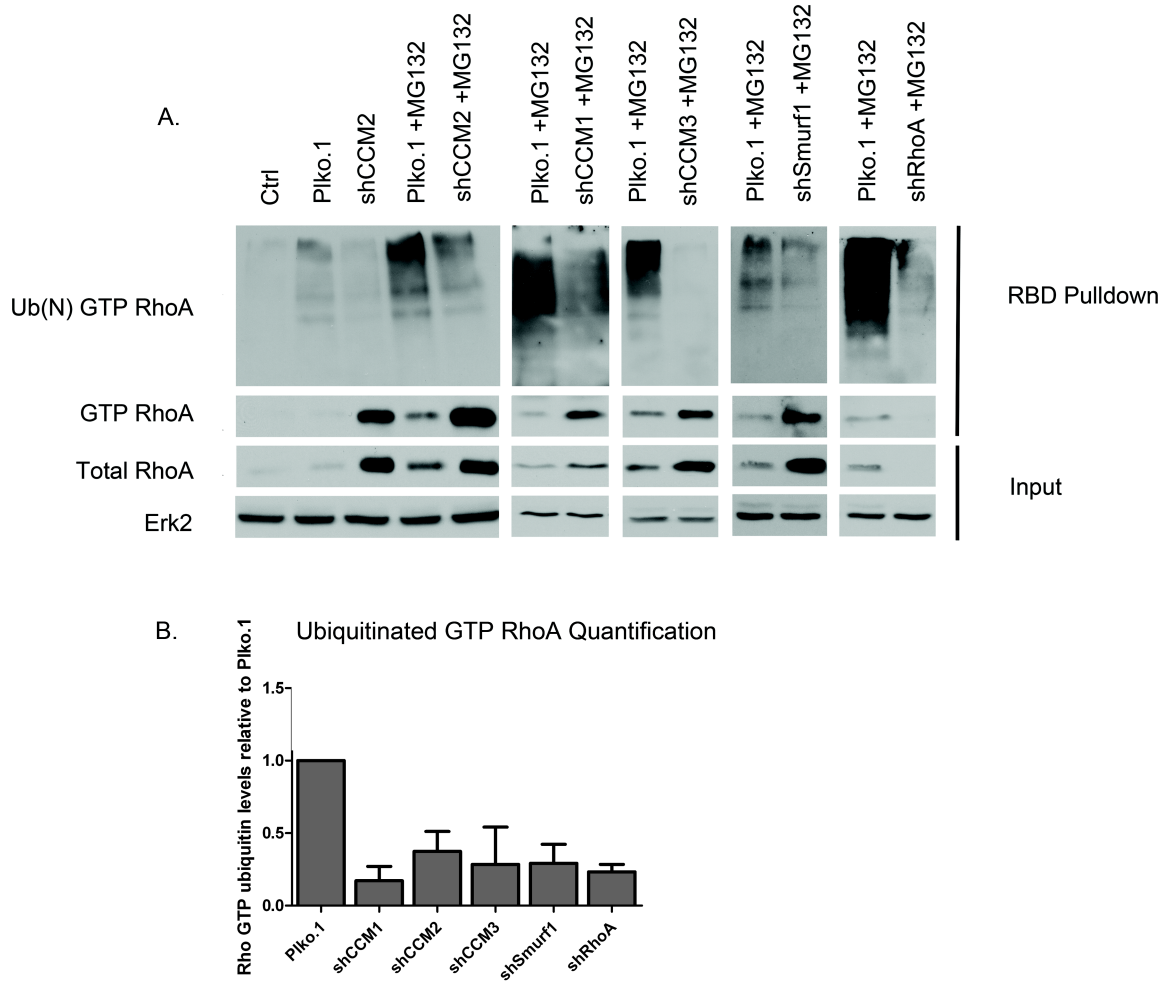

Figure 4.1: Ubiquitinated GTP bound RhoA is decreased after CCM protein loss. A). Stable shRNA knock down CCM1, -2, -3, Smurf1, and RhoA in MEECs were generated and treated with or without 20 μM MG132 for four hours as indicated. The RBD from Rhotekin was used to pull down GTP bound RhoA and a specific ubiquitin antibody was then used to probe for ubiquitinated RhoA. **B).** Quantification of ubiquitinated GTP RhoA. All knock down lines demonstrated a large decrease in ubiquitinated GTP bound RhoA. Quantification was normalized to GTP bound RhoA and Erk2; error bars represent at least 3 independent biological experiments.

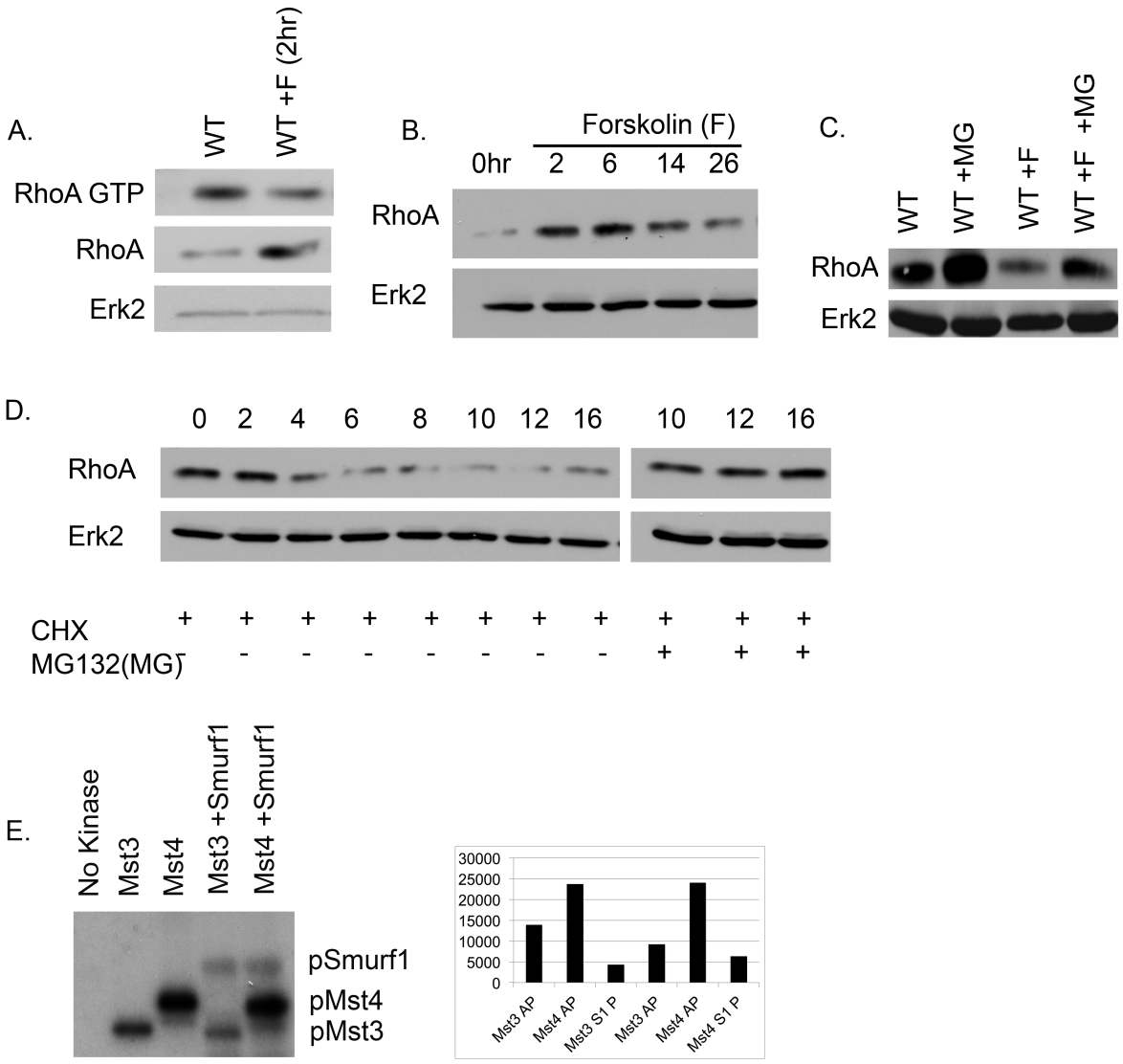

Figure 4.2: Adenylyl cyclase activation by Forskolin promotes RhoA degradation A). Forskolin treatment of Huvecs decreases RhoA GTP levels after two hours and increases total RhoA levels. **B).** Total RhoA protein levels progressively decrease following Forskolin treatment but remain higher than baseline after 26 hours. **C).** Total RhoA protein levels decrease below baseline levels after 36 hours of Forskolin treatment, and this decrease is rescued by the proteasome inhibitor MG132. **D).** The half life of RhoA is approximately 6-8 hours after protein translation inhibition by CHX addition, which is rescued with MG132 proteasome inhibition. **E).** The Mst3 and Mst4 kinases are autophosphorylated and phosphorylated Smurf1, autoradiographic densitometry quantification is shown in the right panel. Forskolin was added at 10 μM and MG132 was added at 20 μM for the indicated times.

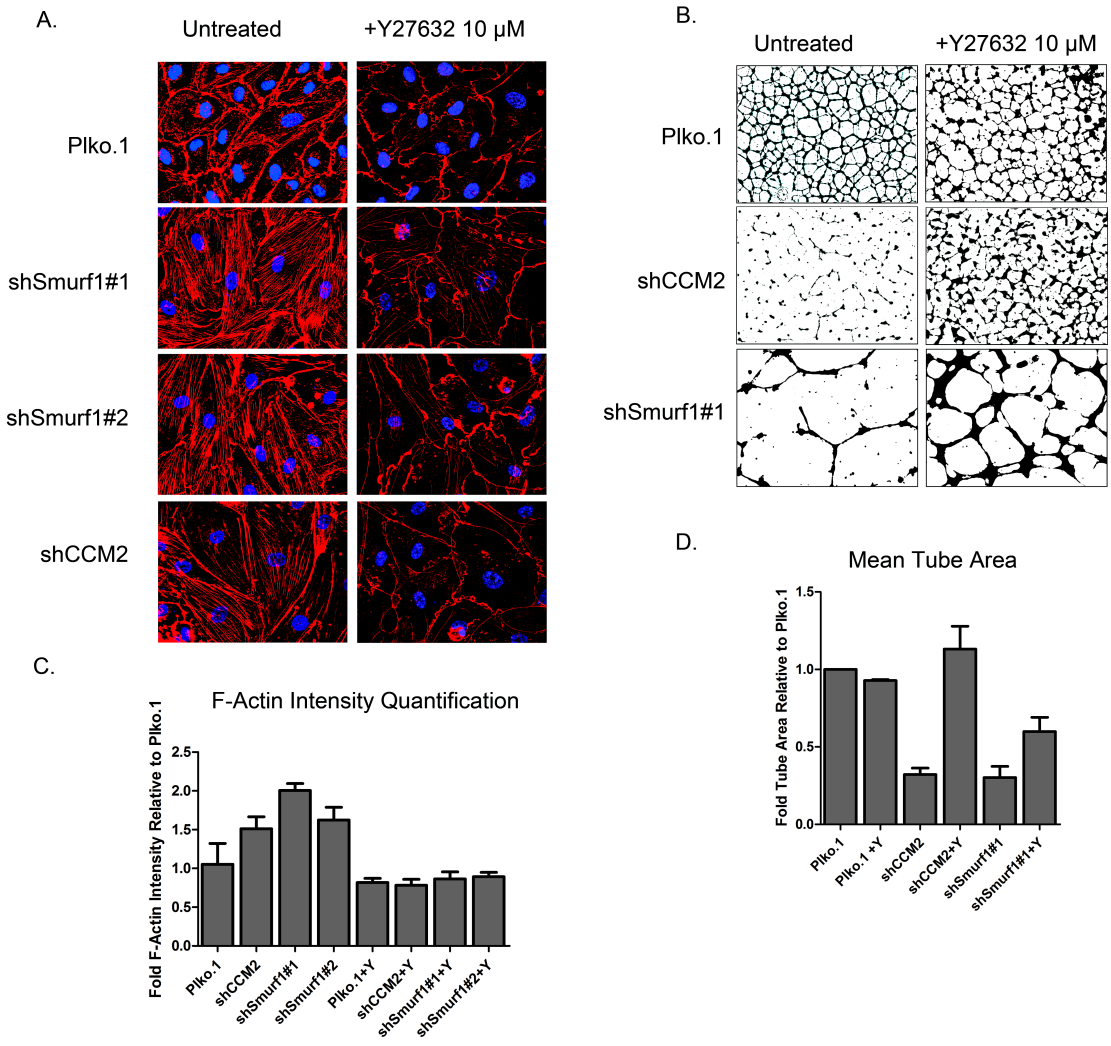

Figure 4.3: Loss of Smurf1 increases stress fiber formation and decreases tube forming ability of Huvecs. A). Huvecs were grown to confluency with knock down of either Smurf1 or CCM2 and were treated with or without ROCK inhibitor Y-27632 (10 μM). Actin was stained with phalloidin, demonstrating that stress fibers were increased with two independent shRNAs for Smurf1 and CCM2, which was rescued with ROCK inhibition. **B).** Smurf1 and CCM2 knock down huvecs were seeded in a Matrigel tube formation assay. WT cells demonstrated robust tube forming ability, where as loss of Smurf1 or CCM2 strongly disrupted tube formation, which was rescuable with ROCK inhibition. **C and D).** Quantifications of stress fibers and tube formation assays; error bars represent at least two independent experiments.

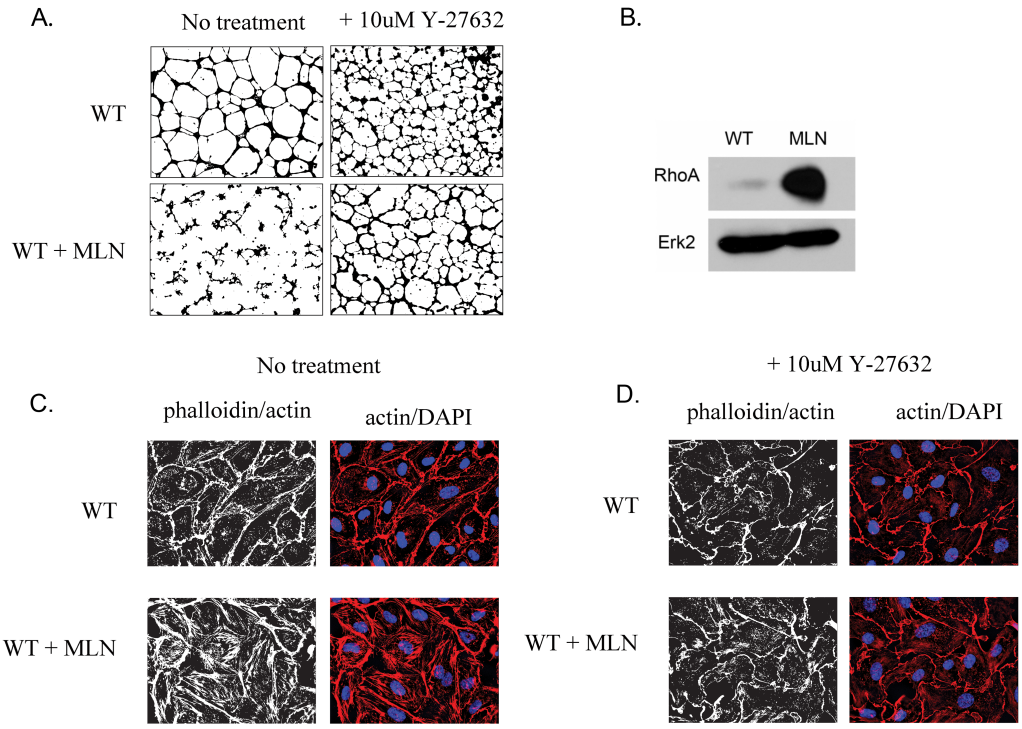

Figure 4.4: Cullin inhibitor MLN 4924 increases stress fibers, decreases tube formation, and increases RhoA protein. A). Tube formation was strongly inhibited in a ROCK dependent fashion after Huvecs were treated with 10 μM MLN 4924 overnight. **B).** RhoA protein levels, assessed by immunoblotting, were substantially increased in huvecs after treatment with 10 μM MLN 4924 overnight. **C and D).** ROCK dependent actin stress fibers were increased in Huvecs treated with 10 μM MLN 4924 overnight.

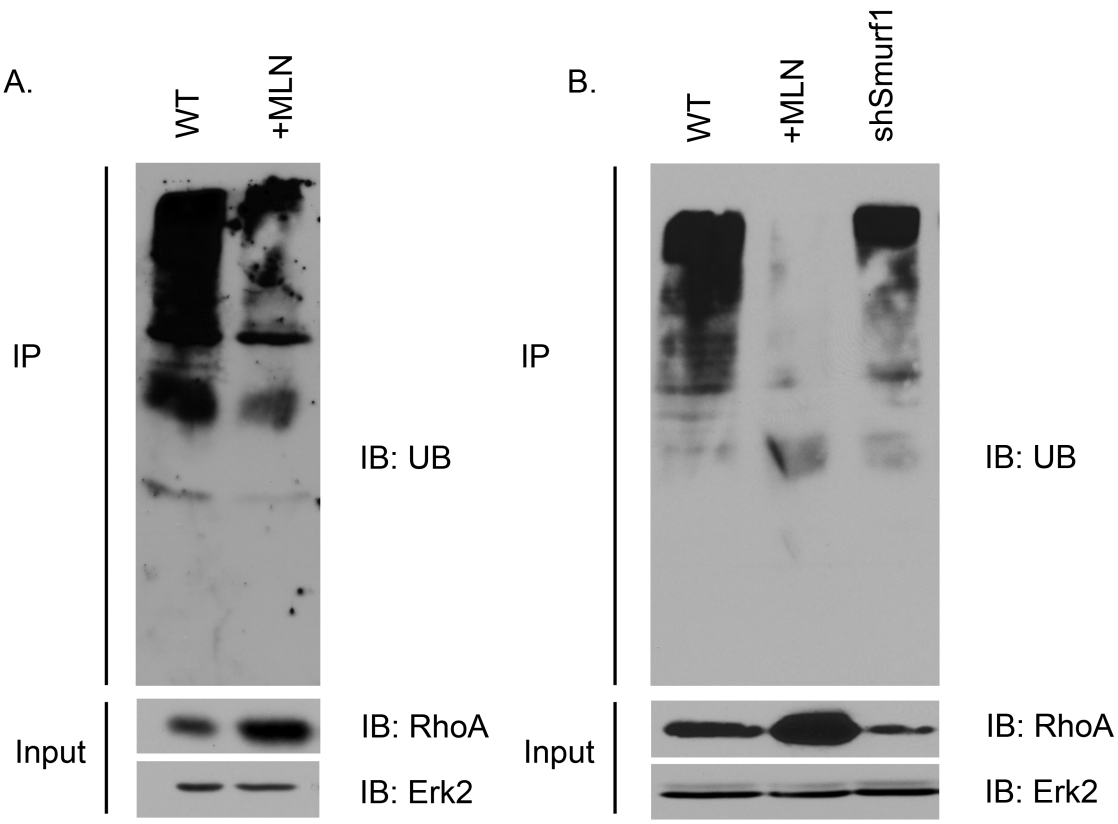

Figure 4.5: MLN 4924 treatment decreases the ubiquitination of total RhoA protein. A). The total RhoA ubiquitin ladder is decreased in huvec cells treated with 10 μM MLN 4924 for 24 hours . **B).** Smurf1 knock down huvecs have a less pronounced decrease in total RhoA ubiquitinated protein levels when compared to MLN 4924 treated huvecs. Cells were treated with MG132 for 4 hours at 20 μM to stabilize poly ubiquitinated proteins.

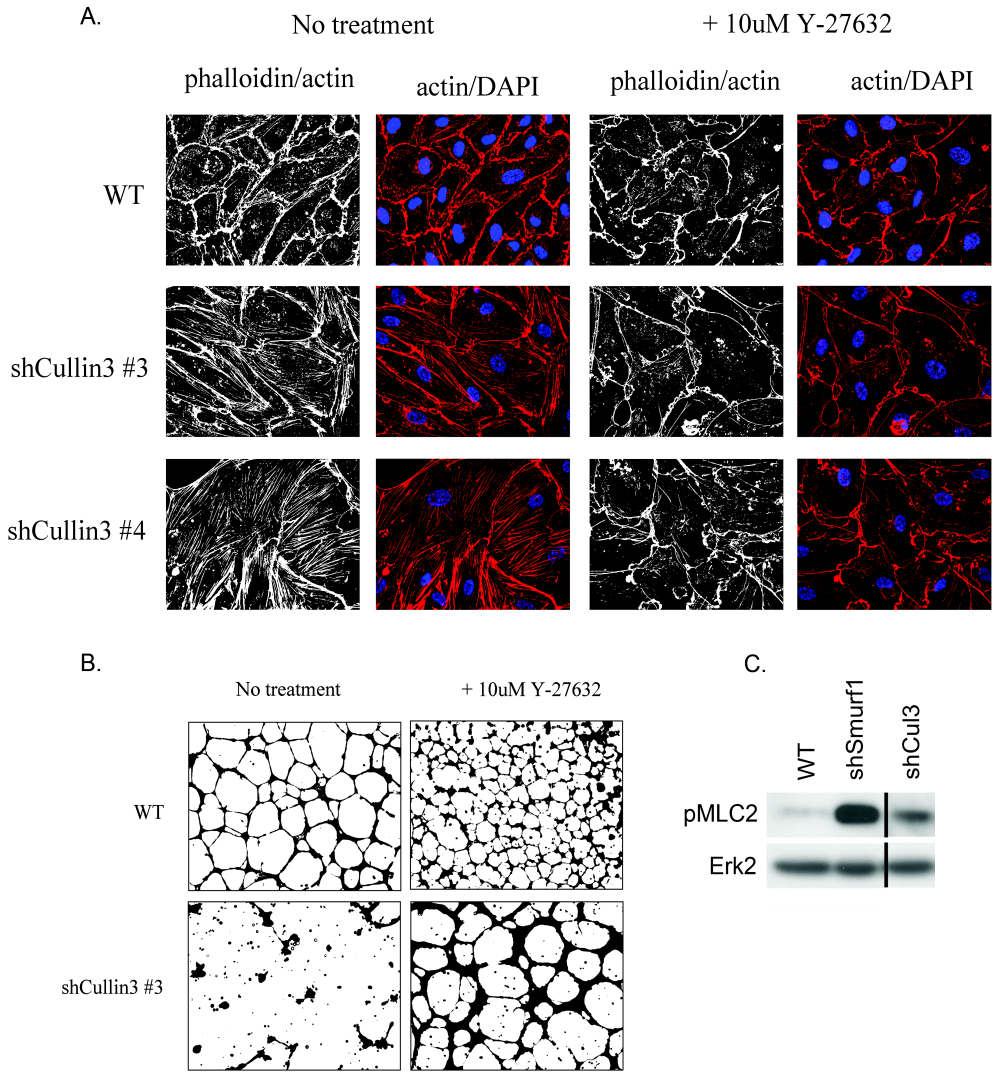

Figure 4.6: Stable cullin 3 knock down increases stress fibers and decreases tube forming ability. A). Tube formation was strongly inhibited in a ROCK dependent fashion after cullin 3 was stably knocked down in Huvecs. **B).** Actin stress fibers were increased in a ROCK dependent fashion after cullin 3 was stably knocked down in Huvecs. **C).** pMLC2 levels were increased after cullin 3 knock down but to a lesser extend than in Smurf1 stable knock down Huvecs.

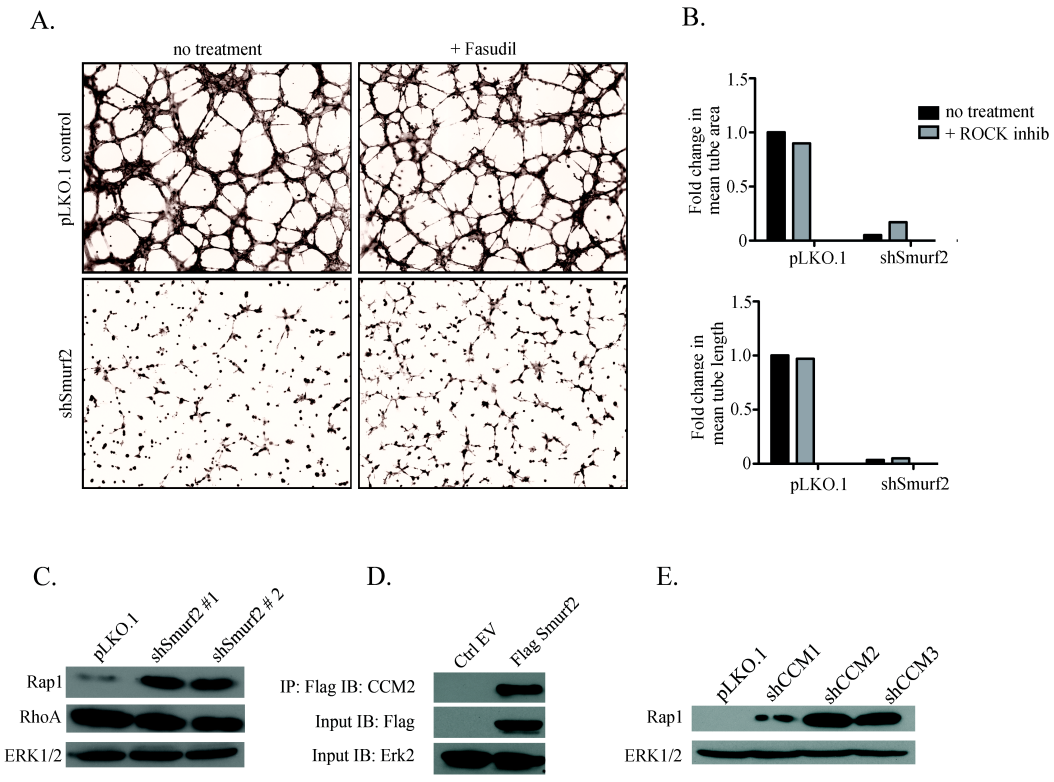

Figure 4.7: Smurf2 regulates the turn over of Rap1. A). Tube formation was strongly inhibited in Huvecs following stable knock down of Smurf2. **B).** Quantification of tube area and length demonstrates that ROCK inhibition does not rescue Smurf2 mediated tube formation defects. **C).** Two independent Smurf2 shRNAs increase Rap1 protein levels but not RhoA in Huvecs. **D).** Flag Smurf2 is able to co-immunoprecipitate CCM2. **E).** Loss of either CCM1, -2, or -3 in Huvecs increases Rap1 protein levels.

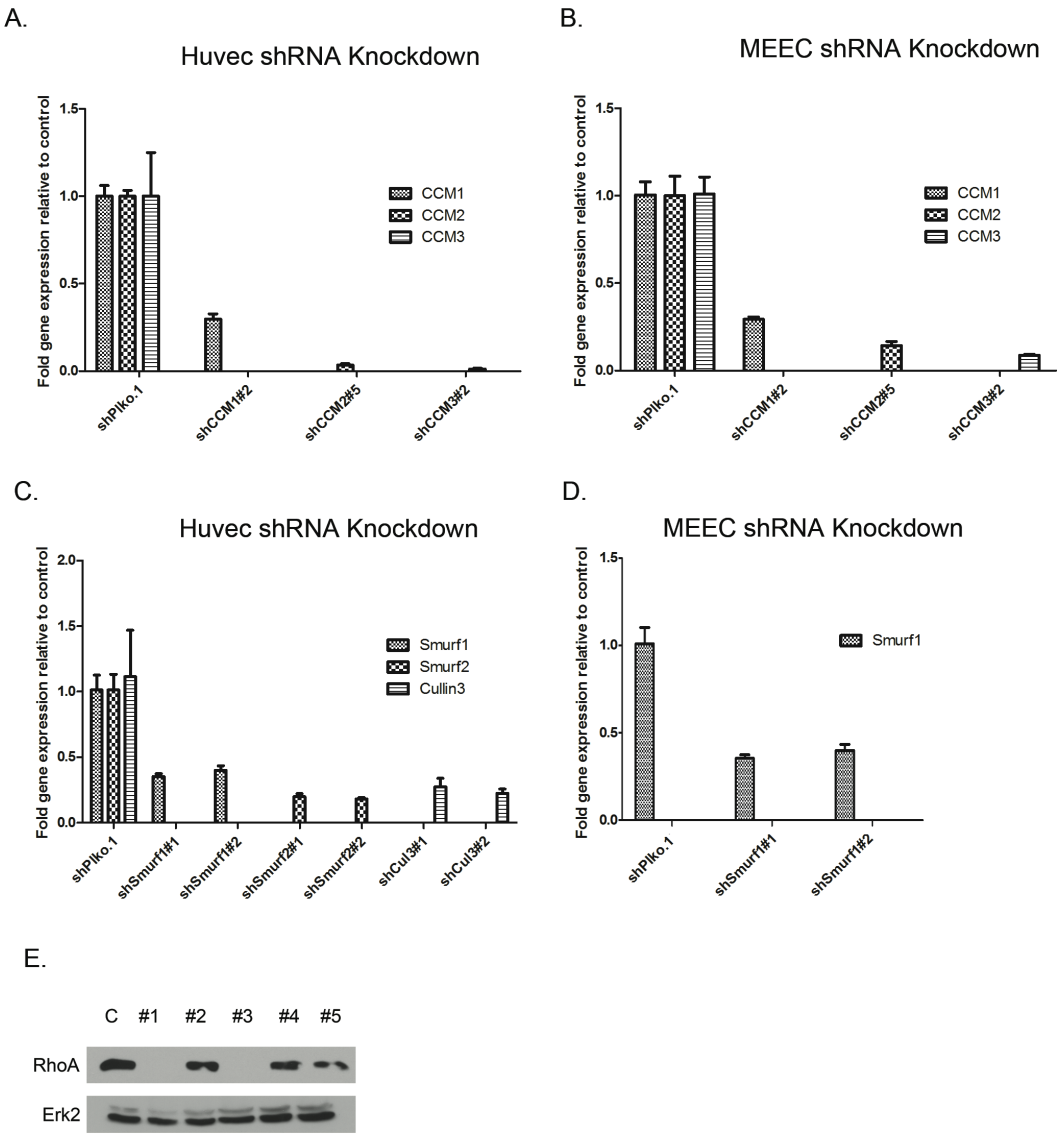

Figure 4.8: qRT-PCR and western blotting analysis of knock down lines used for chapter IV. A). Stable knock down of CCM1, -2, and -3 in Huvecs. **B).** Stable knock down of CCM1, -2, and -3 in MEECs. **C).** Stable knock down of Smurf1, Smurf2, and Cullin3 in Huvecs. **D).** Stable knock down of Smurf1 in MEECs. **E).** Knock of RhoA in MEECs

V. Induced pluripotent stem cells as a new patient specific model for CCM.

Introduction

Currently, the only models available for the study of CCM are various mouse and human endothelial cell lines and mouse genetic models. These model systems have led to the current understanding of signaling mechanisms that underlie CCM. Healthy cell lines are robust in vitro tools for investigation into the signaling mechanisms underlying CCM, and siRNA technology allows for the knock down of each CCM gene followed by observations in cell behavior. Yet these models have not always been consistent. For example, several studies have shown that loss of CCM3 leads to increased RhoA signaling and actin stress fiber formation; whereas another study challenged these findings showing that knock down of CCM3 in human cells had little to no effect on stress fiber formation or pMLC2 levels [4, 6, 87]. Furthermore, several studies have been inconclusive into the effects of CCM1, -2, and -3 in aspects of cellular proliferation and endothelial sprouting in fibrin bead assays [4, 8, 45, 210].

These differences could be a side effect of the type of siRNA approach used to knock down *ccm* gene expression. Transient siRNA efficiently knocks down gene expression in a subset of cells, which are transfected but wanes there after. In contrast, stable shRNA integrates into the host cell genome in most of the plated cells and can knock down genes permanently. Most studies have assessed knock

down through qRT-PCR, which doesn't assess whether residual CCM protein is available after CCM mRNA loss. Thus, the underlying signaling differences may be more sensitive to knock down efficiency and residual protein than broad endothelial cell phenotypic defects. Furthermore, every siRNA or shRNA has potential off target effects to proteins with similar seed sequences. Therefore, some of the phenotypic differences could be attributable to unrelated proteins being targeted by the siRNA. In addition to the problems with siRNA technology, cell culture lines have intrinsic differences. These arise from the many different endothelial cell lines that have been used in CCM studies. The most broadly used in the context of CCM studies are Huvecs. These cells have general shared characteristics with all other endothelial cells; however, they are derived from a tissue, which does not form CCM lesions and may not necessarily recapitulate CCM signaling. More physiologically relevant endothelial cell types are human brain microvascular endothelial cells (Hbmvecs). These cells are from brain tissue where CCM lesions form and likely represent a more relevant cell type to study CCM signaling. In lieu of these suppositions, a recent study found that endothelial cells isolated from CCM patient lesions have enhanced migration, where as CCM knock down Huvecs or Hbmvecs do not [211]. Cell culture practice and passage number can exasperate these differences. Thus, a complex understanding of CCM requires a more rigorous approach that entails the use of diseased endothelial cells from patients.

Mouse models have become a powerful tool for understanding lesion formation in CCM. These models utilize genetic knock out approaches and are not hampered by partial knock down or siRNA off target effects. Developmentally, CCM

protein knock out in the mouse is embryonic lethal due to improper embryonic heart development and vascular patterning [40, 41]. However, unlike human familial carriers, CCM protein heterozygous mouse models never form lesions [8]. Adult mouse lesions could only by generated by breeding CCM heterozygous mice into a p53 null or MSH2 null background, which have increased genomic instability. These mice were powerful tools that potentially proved the loss of heterozygosity hypothesis, allowed for the study of lesion generation, and gave an in vivo evaluation of Rho kinase inhibitor treatments for CCM [8]. However, these second generation models are not representative of CCM patient genomic backgrounds as CCM patients do not have increased rates of tumor formation due to the loss of p53 or DNA repair machinery. Nonetheless, these observations of genomic instability and CCM protein loss have raised important questions as to the heterogeneity of CCM lesion formation in common pedigrees and whether patient genomic background or stability within ECs play an important role in CCM lesions.

Therefore, studying diseased cells from patients is paramount because it is possible to determine if the phenotypes established in heterologous human and mouse cell culture systems are valid. This research strategy will allow for a more confident approach in testing therapeutics and designing CCM clinical trials. Symptomatic CCM lesions typically occur in the brain in areas that are difficult to obtain good biopsies for the extraction of cell culture. To date only one study has been undertaken to isolate CCM lesion endothelial cells [174]. The phenotypic data generated from this study was very limited because of low cell numbers, slow cellular growth rates, and purity. The iPS field has taken disease modeling to task

with substantial progress in numerous rare and hard to study diseases. iPS cells generated from already sequenced CCM patients would allow for the generation of a library of diseased cells encompassing the genomic background of human patients. iPS cells are immortal and have been cultured continuously for a year [212]. Thus, it is thought that they are like hESCs and are an immortal and karyotypically normal cell type due to the expression of telomerase. This characteristic of iPS cells will preserve valuable patient cells for indefinite periods of time and study.

The science behind generating iPS cells has progressed rapidly and is still burgeoning. First generation iPS cells comprising approximately 80% of all published iPS lines were generated by retroviral or lentiviral ectopic expression of reprogramming cocktails including Oct4, Sox2, Klf4 (or Nanog) and a proliferative driver such as cMyc (or SV40) [146]. Each of these genes have been associated with teratocarcinoma growth, cell transformation and genome instability. Second-generation methodologies for generating iPS cells have ameliorated some of the problems with ectopic retroviral integration and have increased the fidelity and genomic stability of the resulting iPS cells. These methods utilize non-integrating approaches, such as RNA transfection, episomal vector electroporation, and sendai virus [146]. These cells are more similar to hESC cells with the only drawback being a lower efficiency of generation. These approaches only transiently express reprogramming factors and the cells are at a lower risk for further transformation with time in culture. Therefore, the generation of CCM patient iPS cells will benefit from the newer methods for iPS cell generation.

iPS cells can be readily differentiated into all major cell lineages including endothelial cells, which are thought to be the cell type most affected by genetic loss of the CCM proteins. iPS cells spontaneously differentiate upon the removal of basic Fibroblast growth factor (bFGF) from the cell culture media into cells representing all three germ layers [213]. Typically, differentiation is initiated by generating embryoid bodies (EBs). EBs are non-adherent spherical structures, which stochastically differentiate into cells of all three developmental germ layers. Appropriate inducing cytokines can be added to direct cells within these EBs to form specific cell types (Fig 1.2). Endothelial vessel like structures cells were shown to differentiate from hESCs in EBs after 13-15 days [214]. These ECs could form tube-like structures both in EBs imaged by confocal microscopy, on Matrigel, and contribute to the vasculature when tissue scaffolds were implanted into mice. They also expressed selective endothelial specific genes such as Tie2, CD34, CD31, CD144, and could uptake acetylated low-density lipo protein. The hESC derived endothelial cells produced in this manor grew slowly and proved to be unstable and quickly were overrun by a secondary population of fibroblast or smooth muscle like cells [215]. This secondary non-EC population arose either from contaminating cells from the initial purification or from a trans differentiation process.

Directed endothelial differentiation methods were established to eliminate these substantial stability problems. Numerous groups found that addition of the cytokine BMP4 promoted EC differentiation. Seminal work from Gordon Keller's lab further defined the timing and development of hESC hematoendothelial differentiation [216]. Accordingly, they found adding mesoderm inducing signaling

cytokines BMP4 and activin A generated a primitive streak like population of cells that expressed brachyury (T). With further time in culture these cells developed three distinct populations when analyzed by flow cytometry and gated on the expression of the vascular endothelial growth factor receptor 2 (VEGFR2) and c-KIT (KDR^{++}c-KIT^{+}, KDR^{+} c-KIT^{-}, $KDR^{-}cKIT^{+}$). Cardiac progenitors were found to be present in the KDR^{+} c-KIT^{-} population and the hemangioblasts, precursor cells that can form blood cells or endothelial cells were present in the KDR^{++}c-KIT^{+} population. Further stimulation with VEGF and FGF promoted this hemangioblast population into the endothelium, where as blocking WNT signaling pushed the KDR^{+} c-KIT^{-} population into cardiomyocytes. While this work established a mechanism for enriching in endothelial progenitors, the problems with EC stability remained. This issue was recently solved through small molecule inhibition of TGF-β signaling [215]. The expression of the endothelial specific markers CD144 and CD31 were present after isolation but so was expression of the smooth muscle marker α-SMA. This indicated that purified cells retained plasticity to differentiate into terminal endothelial or smooth muscle cells. TGF-β inhibition significantly blocked this transition and gave rise to a stable and pure population of ECs. There was a seven-fold increase in the number of end point ECs when compared to the number of hESCs used to initiate the differentiation process.

It is unlikely that CCM patient iPS cells will ever be used for regenerative or corrective cell transplantation due to the nature of disease development. Most applications for regenerative medicine would be those for which cellular replacement would have a major effect such as diseases, which are due to a defective gene that

can be corrected through genome editing technologies or neurodegenerative diseases, which could benefit from replacement neurons. The cell(s) of origin for CCM lesions is unknown; and therefore, it is impossible to replenish CCM proteins to all of the brain microvascular endothelial cells within a patient. While the therapeutic treatment of CCM patients may not be an option with iPS cells, their in vitro theranostics potential is high. It is likely that a CCM patient library could help answer some of the outstanding questions in the CCM field. First and foremost it will be important to establish whether patient cells have the same phenotype as observed in other CCM models. Following this question it will become important to examine how the genetic penetrance of CCM patients affects disease onset, progression, and severity. iPS disease modeling could shed light into this area. For example, the phenotypic severity of LQT2 patient derived iPS cells demonstrated milder phenotypes when obtained from asymptomatic patients when compared to severely symptomatic patients [217]. Most of the mouse models have indicated that homozygous loss of CCM proteins is required for lesion generation; however, at least one study has shown that heterozygous mice for CCM1 and CCM2 demonstrated increased vascular leak [7]. Although it is widely thought that LOH is required for CCM lesion generation, it will be important to confirm this hypothesis in patient cells. Most studies have concluded that CCM proteins act in an endothelial cell autonomous fashion; however, it is possible that there is a neural cell autonomous effects according to data obtained from mice lacking CCM3 in astrocytes [44]. Answering these basic signaling biological questions will be important for rationally designing therapeutics. Small molecule drug discovery is an

additional unexploited avenue in the treatment of CCM. It will be possible to differentiate ECs from patient iPS cells and use a small molecule library to identify compounds that reverse CCM relevant phenotypes, such as stress fiber formation, tight junction marker expression, hyper permeability, tube formation, or EC migration. Once a potential screened therapeutic or rationally designed therapeutic is tested for efficacy in reversing in vitro phenotypes, it will be possible to differentiate patient cells to hepatocytes and cardiomyocytes for in vitro toxicity testing of identified compounds. Thus, CCM specific iPS cells represent a unique and novel way to address many outstanding questions in CCM biology with the eventual hope of developing new CCM patient specific therapeutics.

This study investigated the potential for establishing a hiPS model of CCM. We show that hESCs remain pluripotent following shRNA mediated knock down of CCM1, -2, or -3 and can differentiate to endothelial cells. We further show that endothelial progenitor cell derived ECs can model CCM, and be successfully reprogrammed to a pluripotent state. These novel iPS cells can then be re-differentiated to the endothelium. Thus, our data suggests that CCM can be modeled using human pluripotent stem cells and warrants patient recruitment for patient cell reprogramming.

Results:

hESCs differentiate to the endothelium and can be used to model CCM phenotypes.

hESCs are the gold standard for which all iPS cells are measured. Thus, we elected to use hESCs to establish a method for differentiating pluripotent stem cells

to ECs and to determine whether pluripotent derived ECs recapitulate in vitro CCM phenotypes observed in heterologous EC cell types. The simplest method for deriving endothelial cells was published following the random differentiation of EBs, which generated round 1-2% $CD31^+$ cells, which could be further isolated by flourescence activated cell sorting (FACS) [214]. Accordingly, we generated EBs from H9 hESCs by scoring colonies into squares and gently lifting each section. After 24 hours, characteristically round EBs formed, and bFGF was removed to promote random non-directed differentiation (Fig 5.0 A). EBs were allowed to differentiate for approximately 15 days, a time point where robust endothelial structures have been reported to form [214]. In contrast this previous reported differentiation result for H9 hESCs, we observed very little EC differentiation as reported by CD31 marker expression (Fig 5.0 B). When these cells were isolated they failed to grow enough for validation studies. These differences could be due to different methodologies for growing the hESCs or the health of the resultant EBs. This previously described method used LIF to grow hESCs, which is required for mESCs and has subsequently been shown to be dispensable for the maintenance of hESCs, and thus not included in our growth conditions. Furthermore, we were unable to maintain EB cultures past 18 days due to senescence and cell death of the EBs without addition of differentiation inducing cytokines, and similar results were obtained for the H7 hESC line (data not shown).

Non-directed differentiation was ineffective for two hESC lines, which have been reported to differentiate to ECs. Therefore, we next examined whether hESCs would differentiate to ECs under a directed differentiation method. A protocol was

recently developed, which initiates differentiation through transient mesoderm induction followed by endothelial specification and TGF-β inhibition [215, 216]. This differentiation method utilizes short-term EB growth followed by adherent plating conditions and EC isolation after 14 days (Fig 5.1 A). The mesodermal inducers BMP4 and activin A were added sequentially and were left on cells until day 4. Accordingly, addition of BMP4 increased expression of the mesodermal marker brachyury by day 3, where it rapidly decreased suggesting that these cells were specified into mesodermal lineages (Fig 5.1 B). An increase in CD34, VEGFR2, cKIT, and VEcadherin protein levels were noticeable in a subset of differentiating cells by day 3, indicating that multi-potent vascular progenitors were forming (Fig 5.1 C). At this point EBs were plated on adherent conditions and the vascular specification cytokine VEGF was added to the cultures along with BMP4 and bFGF. At day 7, the TGF-β inhibitor SB431542 was added to the cultures, and a noticeable increase in CD31 and VEcadherin (CDH5) mRNA levels were detected (Fig 5.1 B). VEcadherin protein expression was detected without CD31 protein detected suggesting that the cells were still in an immature state (Fig 5.1 C). CD31 protein expression followed after approximately 14 days (Fig 5.1 D). Putative ECs were isolated by FACs or through CD31 magnetic microbeads to at least 92% purity (Fig 5.1 D). These cells were able to grow in monolayers with VEcadherin expression at cell junctions, up take acetylated low density lipo protein, and form tube-like structures when plated on Matrigel demonstrating that this method of directed differentiation generates bone fide hESCs derived ECs (5.1 E).

Following isolation, ECs maintained endothelial characteristics but grew slowly. Therefore, we ascertained whether a better media could be formulated for the growth and expansion of hESC derived ECs. A major driver of proliferation in ECs is the VEGF cytokine. We titrated VEGF from two separate companies to determine if the slow growth kinetics of hESC derived ECs is due to low concentrations of VEGF. Huvec proliferation was increased in a dose dependent fashion upon VEGF addition (Fig 5.2 A). In contrast, hESC derived ECs remained constant at the maximal 100 ng/mL dose of VEGF from two separate vendors (Fig 5.2 B). This result suggests that hESC ECs are receiving adequate VEGF stimulation and are growing at their maximum growth rate under these conditions. Huvecs rapidly grow in EGM-2 commercial endothelial basal media, which contains EC specific growth factors. Previous studies have suggested that hESC derived ECs proliferate better in EGM-2 media [218, 219]. Therefore, we examined the ability of our hESC derived ECs to proliferate in EGM-2. We thus, grew our hESC derived ECs in EGM-2 media containing TGF-β inhibitor and noted a robust two fold increase in proliferation. However, these ECs rapidly lost endothelial characteristics when grown in EGM-2 with delocalized VEcadherin and loss of tight junctions indicative of transition to a more mesenchymal phenotype (Fig 5.2 C). We obtained similar results by removing serum from EGM-2 and replacing with knock out serum. While these growth conditions are significantly slower in hESC ECs, we empirically concluded that our vascular specification media supplemented with TGF- β inhibitor was the optimal growth media for the hESC derived ECs for future experimentation.

Following this protocol we have been able to consistently isolate hESC derived endothelial cells. Therefore, we sought to determine if differentiation of hESCs lacking CCM1, -2, or -3 retained the ability to differentiate into endothelial cells. Accordingly, H7 hESCs remained pluripotent with loss of CCM1, -2, or -3 by expression of the pluripotency marker Oct4 (Fig 5.3 A). These cells differentiated into $CD31^{+}VEcadherin^{+}$ endothelial cells after 14 days (Fig 5.3 B). Over multiple experiments, the percentage of double positive cells was similar between control, CCM1, -2, and -3. (Fig 5.3 C). Interestingly, during EB differentiation random sprouting of endothelial tube-like structures appeared in control cells but not in CCM2 deficient differentiating EBs when cultured on a thick layer of Matrigel (Fig 5.4 A-C). These tube-like structures grew down into the Matrigel layer. To better quantify potential tube formation defects, control, CCM1, -2, and -3 deficient ECs were isolated from differentiating H7 cultures. After a transient expansion period, these cells were plated on Matrigel to assess endothelial specific tube formation differences in control and CCM deficient cells. Control cells formed tube-like structures that had many nodes and branch points. In contrast, loss of CCM1, -2, or -3 resulted in fragile tubes, which had fewer branch points and connections. Importantly, the defects in tube formation could be rescued with small molecule inhibition of the RhoA effector ROCK by either Y-27632, suggesting that RhoA signaling is defective in these ECs (Fig 5.5 A). This result is consistent with results obtained in heterologous cell culture systems from multiple laboratories. Thus, H7 derived ECs display phenotypic similarities with other endothelial cells lacking CCM proteins. Therefore, we sought to further determine whether these effects were

through deregulated RhoA signaling and the actin cytoskeleton. Accordingly, we detected an increase in total RhoA protein concomitant with an increase in phosphorylated cofilin (Fig 5.5 B). Therefore, H7 derived ECs demonstrate elevated RhoA and a stabilized actin cytoskeleton.

Isolation and characterization of endothelial progenitor derived endothelial cells as a model for CCM.

These data suggest that pluripotent stem cells can be utilized to model CCM. Therefore, we decided to generate novel iPS cells generated from the endothelium that can model the CCM phenotype. There is a growing body of evidence, which suggests that the somatic cell type of choice can influence the differentiation characteristics of the reprogrammed iPS cell [147, 169, 220-222]. These differences are attributable to an epigenetic memory effect. Epigenetic memory is residual epigenetic gene expression marks left behind from the somatic cell of origin on the corresponding iPS cells. Typically, these marks are strongest on genes that are important for cell identity or function. Thus, in certain instances, iPS cells have been shown to preferentially differentiate back to the cell of origin over a different non-related cell types. Recently, the generation of iPS cells from endothelial cells has been described [223, 224]. Similar to other epithelial-like cells, these iPS cells appeared much faster than iPS cells derived from mesenchymal cells. This result is likely because there is no requirement for a mesenchymal to epithelial transition [211]. Thus, our decision to utilize endothelial cells for iPS generation was for

increased efficiency of iPS cell generation coupled with the possibility for increased re-differentiation to the endothelium for the study of CCM phenotypes.

Adult vascular cells require invasive surgery or punch biopsy techniques to obtain. However, circulating endothelial progenitor cells (EPCs) have gained traction as a potential adult source of neovascularization and ECs [225, 226]. Circulating EPCs can be obtained from the adult peripheral blood mononuclear cells (PBMC) after a simple non-invasive blood draw followed by ficoll density gradient centrifugation [227, 228]. These PBMCs can be frozen or shipped and retain functionality and viability. Plating PBMCs on collagen IV in the presence of endothelial specific growth factors allows for early and late outgrowth EPCs to appear. Accordingly, proliferative EPC derived endothelial cells (EPC-ECs) arise one to two weeks after plating. They begin as small colonies of cells that we were able to obtain from 80 mL of peripheral blood with a success rate of 70% in healthy blood donors. These EPC-ECs express VEcadherin, CD31, up take acetylated low density lipo protein (Ac-LDL), and generate tube-like structures when plated on Matrigel (Fig 5.6 A-D). We did observe there was a difference in proliferative ability of EPC-ECs with some clones retaining proliferative ability beyond 5-7 passages and others prematurely senescing after 1-2 passages. This broad variability is likely due to the age and number of cell divisions the circulating EPC had underwent in vivo before isolation and expansion in vitro. We next determined if these cells are able to model the CCM phenotype. This information is important because they can be used as a stand-alone model for patient CCM phenotypes but more importantly because it is hypothesized that iPS cells generated from EPC-ECs will likely

redifferentiate to an EC, which is more similar to the original EPC-EC. Following shRNA mediated knock down of CCM-1, -2, or -3, there was a marked decrease in tube-like structure formation rescuable by ROCK inhibition (Fig 5.7 A-C). Furthermore, two different isolations of EPC-ECs from patients demonstrated an increase in total RhoA protein, phospho-cofilin, and pMLC2. These data indicate that EPC-ECs behave in a similar manner to hESC derived ECs, Huvecs, MEECs and bEND.3 endothelial cells and would be an amenable cell type for reprogramming (Fig 5.8)

Generation of iPS cells from EPC derived ECs

Therefore, we began by generating iPS cells from normal EPC-ECs. IPS cells were also generated de novo from Huvecs and MRC5 fibroblasts for comparison. The most efficient method for generating iPS is through the retro viral transduction of Oct4, Sox2, KLF4, and cMyc. Individual PMX retroviral plasmids containing each transgene were transfected and virus was generated in 293T packaging cells. EPC ECs, MRC5 fibroblasts, and Huvecs were all transduced with the same MOI viral titer. Each cell type was infected for 24 hours prior to being seeded on MEF feeder cells. Huvecs and EPC ECs started forming iPS like colonies as early as 6 days after plating on the feeder layer and changing to iPS cell induction media with a much higher number of iPS like colonies (Fig 5.9). This result is in contrast to what was noted in MRC5 fibroblasts, which took much longer at over 20 days. These results are consistent with what has been previously published in Huvecs, which generate iPS cells quicker and at a higher efficiency than MRC5

fibroblasts [223]. Multiple clones from each line were subcloned and characterized for the establishment of successful reprogramming and pluripotency marker expression. Accordingly, iPS clones from EPC-ECs, MRC5 fibroblasts, and Huvecs had high alkaline phosphatase activity, a functional marker for pluripotency (Fig 5.10 A). In addition, the iPS clones from all cells activated the core pluripotency transcriptional network as evidenced by immunoflourescent imaging and qRT-PCR expression of Oct4, Sox2, and Nanog (Fig 5.10 A and B). To rule out that Oct4 and Sox2 expression was due to residual transgene expression, we designed q-RT-PCR primers that were selective for the 5' UTR region of the virus. The resulting expression data showed that transgene expression was high in OSKM infected EPC-ECs but was efficiently silenced in all stable iPS clones (Fig 5.10 C). Retroviral gene silencing is a hallmark of successful reprogramming [159]. Other markers of pluripotency TDGF1 and Nodal were highly expressed; interestingly a higher expression of Nodal was detected in 3 out of 4 EPC-EC iPS clonal lines (Fig 5.10 B). The consequences of this expression difference were not investigated and are unknown. Thus, iPS cells generated from huvecs and EPC-ECs reprogram faster and express pluripotency markers at levels equivalent to hESCs and MRC5 fibroblast derived iPS cells.

We next determined the differentiation potential of our EPC-EC derived iPS cells. In vitro there are two methods for establishing pluripotency: random and directed differentiation of EBs. To establish whether our EPC-EC clones could differentiate into all germ layers, a hallmark of pluripotency, we generated EBs and differentiated the cells in non adherent conditions for 14 days in hESC basal media

without bFGF. EBs were then stained for SMA, AFP, and Nestin (neural progenitor) as well as MAP2 (neuron) markers of the mesoderm, endoderm, and ectoderm respectively (Fig 5.11 A). In a subset of EBs we detected expression of each of these markers, indicating that EPC-EC iPS cells are pluripotent and are capable of in vitro differentiating to each of the three germ layers (Fig 5.11 A). In addition to random EB mediated differentiation, we sought to determine whether our EPC-ECs could be directed to differentiate into different tissues. Utilizing different cytokine inducers, we were able to drive our EPC-EC iPS lines into $Nestin^+$ neural progenitors, $TuJ1^+$ neurons, $GFAP^+$ astrocytes (Fig 5.11 B). Importantly, we were able to generate CDH5/LDL uptake positive ECs (Fig 5.11 C). These results demonstrate that both random and directed differentiation of EPC-EC iPS cells is possible. The most stringent available assay for pluripotency of human iPS cells is teratoma formation. Teratomas are embryonic tumors, which consist of many different body tissues that originate from the three germ layers. Following injection in the flank of Nude mice, teratoma formation occurred after approximately four weeks with 5 out of 6 injected animals forming tumors. Upon histological analysis, each teratoma displayed tissue structures retinal-pigmented epithelium, ciliated enterocytes, and chondrocytes from the ectoderm, endoderm, and mesoderm, respectively (Fig 5.11 D). Thus, these characterizing studies demonstrate that we were able to generate iPS cells from a completely novel cell type (denoted now as epiPS).

We next to investigated the differentiation potential of huvec and epiPS to endothelium and whether the proposed epigenetic memory mechanism promotes the differentiation to endothelial cells. We utilized the same differentiation protocol

as we had established for the differentiation of hESCs to ECs to differentiate the huvec, and epiPS cells to endothelium. Interestingly, we found that the differentiation kinetics of the EC derived iPS cell lines (Huvecs iPS and epiPS) differed from hESCs. There was a greatly enhanced induction of VEcadherin expression that persisted for up to 20 days followed by an increase a progressive and slower increase in CD31 (Fig 5.12). Microbead isolation of epiPS derived ECs showed that these cells express the endothelial specific markers VEcadherin, CD31, and were capable of acetylated LDL uptake (Fig 5.11 C) however, the total number of epiPS-ECs cwas comparable to H7 hESCs. These data suggest that epiPS cells can generate ECs. The epigenetic memory effect is restricted to VEcadherin, which is expressed on other cells other than ECs. Therefore, we observed an epigenetic memory on one endothelial marker but this did not enhance EC derivation from epiPS. Further investigation into the differentiation kinetics of epiPS may yield better EC yields. Perhaps following a similar differentiation kinetic that EPCs follow to generate EPC-ECs will be more applicable to the differentiation of epiPS to the endothelium.

Discussion:

These studies demonstrate that hESC derived ECs can be used for the study of CCM. The cell phenotypes that other groups have observed in heterologous EC systems from both mouse and human are conserved with hESCs. We have also demonstrated that CCM regulates RhoA levels and downstream signaling in hESC derived ECs. hESCs undergo apoptosis when in single cell conditions due to over

activation of the RhoA/ROCK pathway. Our knock down hESC lines were completely healthy and maintained equal growth rates compared to control lines even when split at sparse ratios. These observations were confirmed, as there was no deregulation of RhoA/ROCK signaling in hESCs by phospho-cofilin or pMLC2 immunoblotting. These data demonstrate for the first time that loss of CCM proteins effect angiogenesis and not the endothelial differentiation of human cells, which is consistent with what has been observed from multiple mouse models. Using hESCs has demonstrated that the development of a patient specific iPS cell model is possible, and more broadly, this is the first data that has attempted to model an endothelial specific disease in pluripotent stem cells.

It is important to consider multiple cell types when deriving iPS cells from patients. Fibroblasts and keratinocytes are well proven, but are invasive to obtain. Blood represents a minimally invasive and easily obtained source of cells from which iPS cells can be generated from relatively small amounts. Using this logic, we were able to generate peripheral blood EPC derived ECs. These cells demonstrated robust phenotypes after shRNA knock down of the CCM proteins. More importantly, these cells rapidly generated high quality iPS clones that demonstrate all of the hallmarks of pluripotent hESCs. These epiPS cells are capable of differentiating along the three germ layers and form endothelial cells. Unexpectedly, these cells only retained an epigenetic memory of VEcadherin expression, which is not as specific an endothelial marker as CD31 or Tie2 and did not display any enhanced differentiation kinetics to the endothelium when compared to hESCs. Further work may need to be done to fully demonstrate CCM phenotypes following shRNA knock

down of the CCM proteins in epiPS cells, but these validation studies suggest that EPCs can be utilized to generate iPS cells for the study of CCM. Other peripheral blood cells, including erthyroblasts can be used to obtain iPS cells from as little as 10 mL and are actively being tested in the laboratory. Thus, this study has overall demonstrated the generation of iPS cells from a novel cell source and that making patient specific iPS cells to model CCM is feasible

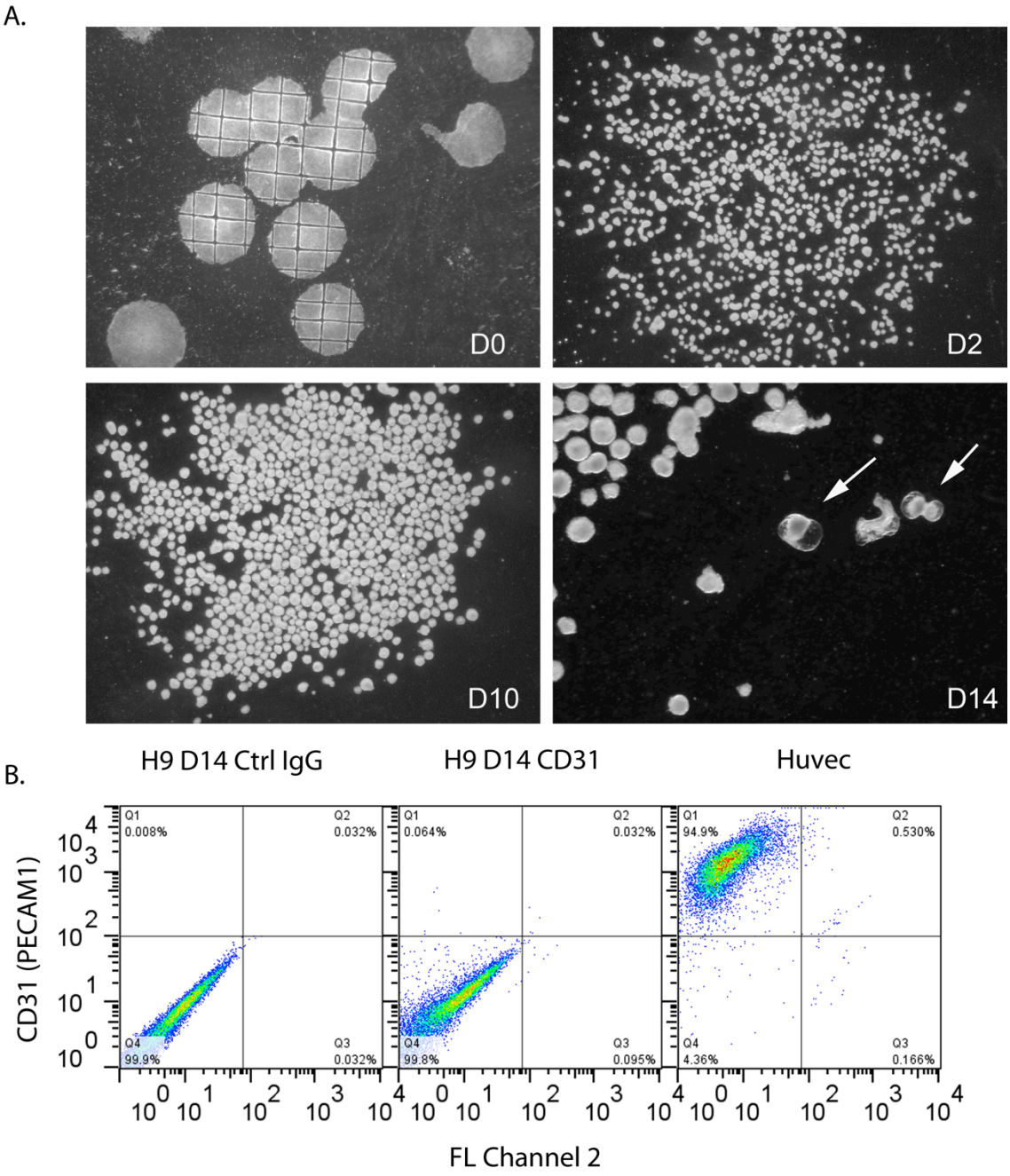

Figure 5.0: H9 hESCs do not randomly differentiate efficiently to CD31^{+} ECs. A). Images showing the scoring of healthy H9 hESCs for EB formation at D0. D2 and D10 images are of EBs grown in adherent conditions without bFGF, and D14 image shows the formation of fully differentiated cystic embryoid bodies. **B).** Flow cytometry analysis demonstrates a less than .1% differentiation efficiency of H9 hESCs compared to fully differentiated Huvecs, which are 95% positive for the endothelial specific marker CD31 (PECAM1)

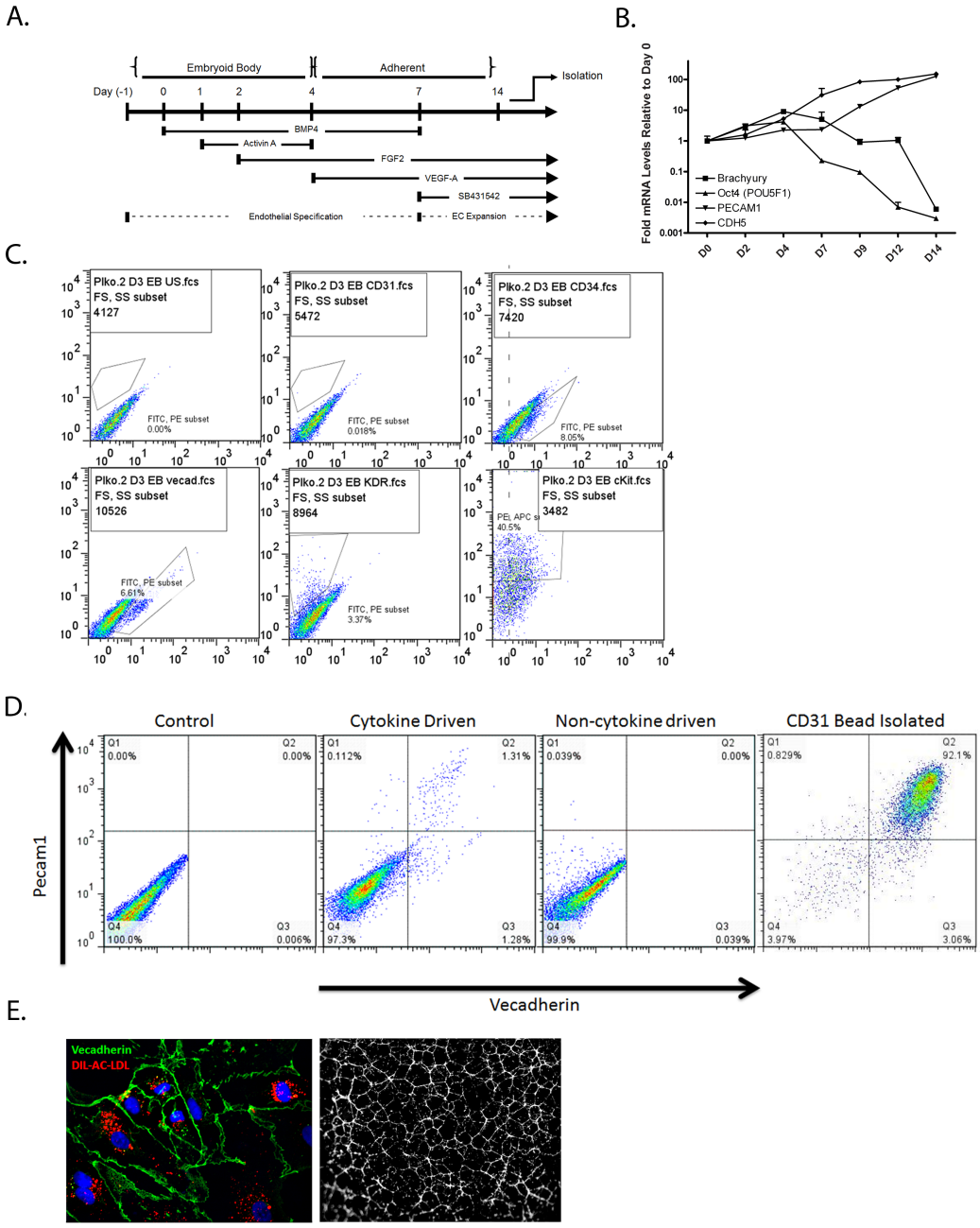

Figure 5.1: Mesodermal inducing cytokines followed by TGF-β inhibition promote H7 hESC differentiation to CD31^{+}CDH5^{+} ECs. A). Differentiation timeline protocol. **B).** qRT-PCR analysis of the vascular markers Pecam1 (CD31) and CDH5 (VEcadherin), the pluripotency marker Oct4, and the early mesoderm marker Brachyury. **C).** Flow cytometry analysis of H7 hESC differentiating EBs. **D).** Flow cytometry analysis of differentiating EBs pre and post CD31 bead isolation. **E).** Isolated ECs express VEcadherin and uptake acetylated low-density lipoprotein (left panel 40x objective) and form tube-like structures (right panel 10x objective)

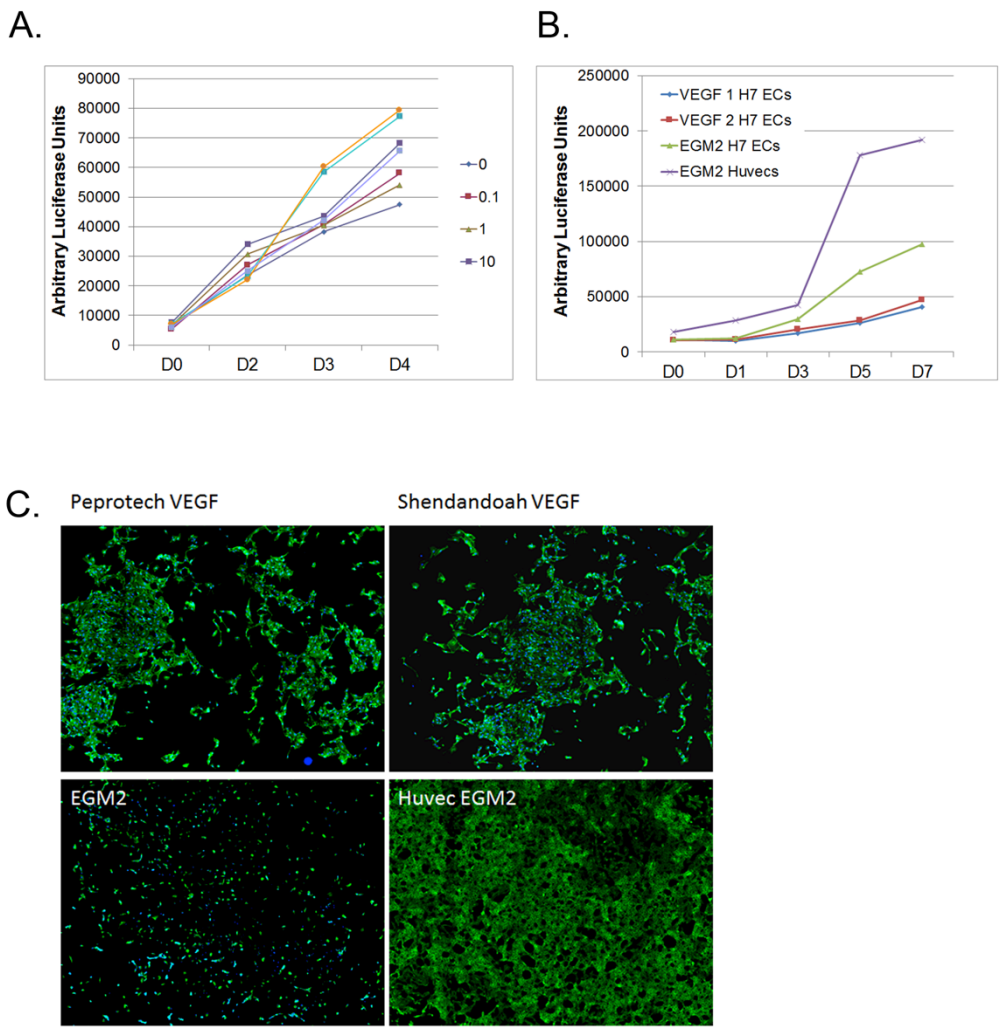

Figure 5.2: hESC derived ECs grow best in the vascular specification media. A). Dose-dependent Proliferation of Huvecs following VEGF stimulation, indicating that the VEGF used in this study is functional. **B).** Proliferation profile of Huvecs and H7 derived ECs in vascular specification media with two different forms of VEGF or grown in EGM-2, demonstrating that proliferation is increased in EGM-2 media with no differences in VEGF vendor source. **C).** Immunoflourescent imaging of H7 ECs or Huvecs grown in different media formulations. Cells grown in two different sources of VEGF were identical; where as, H7 ECs grown in EGM-2 lost endothelial characteristics. Images were taken at 10X magnification for monolayer visualization.

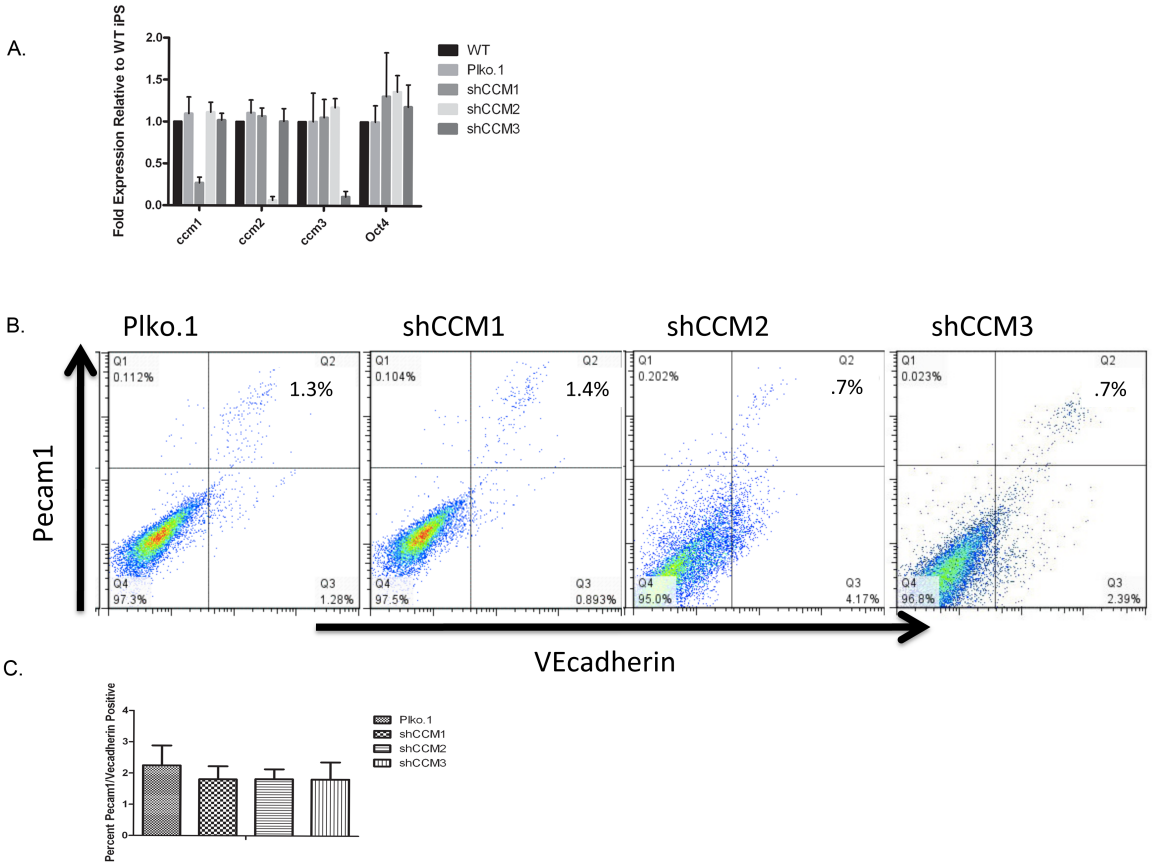

Figure 5.3: CCM protein knock down does not affect hESC pluripotency or differentiation to the endothelium. A). qRT-PCR analysis demonstrating that CCM proteins are effectively silenced by specific shRNAs in hESCs, and loss of CCM proteins does not effect the expression of the pluripotency marker Oct4. **B).** Representative flow cytometry plot demonstrating that CCM protein deficient knock hESCs are able to differentiate to Pecam1^{+}VEcadherin^{+} ECs. **C).** Quantification of multiple experiments, showing that CCM protein knock down does not significantly effect endothelial differentiation (n=4 experiments).

A.

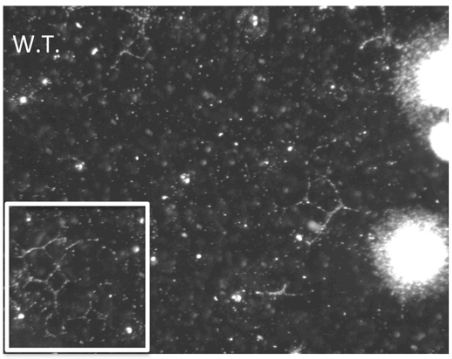

B.

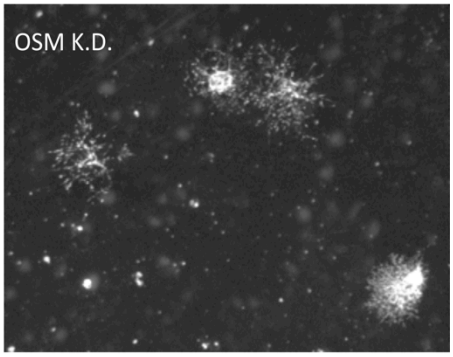

C.

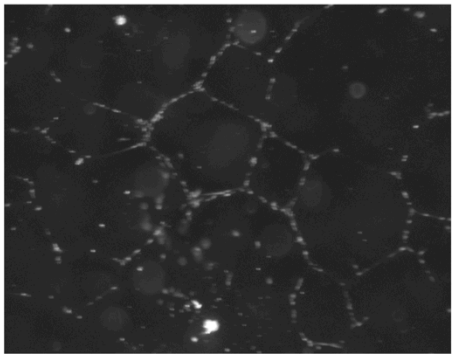

Figure 5.4: WT but not CCM knock down EBs sprout tube-like structures from differentiating EBs. A). WT differentiating EBs seeded on Matrigel send out multiple sprouts from EBs, indicating that active angiogenesis is occurring in these cultures. **B).** CCM2 (OSM) stable knock down differentiating EBs are smaller and demonstrate high levels of migration but no tube-like structurers form. **C).** Higher magnification (20X objective) of panel A (10X objective).

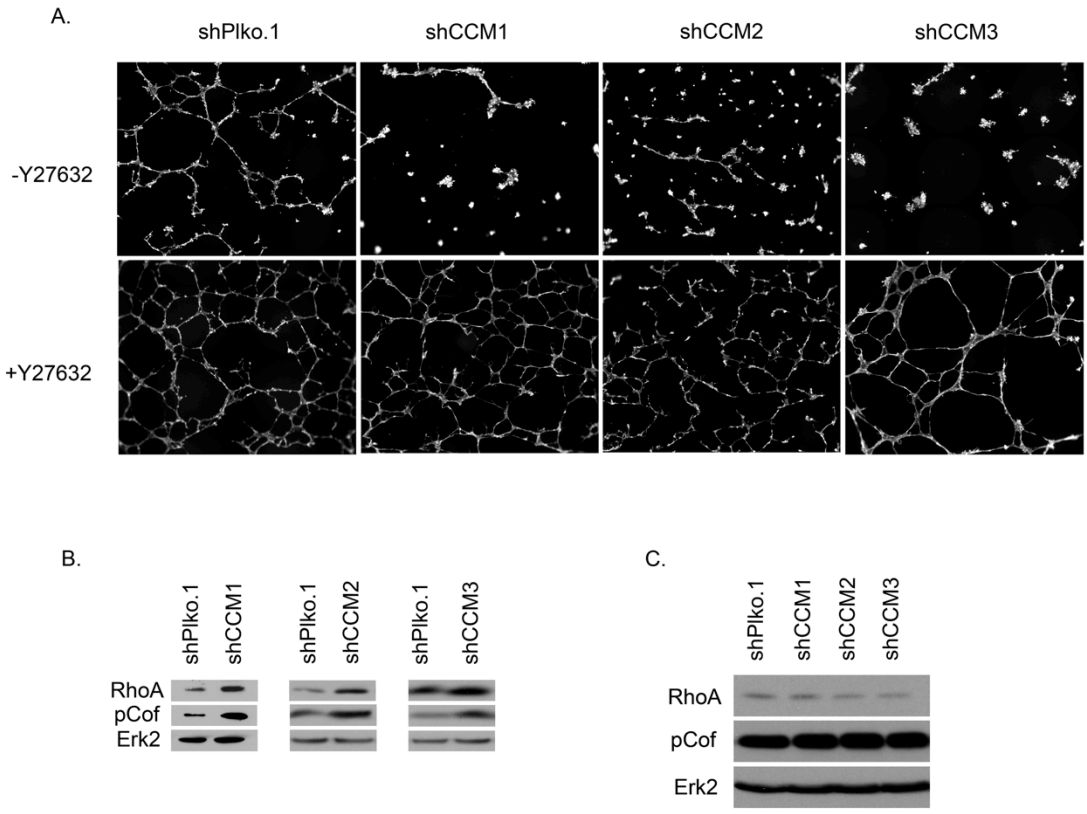

Figure 5.5: CCM proteins regulate endothelial function through RhoA in hESC derived ECs. A). shPlko.1 control ECs generate tube-like structures where as CCM1, -2, or -3 knock down cells are deficient in their ability to form tubes. These phenotypes are rescued by treatment with 10 μM Y-27632 **B).** ECs derived from hESCs with stable CCM protein knock down demonstrate elevated RhoA levels and pCofilin, suggesting that the phenotypes detected are due to deregulated RhoA signaling. **C).** hESCs do not have deregulated RhoA levels or elevated pCofilin, suggesting that RhoA is not deregulated in the pluripotent parental stem cell with CCM protein loss.

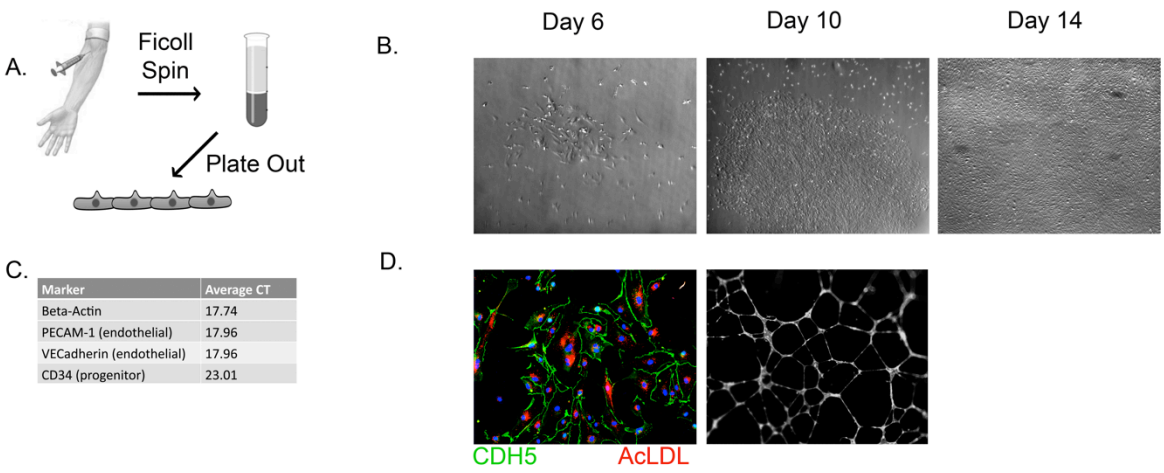

Marker	Average CT
Beta-Actin	17.74
PECAM-1 (endothelial)	17.96
VECadherin (endothelial)	17.96
CD34 (progenitor)	23.01

Figure 5.6: Endothelial progenitor cell derived ECs can be derived from peripheral blood. A). Peripheral blood is drawn from patients, spun on a ficoll gradient, the PBMCs are isolated and then plated on collagen IV. **B).** Late out growth endothelial progenitor cells start forming small colonies around 6 days and continue to grow. **C).** These EPC-ECs express high levels of Pecam-1, VEcadherin, and CD34. **D).** EPC-ECs form tight juntions with VEcadherin (CDH5) expressed at the membrane and are capable of uptaking acetylated low density lipo protein. EPC-ECs also form tube-like structures when plated on Matrigel.

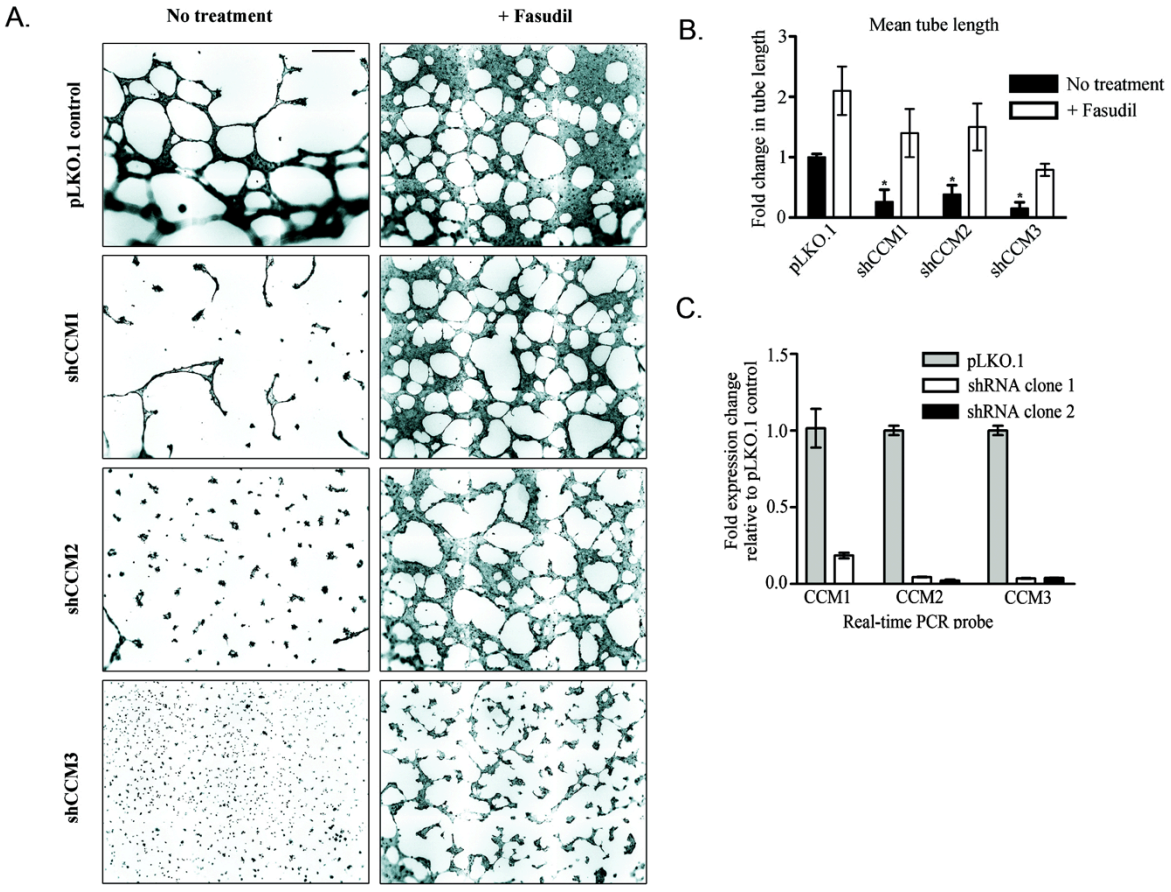

Figure 5.7: CCM1, -2, and -3 deficient endothelial progenitor cells are unable to form tube-like structures A). Knock down of CCM proteins abrogates proper tube formation ability in EPC-ECs, which is rescuable with ROCK inhibition. **B).** Quantification of tube formation assays from multiple independent experiments (*P= < .05). **C).** qRT-PCR validation of mRNA knock down in EPC-ECs.

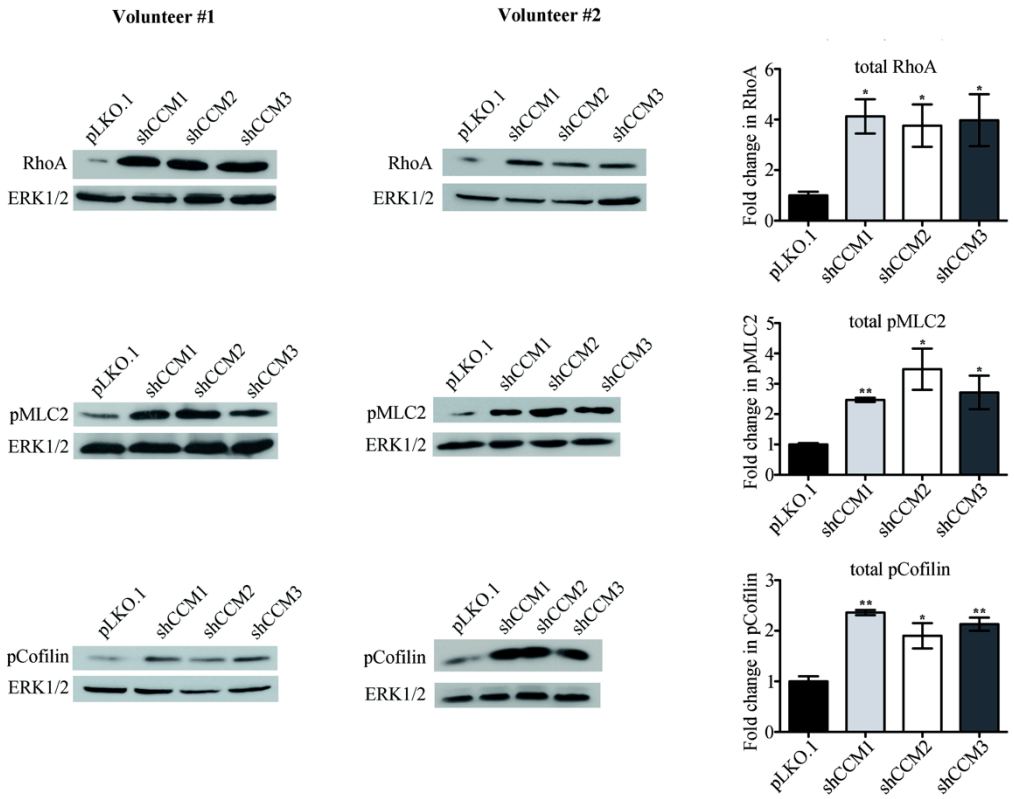

Figure 5.8: Two independent sources of EPC-ECs demonstrate elevated RhoA signaling. RhoA, pMLC2, and pCofilin are all increased in CCM protein deficient EPC-ECs indicating that RhoA and its downstream effectors are over activated. Right panels are the quantifications from multiple western blots (*P= < .05).

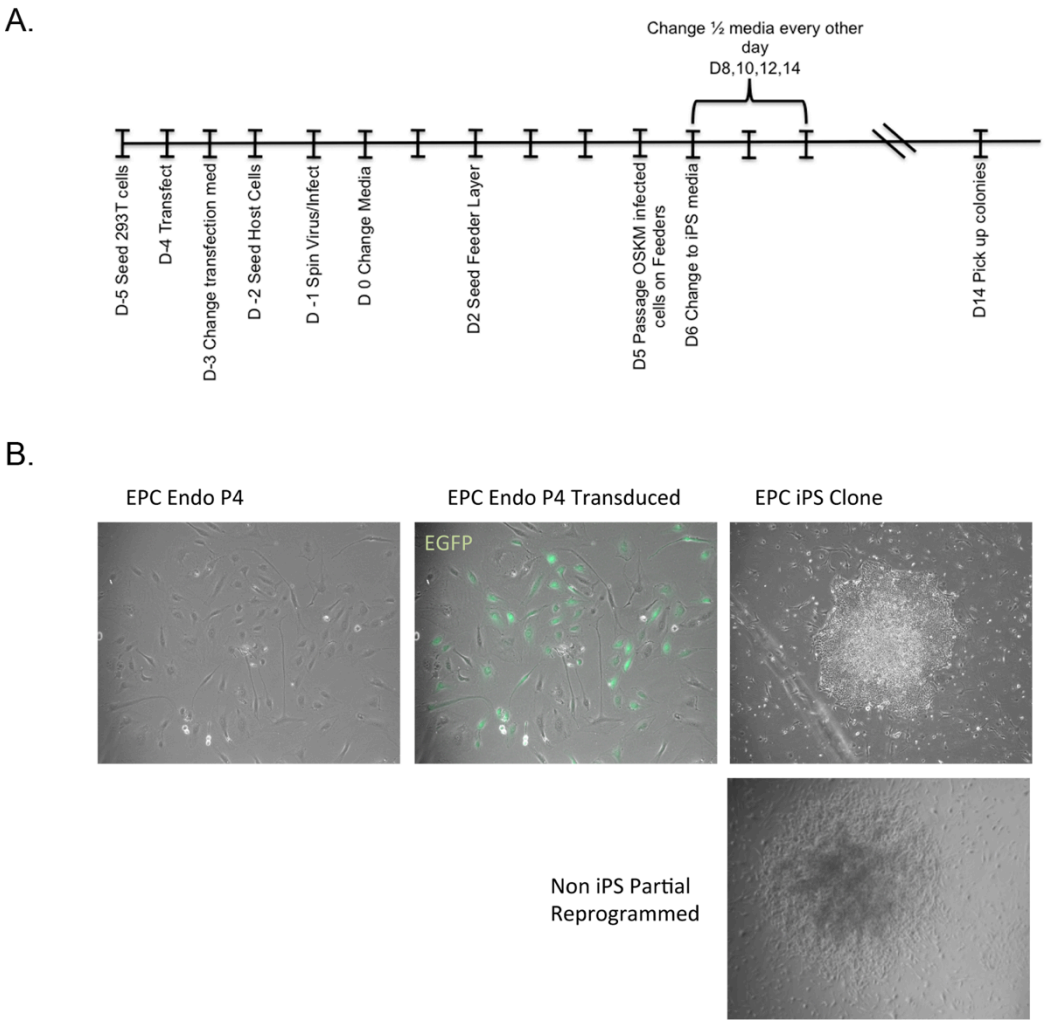

Figure 5.9: EPC-ECs form iPS colonies after retroviral transduction with Oct4, Sox2, Klf4, and cMyc. A). iPS reprogramming timeline used for the generation of all iPS clones. **B).** EPC-ECs were transduced at approximately 50% as estimated by GFP expression. Mature colonies started forming as little as 6 days after transduction; panel below shows an example of partially reprogrammed colonies.

A.

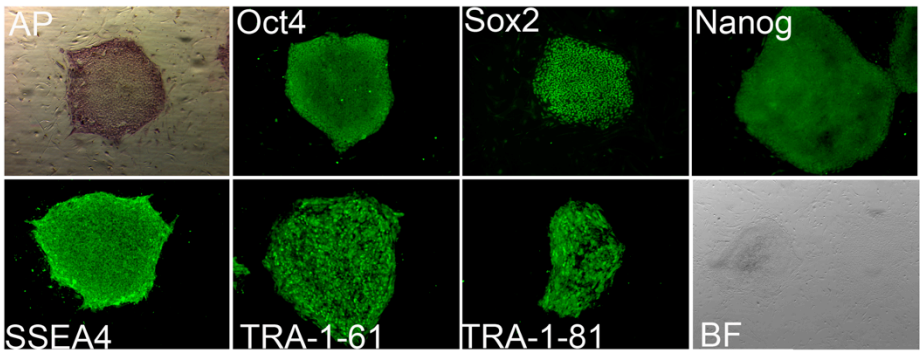

B.

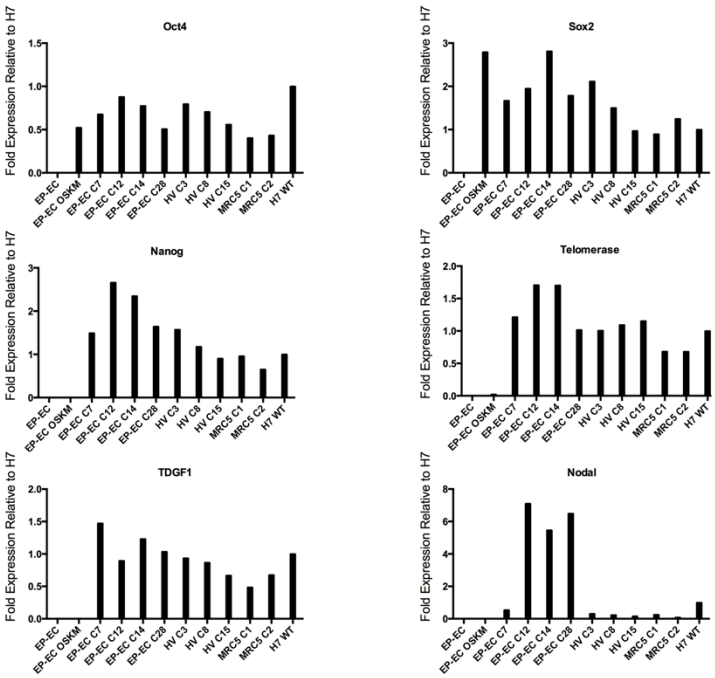

C.

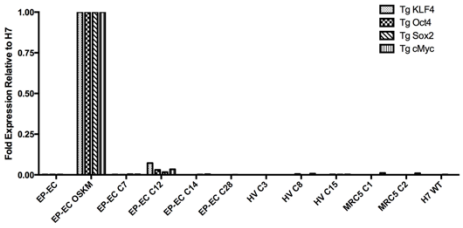

Figure 5.10: EPC-EC derived iPS cells express a panel of pluripotent stem cell markers. A). Reprogrammed EPC-ECs express pluripotency markers by immunoflourescence. **B).** qRT-PCR analysis shows that EPC-EC iPS cells express pluripotency markers to levels comparable to H7 hESCs. **C).** EPC-EC iPS cells have shut down the expression of Oct4, Sox2, KLF4, and cMyc transgenes.

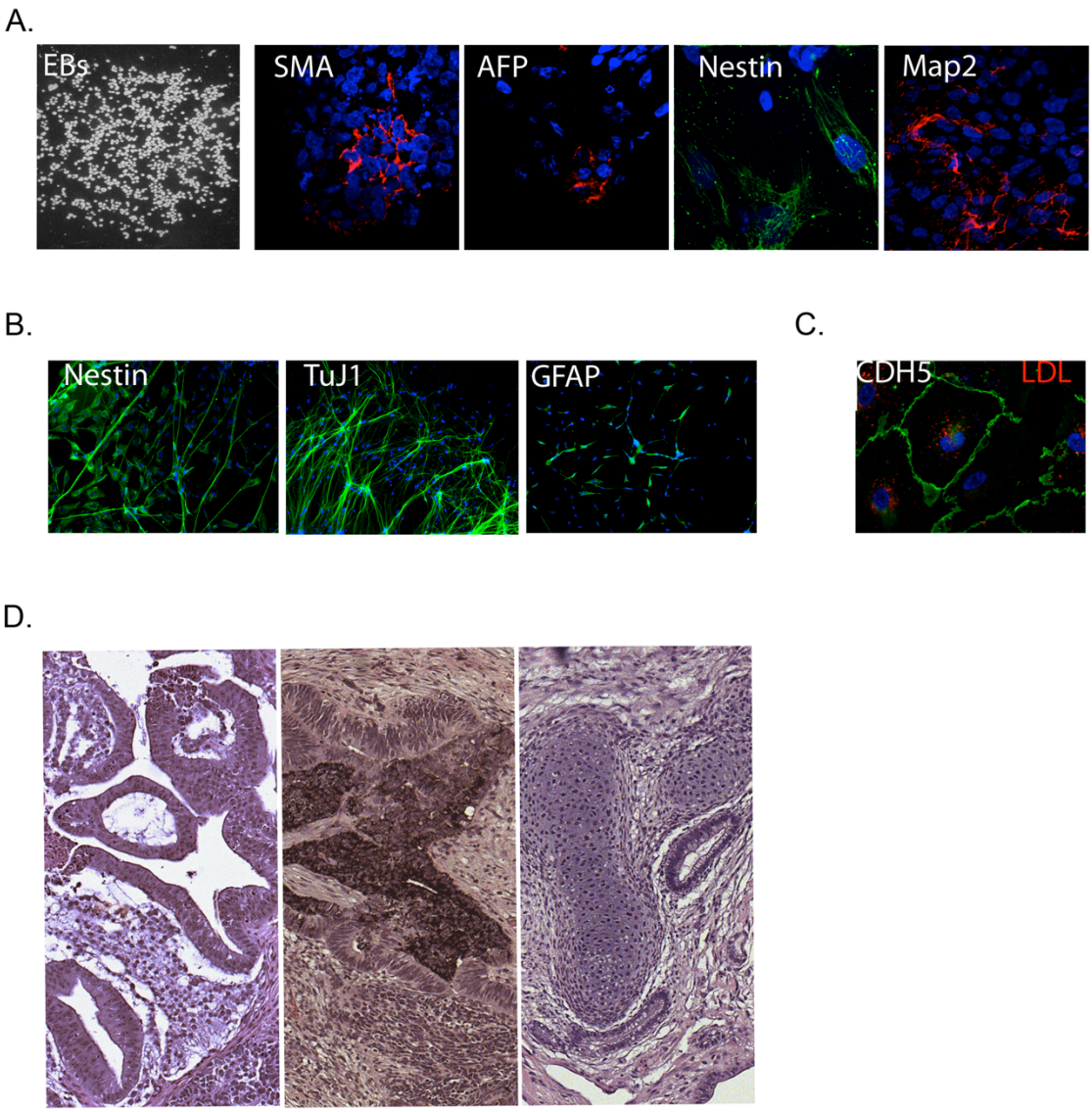

Figure 5.11: EPC-EC derived iPS cells are able to differentiate to all three germ layers A). EPC-EC iPS cells are able to differentiate to the mesoderm (smooth muscle actin; SMA), endoderm (alpha fetoprotein; AFP), and ectoderm (nestin and Map2) germ layer tissues by immunoflourescence. **B).** EPC-EC iPS cells can be cytokine directed to differentiate to neural rosette structures which contain Nestin^{+} neural progenitors, TuJ1^{+} neurons, or GFAP^{+} astrocyctes. **C).** EPC-EC iPS cells can be re-differentiated back to ECs that express CDH5 (VEcadherin) and can uptake AC-LDL. **D).** EPC-EC iPS cells form teratomas in vivo, which form endodermal tissues (left panel; ciliated enterocytes), ectodermal tissues (middle panel; pigmented retinal epithelium), and mesodermal tissues (right panel; immature cartilage).

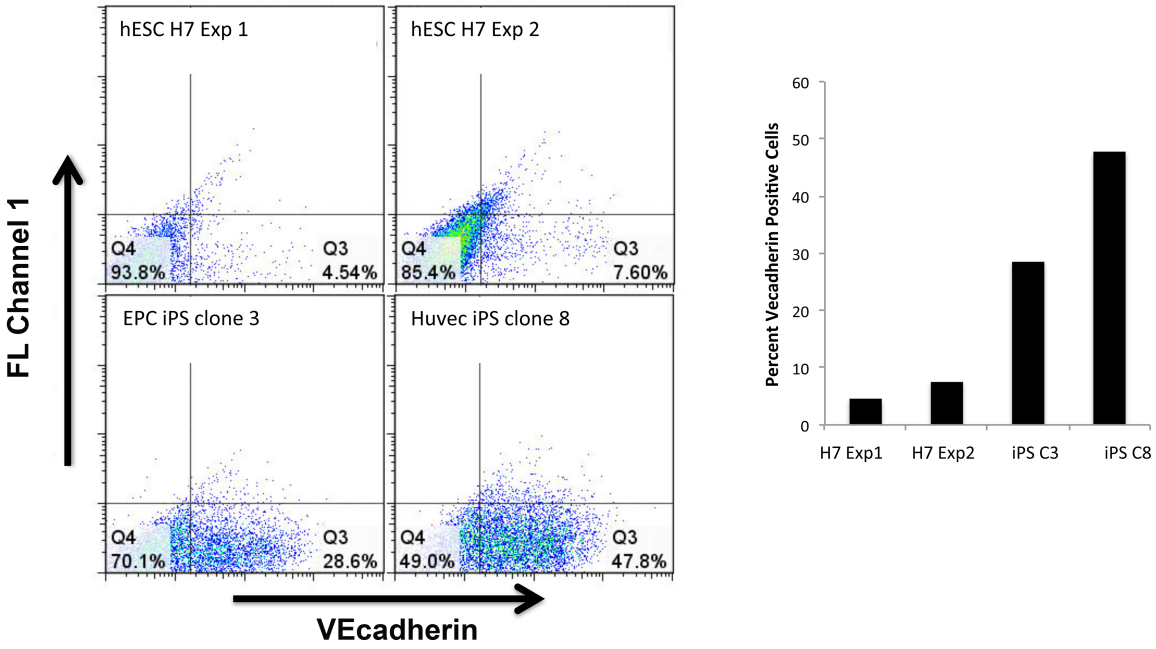

Figure 5.12: Endothelial derived iPS cells have enhanced VEcadherin expression during differentiation A). Flow cytometry analysis of VEcadherin expression in H7 hESC, epiPS, and Huvec iPS differentiating cultures. VEcadherin expression was greatly increased after 14 days of differentiation when compared to hESC control lines.

VI. Concluding remarks

Summary

CCM is a relatively common blood vascular disease, which has broad phenotypic and psychological effects. In many aspects CCM is similar to tumor formation as CCM lesions may form randomly and effect people, which have no genetic predisposition for the disease. CCM lesions can be both completely physically disabling, but perhaps equally psychologically damaging; patients neither know when a lesion may hemorrhage nor when they may become disabled. There is no cure, and the options for treatment is limited to invasive surgery. Thus, the goal of the collective CCM field is to develop new pharmacological treatment options for CCM patients, which both inhibits lesion genesis and recesses current lesions. To address this challenge, this body of work has attempted to further define the CCM signaling network and establish whether CCM patient specific pluripotent stem cell disease modeling is possible.

To date, there are no known prior studies investigating the involvement of the kinome in CCM. Kinases are the major class of proteins that integrate extracellular signaling cues to cellular responses, and represent a vastly understudied component of CCM. Indeed, the effects of RhoA and ROCK in driving CCM phenotypes are well described and represent an important therapeutic strategy for the pharmacological treatment of CCM. However, there may be a wealth of other potential targetable kinases driving the CCM disease process. Thus, to investigate this greatly

understudied aspect of CCM, we utilized MIB/MS, a novel technology that identifies unknown kinases in a completely unbiased manner. Our analysis showed that we were able to detect approximately 30% of the known kinome in our ECs. Many of these kinases were changed following the loss of the CCM proteins, many of which directly regulate the actin cytoskeleton. Moreover, many of the upregulated kinases have small molecule inhibitors available and were common between CCM1, -2, and -3 deficient ECs. We validated LIMK1 from our kinome profiling as being overactive and a major driver of a stabilized actin cytoskeleton downstream of RhoA and ROCK. Inhibition of LIMK1 by specific shRNAs rescued CCM phenotypes to the same extent as upstream ROCK inhibition. This finding is highly relevant to CCM as this kinase has cofilin as its one known substrate. The only other pharmacological avenues currently available for CCM are direct RhoA inhibition with Simvastatin or ROCK inhibition with hydroxyfasudil. RhoA and ROCK carry out a myriad of functions, and inhibiting them would be intrinsically less specific than an approach targeting LIMK1. Inhibitors of LIMK1 are currently being developed, and the effect of these inhibitors in vivo will be important to establish whether lesion recession is equal to that of hydroxyfasudil administration. The overall data generated from these kinome studies will be a resource for the CCM field to interrogate novel kinase networks involved in CCM, which may contribute to the development of new therapeutic strategies.

In addition to interrogating kinome networks in CCM, we have further established the role of deregulated degradation of the small GTPase RhoA as a molecular mechanism driving CCM phenotypes. These data suggest that the CCM

protein complex promotes Smurf1 ubiquitination of GTP bound RhoA in ECs, which is required for normal endothelial function. Increased GTP bound RhoA is found in numerous pathological conditions and ubiquitin modification is an emerging theme in the regulation of small GTPases. Thus, more broadly this work demonstrates for the first time that decreased ubiquitination of GTP bound RhoA contributes to the molecular biology behind a genetic disease and may represent a new paradigm when thinking about diseases affected by deregulated GTPase activity.

It is critical to study diseased cells from CCM patients to determine whether these in vitro and in vivo model phenotypes are relevant with the complex genetics of CCM patients. To begin to address this need, we developed a hESC model system of CCM to validate the feasibility of modeling diseased patient ECs from iPS cells. Accordingly, we found that hESCs remain pluripotent following CCM protein loss, and differentiated ECs demonstrate in vitro CCM phenotypes. We further demonstrated that EPC-ECs can be generated from normal healthy donors, and these cells also can be used to model CCM phenotypes following shRNA knock down of the CCM1, -2, and -3. Lastly, we showed that iPS cells can be successfully generated from these EPC-ECs and can be re-differentiated to the endothelium for CCM disease modeling. These data importantly demonstrate the feasibility of pluripotent stem cell disease modeling of CCM. Thus, a library of CCM patient iPS cells will allow the study of CCM in a patient specific way and may aid in elucidating the molecular mechanistic differences between CCM1, -2, and-3 patients.

Future Directions

Many challenges and outstanding basic research questions still face the CCM field. There is a great unmet need for treatment options for CCM patients, and it is important to remain focused on first answering those questions that will lead to the development of a feasible pharmacological strategy for the treatment of CCM. Broad genomic and proteomic approaches carried out in actual diseased CCM cells are paramount to understanding the relevant molecular mechanisms behind CCM pathology. The elucidation of at least one of these pathways has already led to the first clinical trial in CCM with Simvastatin. While this news is encouraging, more options are needed and collaborations between clinicians, basic research scientists, and patient advocacy groups will greatly increase the speed at which CCM biology is understood and new therapeutics generated.

Through our kinome profiling studies, we provide the first information into the global deregulation of kinase signaling in CCM deficient ECs. These data will be best used in concert with other broad discovery based technologies. For example, RNA sequencing of CCM deficient cells coupled with these kinome profiling studies will allow for the identification of gene signature changes that may be driving important previously unknown cellular changes. A major goal of the Angioma Alliance CCM patient advocacy group is to collect blood samples for genomic sequencing and tissue lesion samples for basic research. In the future, proteomic studies coupled with RNA and whole genome sequencing from patients will allow for the identification of protein and transcription networks deregulated in CCM and the baseline genomic mutations that may underlie these aberrant networks. Thus, a

more accurate picture of what is happening at transcriptional, genomic, and proteomic levels will serve as a resource for the CCM community to drive new hypotheses of pathways currently not recognized as being important in CCM biology.

There is a consensus in the field that deregulated RhoA signaling contributes to an aberrant cytoskeletal state in CCM deficient ECs, which gives rise to CCM phenotypes. Understanding how the cytoskeleton is regulated in ECs may provide immediate therapeutic avenues. We describe the importance of the CCM proteins in coordinating Smurf1 and Smurf2 regulation of RhoA and Rap1, respectively. RhoA is thought to antagonize Rap1 function by increasing monolayer permeability. Therefore, further understanding the interplay of these two small GTPases and potentially increasing Rap1 activity over RhoA may represent a new therapeutic avenue for CCM.

Many fascinating basic science questions remain unanswered. Perhaps the most difficult question to answer is how lesions initially form. Genomic instability seems to be an obvious answer; however, CCM patients do not have increased rates of cancer through genomic mutations. What makes the *ccm* gene loci so predisposed for genetic mutations; what is the selective pressure for these mutations? The CCM cell of origin may shed light into this question, especially if there is a defective circulating endothelial progenitor cell or other stem cell, which can hone to sites of active angiogenesis and contribute to CCM lesion formation.

In addition to the genetics of CCM, many questions remain into where and how the CCM proteins function. Our lab demonstrated that the CCM proteins are in complex with each other. What is the stoichiometry of this complex; when during the

many complex functions of an EC do these proteins interact? Undoubtedly endogenous fluorescent or epitope tagging approaches coupled with live cell high-resolution microscopy will help answer these questions. Along these lines, this thesis provides proof of concept studies using hESCs and hiPS cells as a first step to developing these tools to answer these types of questions. Thus, these cells can be used for both the study of disease patient cells and targeted with next generation gene targeting strategies for endogenous protein tagging. Overall, research in the CCM field is moving at a rapid pace with many novel avenues of research from the constant growth of new CCM researchers, and work in the near future will couple these basic science discoveries to the development of a novel therapeutic for CCM patients.

REFERENCES

1. Moriarity, J.L., R.E. Clatterbuck, and D. Rigamonti, *The natural history of cavernous malformations.* Neurosurg Clin N Am, 1999. **10**(3): p. 411-7.

2. Labauge, P., et al., *Genetics of cavernous angiomas.* Lancet Neurol, 2007. **6**(3): p. 237-44.

3. Whitehead, K.J., et al., *The cerebral cavernous malformation signaling pathway promotes vascular integrity via Rho GTPases.* Nat Med, 2009. **15**(2): p. 177-84.

4. Borikova, A.L., et al., *Rho kinase inhibition rescues the endothelial cell cerebral cavernous malformation phenotype.* J Biol Chem, 2010. **285**(16): p. 11760-4.

5. Crose, L.E., et al., *Cerebral cavernous malformation 2 protein promotes smad ubiquitin regulatory factor 1-mediated RhoA degradation in endothelial cells.* J Biol Chem, 2009. **284**(20): p. 13301-5.

6. Zheng, X., et al., *CCM3 signaling through sterile 20-like kinases plays an essential role during zebrafish cardiovascular development and cerebral cavernous malformations.* J Clin Invest, 2010. **120**(8): p. 2795-804.

7. Stockton, R.A., et al., *Cerebral cavernous malformations proteins inhibit Rho kinase to stabilize vascular integrity.* J Exp Med, 2010. **207**(4): p. 881-96.

8. McDonald, D.A., et al., *A novel mouse model of cerebral cavernous malformations based on the two-hit mutation hypothesis recapitulates the human disease.* Hum Mol Genet, 2011. **20**(2): p. 211-22.

9. Rigamonti, D., et al., *Cerebral cavernous malformations. Incidence and familial occurrence.* N Engl J Med, 1988. **319**(6): p. 343-7.

10. Gunel, M., et al., *A founder mutation as a cause of cerebral cavernous malformation in Hispanic Americans.* N Engl J Med, 1996. **334**(15): p. 946-51.

11. Bertalanffy, H., et al., *Cerebral cavernomas in the adult. Review of the literature and analysis of 72 surgically treated patients.* Neurosurg Rev, 2002. **25**(1-2): p. 1-53; discussion 54-5.

12. Moriarity, J.L., et al., *The natural history of cavernous malformations: a prospective study of 68 patients.* Neurosurgery, 1999. **44**(6): p. 1166-71; discussion 1172-3.

13. Bergametti, F., et al., *Mutations within the programmed cell death 10 gene cause cerebral cavernous malformations.* Am J Hum Genet, 2005. **76**(1): p. 42-51.

14. Cave-Riant, F., et al., *Spectrum and expression analysis of KRIT1 mutations in 121 consecutive and unrelated patients with Cerebral Cavernous Malformations.* Eur J Hum Genet, 2002. **10**(11): p. 733-40.

15. Craig, H.D., et al., *Multilocus linkage identifies two new loci for a mendelian form of stroke, cerebral cavernous malformation, at 7p15-13 and 3q25.2-27.* Hum Mol Genet, 1998. **7**(12): p. 1851-8.

16. Denier, C., et al., *Mutations within the MGC4607 gene cause cerebral cavernous malformations.* Am J Hum Genet, 2004. **74**(2): p. 326-37.

17. Del Curling, O., Jr., et al., *An analysis of the natural history of cavernous angiomas.* J Neurosurg, 1991. **75**(5): p. 702-8.

18. Scott, R.M., et al., *Cavernous angiomas of the central nervous system in children.* J Neurosurg, 1992. **76**(1): p. 38-46.

19. Herter, T., M. Brandt, and U. Szuwart, *Cavernous hemangiomas in children.* Childs Nerv Syst, 1988. **4**(3): p. 123-7.

20. Kondziolka, D., L.D. Lunsford, and J.R. Kestle, *The natural history of cerebral cavernous malformations.* J Neurosurg, 1995. **83**(5): p. 820-4.

21. Englot, D.J., et al., *Predictors of seizure freedom in the surgical treatment of supratentorial cavernous malformations.* J Neurosurg, 2011. **115**(6): p. 1169-74.

22. Labauge, P., et al., *Hereditary cerebral cavernous angiomas: clinical and genetic features in 57 French families. Societe Francaise de Neurochirurgie.* Lancet, 1998. **352**(9144): p. 1892-7.

23. Riant, F., et al., *Recent insights into cerebral cavernous malformations: the molecular genetics of CCM.* FEBS J, 2010. **277**(5): p. 1070-5.

24. Zabramski, J.M., et al., *The natural history of familial cavernous malformations: results of an ongoing study.* J Neurosurg, 1994. **80**(3): p. 422-32.

25. McCormick, W.F., *The pathology of vascular ("arteriovenous") malformations.* J Neurosurg, 1966. **24**(4): p. 807-16.

26. Robinson, J.R., I.A. Awad, and J.R. Little, *Natural history of the cavernous angioma.* J Neurosurg, 1991. **75**(5): p. 709-14.

27. Zabramski, J.M., J.S. Henn, and S. Coons, *Pathology of cerebral vascular malformations.* Neurosurg Clin N Am, 1999. **10**(3): p. 395-410.

28. Barrow, D.L. and A. Reisner, *Natural history of intracranial aneurysms and vascular malformations.* Clin Neurosurg, 1993. **40**: p. 3-39.

29. Wong, J.H., I.A. Awad, and J.H. Kim, *Ultrastructural pathological features of cerebrovascular malformations: a preliminary report.* Neurosurgery, 2000. **46**(6): p. 1454-9.

30. Clatterbuck, R.E., et al., *Ultrastructural and immunocytochemical evidence that an incompetent blood-brain barrier is related to the pathophysiology of cavernous malformations.* J Neurol Neurosurg Psychiatry, 2001. **71**(2): p. 188-92.

31. He, Y., et al., *Stabilization of VEGFR2 signaling by cerebral cavernous malformation 3 is critical for vascular development.* Sci Signal, 2010. **3**(116): p. ra26.

32. Fritschi, J.A., et al., *Cavernous malformations of the brain stem. A review of 139 cases.* Acta Neurochir (Wien), 1994. **130**(1-4): p. 35-46.

33. Brunereau, L., et al., *De novo lesions in familial form of cerebral cavernous malformations: clinical and MR features in 29 non-Hispanic families.* Surg Neurol, 2000. **53**(5): p. 475-82; discussion 482-3.

34. Awad, I. and P. Jabbour, *Cerebral cavernous malformations and epilepsy.* Neurosurg Focus, 2006. **21**(1): p. e7.

35. Amin-Hanjani, S., et al., *Stereotactic radiosurgery for cavernous malformations: Kjellberg's experience with proton beam therapy in 98 cases at the Harvard Cyclotron.* Neurosurgery, 1998. **42**(6): p. 1229-36; discussion 1236-8.

36. Amin-Hanjani, S., et al., *Risks of surgical management for cavernous malformations of the nervous system.* Neurosurgery, 1998. **42**(6): p. 1220-7; discussion 1227-8.

37. Pagenstecher, A., et al., *A two-hit mechanism causes cerebral cavernous malformations: complete inactivation of CCM1, CCM2 or CCM3 in affected endothelial cells.* Hum Mol Genet, 2009. **18**(5): p. 911-8.

38. Knudson, A.G., Jr., *Mutation and cancer: statistical study of retinoblastoma.* Proc Natl Acad Sci U S A, 1971. **68**(4): p. 820-3.

39. Kleaveland, B., et al., *Regulation of cardiovascular development and integrity by the heart of glass-cerebral cavernous malformation protein pathway.* Nat Med, 2009. **15**(2): p. 169-76.

40. Whitehead, K.J., et al., *Ccm1 is required for arterial morphogenesis: implications for the etiology of human cavernous malformations.* Development, 2004. **131**(6): p. 1437-48.

41. Boulday, G., et al., *Tissue-specific conditional CCM2 knockout mice establish the essential role of endothelial CCM2 in angiogenesis: implications for human cerebral cavernous malformations.* Dis Model Mech, 2009. **2**(3-4): p. 168-77.

42. Plummer, N.W., et al., *Loss of p53 sensitizes mice with a mutation in Ccm1 (KRIT1) to development of cerebral vascular malformations.* Am J Pathol, 2004. **165**(5): p. 1509-18.

43. Plummer, N.W., et al., *Neuronal expression of the Ccm2 gene in a new mouse model of cerebral cavernous malformations.* Mamm Genome, 2006. **17**(2): p. 119-28.

44. Louvi, A., et al., *Loss of cerebral cavernous malformation 3 (Ccm3) in neuroglia leads to CCM and vascular pathology.* Proc Natl Acad Sci U S A, 2011. **108**(9): p. 3737-42.

45. Wustehube, J., et al., *Cerebral cavernous malformation protein CCM1 inhibits sprouting angiogenesis by activating DELTA-NOTCH signaling.* Proc Natl Acad Sci U S A, 2010. **107**(28): p. 12640-5.

46. Boulday, G., et al., *Developmental timing of CCM2 loss influences cerebral cavernous malformations in mice.* J Exp Med, 2011. **208**(9): p. 1835-47.

47. Grunewald, M., et al., *VEGF-induced adult neovascularization: recruitment, retention, and role of accessory cells.* Cell, 2006. **124**(1): p. 175-89.

48. Sahoo, T., et al., *Mutations in the gene encoding KRIT1, a Krev-1/rap1a binding protein, cause cerebral cavernous malformations (CCM1).* Hum Mol Genet, 1999. **8**(12): p. 2325-33.

49. Laberge-le Couteulx, S., et al., *Truncating mutations in CCM1, encoding KRIT1, cause hereditary cavernous angiomas.* Nat Genet, 1999. **23**(2): p. 189-93.

50. Chen, D.H., et al., *Cerebral cavernous malformation: novel mutation in a Chinese family and evidence for heterogeneity.* J Neurol Sci, 2002. **196**(1-2): p. 91-6.

51. Laurans, M.S., et al., *Mutational analysis of 206 families with cavernous malformations.* J Neurosurg, 2003. **99**(1): p. 38-43.

52. Lucas, M., et al., *Germline mutations in the CCM1 gene, encoding Krit1, cause cerebral cavernous malformations.* Ann Neurol, 2001. **49**(4): p. 529-32.

53. Marini, V., et al., *Identification of a novel KRIT1 mutation in an Italian family with cerebral cavernous malformation by the protein truncation test.* J Neurol Sci, 2003. **212**(1-2): p. 75-8.

54. Musunuru, K., V.H. Hillard, and R. Murali, *Widespread central nervous system cavernous malformations associated with cafe-au-lait skin lesions. Case report.* J Neurosurg, 2003. **99**(2): p. 412-5.

55. Sahoo, T., et al., *Computational and experimental analyses reveal previously undetected coding exons of the KRIT1 (CCM1) gene.* Genomics, 2001. **71**(1): p. 123-6.

56. Verlaan, D.J., et al., *Cerebral cavernous malformations: mutations in Krit1.* Neurology, 2002. **58**(6): p. 853-7.

57. Zhang, J., et al., *Mutations in KRIT1 in familial cerebral cavernous malformations.* Neurosurgery, 2000. **46**(5): p. 1272-7; discussion 1277-9.

58. Serebriiskii, I., et al., *Association of Krev-1/rap1a with Krit1, a novel ankyrin repeat-containing protein encoded by a gene mapping to 7q21-22.* Oncogene, 1997. **15**(9): p. 1043-9.

59. Retta, S.F., et al., *Identification of Krit1B: a novel alternative splicing isoform of cerebral cavernous malformation gene-1.* Gene, 2004. **325**: p. 63-78.

60. Kitzmann, A.S., et al., *A splice-site mutation in CCM1/KRIT1 is associated with retinal and cerebral cavernous hemangioma.* Ophthalmic Genet, 2006. **27**(4): p. 157-9.

61. Toll, A., et al., *Cutaneous venous malformations in familial cerebral cavernomatosis caused by KRIT1 gene mutations.* Dermatology, 2009. **218**(4): p. 307-13.

62. Glading, A., et al., *KRIT-1/CCM1 is a Rap1 effector that regulates endothelial cell cell junctions.* J Cell Biol, 2007. **179**(2): p. 247-54.

63. Beraud-Dufour, S., et al., *Krit 1 interactions with microtubules and membranes are regulated by Rap1 and integrin cytoplasmic domain associated protein-1.* FEBS J, 2007. **274**(21): p. 5518-32.

64. Faurobert, E., et al., *CCM1-ICAP-1 complex controls beta1 integrin-dependent endothelial contractility and fibronectin remodeling.* J Cell Biol, 2013. **202**(3): p. 545-61.

65. Zawistowski, J.S., et al., *CCM1 and CCM2 protein interactions in cell signaling: implications for cerebral cavernous malformations pathogenesis.* Hum Mol Genet, 2005. **14**(17): p. 2521-31.

66. Mably, J.D., et al., *santa and valentine pattern concentric growth of cardiac myocardium in the zebrafish.* Development, 2006. **133**(16): p. 3139-46.

67. Goitre, L., et al., *KRIT1 regulates the homeostasis of intracellular reactive oxygen species.* PLoS One, 2010. **5**(7): p. e11786.

68. Kalluri, R. and R.A. Weinberg, *The basics of epithelial-mesenchymal transition.* J Clin Invest, 2009. **119**(6): p. 1420-8.

69. Maddaluno, L., et al., *EndMT contributes to the onset and progression of cerebral cavernous malformations.* Nature, 2013. **498**(7455): p. 492-6.

70. Uhlik, M.T., et al., *Rac-MEKK3-MKK3 scaffolding for p38 MAPK activation during hyperosmotic shock.* Nat Cell Biol, 2003. **5**(12): p. 1104-10.

71. Adams, R.H., et al., *Essential role of p38alpha MAP kinase in placental but not embryonic cardiovascular development.* Mol Cell, 2000. **6**(1): p. 109-16.

72. Yang, J., et al., *Mekk3 is essential for early embryonic cardiovascular development.* Nat Genet, 2000. **24**(3): p. 309-13.

73. Liquori, C.L., et al., *Mutations in a gene encoding a novel protein containing a phosphotyrosine-binding domain cause type 2 cerebral cavernous malformations.* Am J Hum Genet, 2003. **73**(6): p. 1459-64.

74. Hilder, T.L., et al., *Proteomic identification of the cerebral cavernous malformation signaling complex.* J Proteome Res, 2007. **6**(11): p. 4343-55.

75. Li, X., et al., *Crystal structure of CCM3, a cerebral cavernous malformation protein critical for vascular integrity.* J Biol Chem, 2010. **285**(31): p. 24099-107.

76. Wang, H.R., et al., *Regulation of cell polarity and protrusion formation by targeting RhoA for degradation.* Science, 2003. **302**(5651): p. 1775-9.

77. Zheng, X., et al., *Dynamic regulation of the cerebral cavernous malformation pathway controls vascular stability and growth.* Dev Cell, 2012. **23**(2): p. 342-55.

78. Harel, L., et al., *CCM2 mediates death signaling by the TrkA receptor tyrosine kinase.* Neuron, 2009. **63**(5): p. 585-91.

79. Costa, B., et al., *STK25 protein mediates TrkA and CCM2 protein-dependent death in pediatric tumor cells of neural origin.* J Biol Chem, 2012. **287**(35): p. 29285-9.

80. Guclu, B., et al., *Mutations in apoptosis-related gene, PDCD10, cause cerebral cavernous malformation 3.* Neurosurgery, 2005. **57**(5): p. 1008-13.

81. Goudreault, M., et al., *A PP2A phosphatase high density interaction network identifies a novel striatin-interacting phosphatase and kinase complex linked to the cerebral cavernous malformation 3 (CCM3) protein.* Mol Cell Proteomics, 2009. **8**(1): p. 157-71.

82. Fidalgo, M., et al., *CCM3/PDCD10 stabilizes GCKIII proteins to promote Golgi assembly and cell orientation.* J Cell Sci, 2010. **123**(Pt 8): p. 1274-84.

83. Richardson, B.T., et al., *Cerebral cavernous malformation is a vascular disease associated with activated RhoA signaling.* Biol Chem, 2013. **394**(1): p. 35-42.

84. Altas, M., et al., *Angiotensin-converting enzyme insertion/deletion gene polymorphism in patients with familial multiple cerebral cavernous malformations.* J Clin Neurosci, 2010. **17**(8): p. 1034-7.

85. You, C., et al., *Loss of CCM3 impairs DLL4-Notch signalling: implication in endothelial angiogenesis and in inherited cerebral cavernous malformations.* J Cell Mol Med, 2013. **17**(3): p. 407-18.

86. Etienne-Manneville, S. and A. Hall, *Rho GTPases in cell biology.* Nature, 2002. **420**(6916): p. 629-35.

87. Chan, A.C., et al., *Mutations in 2 distinct genetic pathways result in cerebral cavernous malformations in mice.* J Clin Invest, 2011. **121**(5): p. 1871-81.

88. London, N.R., K.J. Whitehead, and D.Y. Li, *Endogenous endothelial cell signaling systems maintain vascular stability.* Angiogenesis, 2009. **12**(2): p. 149-58.

89. De Smet, F., et al., *Mechanisms of vessel branching: filopodia on endothelial tip cells lead the way.* Arterioscler Thromb Vasc Biol, 2009. **29**(5): p. 639-49.

90. Galan Moya, E.M., A. Le Guelte, and J. Gavard, *PAKing up to the endothelium.* Cell Signal, 2009. **21**(12): p. 1727-37.

91. Jaffe, A.B. and A. Hall, *Rho GTPases: biochemistry and biology.* Annu Rev Cell Dev Biol, 2005. **21**: p. 247-69.

92. Maekawa, M., et al., *Signaling from Rho to the actin cytoskeleton through protein kinases ROCK and LIM-kinase.* Science, 1999. **285**(5429): p. 895-8.

93. Wang, H.R., et al., *Degradation of RhoA by Smurf1 ubiquitin ligase.* Methods Enzymol, 2006. **406**: p. 437-47.

94. Liu, Z., et al., *Mechanical tugging force regulates the size of cell-cell junctions.* Proc Natl Acad Sci U S A, 2010. **107**(22): p. 9944-9.

95. Glading, A.J. and M.H. Ginsberg, *Rap1 and its effector KRIT1/CCM1 regulate beta-catenin signaling.* Dis Model Mech, 2010. **3**(1-2): p. 73-83.

96. Pannekoek, W.J., et al., *Cell-cell junction formation: the role of Rap1 and Rap1 guanine nucleotide exchange factors.* Biochim Biophys Acta, 2009. **1788**(4): p. 790-6.

97. Bustos, R.I., et al., *Coordination of Rho and Rac GTPase function via p190B RhoGAP.* Curr Biol, 2008. **18**(20): p. 1606-11.

98. Wildenberg, G.A., et al., *p120-catenin and p190RhoGAP regulate cell-cell adhesion by coordinating antagonism between Rac and Rho.* Cell, 2006. **127**(5): p. 1027-39.

99. Ding, F., Z. Yin, and H.R. Wang, *Ubiquitination in Rho signaling.* Curr Top Med Chem, 2011. **11**(23): p. 2879-87.

100. Cui, Y., et al., *SCFFBXL(1)(5) regulates BMP signalling by directing the degradation of HECT-type ubiquitin ligase Smurf1.* EMBO J, 2011. **30**(13): p. 2675-89.

101. Lu, K., et al., *Targeting WW domains linker of HECT-type ubiquitin ligase Smurf1 for activation by CKIP-1.* Nat Cell Biol, 2008. **10**(8): p. 994-1002.

102. Horiki, M., et al., *Smad6/Smurf1 overexpression in cartilage delays chondrocyte hypertrophy and causes dwarfism with osteopenia.* J Cell Biol, 2004. **165**(3): p. 433-45.

103. Moren, A., et al., *Degradation of the tumor suppressor Smad4 by WW and HECT domain ubiquitin ligases.* J Biol Chem, 2005. **280**(23): p. 22115-23.

104. Suzuki, C., et al., *Smurf1 regulates the inhibitory activity of Smad7 by targeting Smad7 to the plasma membrane.* J Biol Chem, 2002. **277**(42): p. 39919-25.

105. Zhu, H., et al., *A SMAD ubiquitin ligase targets the BMP pathway and affects embryonic pattern formation.* Nature, 1999. **400**(6745): p. 687-93.

106. Murakami, G., et al., *Cooperative inhibition of bone morphogenetic protein signaling by Smurf1 and inhibitory Smads.* Mol Biol Cell, 2003. **14**(7): p. 2809-17.

107. Ebisawa, T., et al., *Smurf1 interacts with transforming growth factor-beta type I receptor through Smad7 and induces receptor degradation.* J Biol Chem, 2001. **276**(16): p. 12477-80.

108. Cheng, P.L., et al., *Phosphorylation of E3 ligase Smurf1 switches its substrate preference in support of axon development.* Neuron, 2011. **69**(2): p. 231-43.

109. Asanuma, K., et al., *Synaptopodin orchestrates actin organization and cell motility via regulation of RhoA signalling.* Nat Cell Biol, 2006. **8**(5): p. 485-91.

110. Dejana, E., F. Orsenigo, and M.G. Lampugnani, *The role of adherens junctions and VE-cadherin in the control of vascular permeability.* J Cell Sci, 2008. **121**(Pt 13): p. 2115-22.

111. Schwamborn, J.C., et al., *Ubiquitination of the GTPase Rap1B by the ubiquitin ligase Smurf2 is required for the establishment of neuronal polarity.* EMBO J, 2007. **26**(5): p. 1410-22.

112. Schwamborn, J.C., M.R. Khazaei, and A.W. Puschel, *The interaction of mPar3 with the ubiquitin ligase Smurf2 is required for the establishment of neuronal polarity.* J Biol Chem, 2007. **282**(48): p. 35259-68.

113. Fukunaga, E., et al., *Smurf2 induces ubiquitin-dependent degradation of Smurf1 to prevent migration of breast cancer cells.* J Biol Chem, 2008. **283**(51): p. 35660-7.

114. Emanuele, M.J., et al., *Global identification of modular cullin-RING ligase substrates.* Cell, 2011. **147**(2): p. 459-74.

115. Genschik, P., I. Sumara, and E. Lechner, *The emerging family of CULLIN3-RING ubiquitin ligases (CRL3s): cellular functions and disease implications.* EMBO J, 2013. **32**(17): p. 2307-20.

116. Chen, Y., et al., *Cullin mediates degradation of RhoA through evolutionarily conserved BTB adaptors to control actin cytoskeleton structure and cell movement.* Mol Cell, 2009. **35**(6): p. 841-55.

117. Pelham, C.J., et al., *Cullin-3 regulates vascular smooth muscle function and arterial blood pressure via PPARgamma and RhoA/Rho-kinase.* Cell Metab, 2012. **16**(4): p. 462-72.

118. Leung, T., et al., *A novel serine/threonine kinase binding the Ras-related RhoA GTPase which translocates the kinase to peripheral membranes.* J Biol Chem, 1995. **270**(49): p. 29051-4.

119. Nakagawa, O., et al., *ROCK-I and ROCK-II, two isoforms of Rho-associated coiled-coil forming protein serine/threonine kinase in mice.* FEBS Lett, 1996. **392**(2): p. 189-93.

120. Shatanawi, A., et al., *Angiotensin II-induced vascular endothelial dysfunction through RhoA/Rho kinase/p38 mitogen-activated protein kinase/arginase pathway.* Am J Physiol Cell Physiol, 2011. **300**(5): p. C1181-92.

121. Riento, K. and A.J. Ridley, *Rocks: multifunctional kinases in cell behaviour.* Nat Rev Mol Cell Biol, 2003. **4**(6): p. 446-56.

122. Chen, X.Q., et al., *Characterization of RhoA-binding kinase ROKalpha implication of the pleckstrin homology domain in ROKalpha function using region-specific antibodies.* J Biol Chem, 2002. **277**(15): p. 12680-8.

123. Matsui, T., et al., *Rho-associated kinase, a novel serine/threonine kinase, as a putative target for small GTP binding protein Rho.* EMBO J, 1996. **15**(9): p. 2208-16.

124. Amano, M., et al., *Phosphorylation and activation of myosin by Rho-associated kinase (Rho-kinase).* J Biol Chem, 1996. **271**(34): p. 20246-9.

125. Kawano, Y., et al., *Phosphorylation of myosin-binding subunit (MBS) of myosin phosphatase by Rho-kinase in vivo.* J Cell Biol, 1999. **147**(5): p. 1023-38.

126. Ohashi, K., et al., *Rho-associated kinase ROCK activates LIM-kinase 1 by phosphorylation at threonine 508 within the activation loop.* J Biol Chem, 2000. **275**(5): p. 3577-82.

127. Sumi, T., K. Matsumoto, and T. Nakamura, *Specific activation of LIM kinase 2 via phosphorylation of threonine 505 by ROCK, a Rho-dependent protein kinase.* J Biol Chem, 2001. **276**(1): p. 670-6.

128. Arber, S., et al., *Regulation of actin dynamics through phosphorylation of cofilin by LIM-kinase.* Nature, 1998. **393**(6687): p. 805-9.

129. Dong, M., et al., *Rho-kinase inhibition: a novel therapeutic target for the treatment of cardiovascular diseases.* Drug Discov Today, 2010. **15**(15-16): p. 622-9.

130. Xie, H., et al., *Role of RhoA/ROCK signaling in endothelial-monocyte-activating polypeptide II opening of the blood-tumor barrier: role of RhoA/ROCK signaling in EMAP II opening of the BTB.* J Mol Neurosci, 2012. **46**(3): p. 666-76.

131. Schneider, H., et al., *Impairment of tight junctions and glucose transport in endothelial cells of human cerebral cavernous malformations.* J Neuropathol Exp Neurol, 2011. **70**(6): p. 417-29.

132. Takemoto, M., et al., *Rho-kinase mediates hypoxia-induced downregulation of endothelial nitric oxide synthase.* Circulation, 2002. **106**(1): p. 57-62.

133. Rochette, L., et al., *Nitric oxide synthase inhibition and oxidative stress in cardiovascular diseases: Possible therapeutic targets?* Pharmacol Ther, 2013. **140**(3): p. 239-57.

134. Shenkar, R., et al., *Concepts and hypotheses: inflammatory hypothesis in the pathogenesis of cerebral cavernous malformations.* Neurosurgery, 2007. **61**(4): p. 693-702; discussion 702-3.

135. Xie, X., et al., *Activation of RhoA/ROCK regulates NF-kappaB signaling pathway in experimental diabetic nephropathy.* Mol Cell Endocrinol, 2013. **369**(1-2): p. 86-97.

136. Taylor, F., et al., *Statins for the primary prevention of cardiovascular disease.* Cochrane Database Syst Rev, 2013. **1**: p. CD004816.

137. Futterman, L.G. and L. Lemberg, *Statin pleiotropy: fact or fiction?* Am J Crit Care, 2004. **13**(3): p. 244-9.

138. Park, H.J., et al., *3-hydroxy-3-methylglutaryl coenzyme A reductase inhibitors interfere with angiogenesis by inhibiting the geranylgeranylation of RhoA.* Circ Res, 2002. **91**(2): p. 143-50.

139. Suzuki, Y., et al., *A postmarketing surveillance study of fasudil treatment after aneurysmal subarachnoid hemorrhage.* Surg Neurol, 2007. **68**(2): p. 126-31; discussion 131-2.

140. Satoh, K., Y. Fukumoto, and H. Shimokawa, *Rho-kinase: important new therapeutic target in cardiovascular diseases.* Am J Physiol Heart Circ Physiol, 2011. **301**(2): p. H287-96.

141. Takahashi, K., et al., *Induction of pluripotent stem cells from fibroblast cultures.* Nat Protoc, 2007. **2**(12): p. 3081-9.

142. Takahashi, K. and S. Yamanaka, *Induction of pluripotent stem cells from mouse embryonic and adult fibroblast cultures by defined factors.* Cell, 2006. **126**(4): p. 663-76.

143. Dey, D. and G.R. Evans, *Generation of Induced Pluripotent Stem (iPS) Cells by Nuclear Reprogramming.* Stem Cells Int, 2011. **2011**: p. 619583.

144. Thomson, J.A., et al., *Embryonic stem cell lines derived from human blastocysts.* Science, 1998. **282**(5391): p. 1145-7.

145. Boyer, L.A., et al., *Core transcriptional regulatory circuitry in human embryonic stem cells.* Cell, 2005. **122**(6): p. 947-56.

146. Bellin, M., et al., *Induced pluripotent stem cells: the new patient?* Nat Rev Mol Cell Biol, 2012. **13**(11): p. 713-26.

147. Hu, Q., et al., *Memory in induced pluripotent stem cells: reprogrammed human retinal-pigmented epithelial cells show tendency for spontaneous redifferentiation.* Stem Cells, 2010. **28**(11): p. 1981-91.

148. Polo, J.M., et al., *Cell type of origin influences the molecular and functional properties of mouse induced pluripotent stem cells.* Nat Biotechnol, 2010. **28**(8): p. 848-55.

149. Bar-Nur, O., et al., *Epigenetic memory and preferential lineage-specific differentiation in induced pluripotent stem cells derived from human pancreatic islet beta cells.* Cell Stem Cell, 2011. **9**(1): p. 17-23.

150. Kim, K., et al., *Epigenetic memory in induced pluripotent stem cells.* Nature, 2010. **467**(7313): p. 285-90.

151. Murry, C.E. and G. Keller, *Differentiation of embryonic stem cells to clinically relevant populations: lessons from embryonic development.* Cell, 2008. **132**(4): p. 661-80.

152. Marion, R.M., et al., *Telomeres acquire embryonic stem cell characteristics in induced pluripotent stem cells.* Cell Stem Cell, 2009. **4**(2): p. 141-54.

153. Hanna, J., et al., *Treatment of sickle cell anemia mouse model with iPS cells generated from autologous skin.* Science, 2007. **318**(5858): p. 1920-3.

154. Wernig, M., et al., *Neurons derived from reprogrammed fibroblasts functionally integrate into the fetal brain and improve symptoms of rats with Parkinson's disease.* Proc Natl Acad Sci U S A, 2008. **105**(15): p. 5856-61.

155. Chapman, A.R. and C.C. Scala, *Evaluating the first-in-human clinical trial of a human embryonic stem cell-based therapy.* Kennedy Inst Ethics J, 2012. **22**(3): p. 243-61.

156. Lee, J.E., et al., *Evaluation of 28 human embryonic stem cell lines for use as unrelated donors in stem cell therapy: implications of HLA and ABO genotypes.* Cell Transplant, 2010. **19**(11): p. 1383-95.

157. Jacquet, L., et al., *Strategy for the creation of clinical grade hESC line banks that HLA-match a target population.* EMBO Mol Med, 2013. **5**(1): p. 10-7.

158. Taylor, C.J., E.M. Bolton, and J.A. Bradley, *Immunological considerations for embryonic and induced pluripotent stem cell banking.* Philos Trans R Soc Lond B Biol Sci, 2011. **366**(1575): p. 2312-22.

159. Okita, K., T. Ichisaka, and S. Yamanaka, *Generation of germline-competent induced pluripotent stem cells.* Nature, 2007. **448**(7151): p. 313-7.

160. Miura, K., et al., *Variation in the safety of induced pluripotent stem cell lines.* Nat Biotechnol, 2009. **27**(8): p. 743-5.

161. Zhao, T., et al., *Immunogenicity of induced pluripotent stem cells.* Nature, 2011. **474**(7350): p. 212-5.

162. Inoue, H. and S. Yamanaka, *The use of induced pluripotent stem cells in drug development.* Clin Pharmacol Ther, 2011. **89**(5): p. 655-61.

163. Robinton, D.A. and G.Q. Daley, *The promise of induced pluripotent stem cells in research and therapy.* Nature, 2012. **481**(7381): p. 295-305.

164. Lee, G., et al., *Modelling pathogenesis and treatment of familial dysautonomia using patient-specific iPSCs.* Nature, 2009. **461**(7262): p. 402-6.

165. Doetschman, T., et al., *Targetted correction of a mutant HPRT gene in mouse embryonic stem cells.* Nature, 1987. **330**(6148): p. 576-8.

166. Wei, C., et al., *TALEN or Cas9 - rapid, efficient and specific choices for genome modifications.* J Genet Genomics, 2013. **40**(6): p. 281-9.

167. Zou, J., et al., *Gene targeting of a disease-related gene in human induced pluripotent stem and embryonic stem cells.* Cell Stem Cell, 2009. **5**(1): p. 97-110.

168. Voss, K., et al., *CCM3 interacts with CCM2 indicating common pathogenesis for cerebral cavernous malformations.* Neurogenetics, 2007. **8**(4): p. 249-56.

169. Iwabuchi, S., et al., *Intra-arterial Administration of Fasudil Hydrochloride for Vasospasm Following Subarachnoid Haemorrhage: Experience of 90 Cases.* Acta Neurochir Suppl, 2011. **110**(Pt 2): p. 179-81.

170. Zhao, J., et al., *Effect of fasudil hydrochloride, a protein kinase inhibitor, on cerebral vasospasm and delayed cerebral ischemic symptoms after aneurysmal subarachnoid hemorrhage.* Neurol Med Chir (Tokyo), 2006. **46**(9): p. 421-8.

171. Daub, H., et al., *Kinase-selective enrichment enables quantitative phosphoproteomics of the kinome across the cell cycle.* Mol Cell, 2008. **31**(3): p. 438-48.

172. Oppermann, F.S., et al., *Large-scale proteomics analysis of the human kinome.* Mol Cell Proteomics, 2009. **8**(7): p. 1751-64.

173. Duncan, J.S., et al., *Dynamic reprogramming of the kinome in response to targeted MEK inhibition in triple-negative breast cancer.* Cell, 2012. **149**(2): p. 307-21.

174. Baev, N.I. and I.A. Awad, *Endothelial cell culture from human cerebral cavernous malformations.* Stroke, 1998. **29**(11): p. 2426-34.

175. Watanabe, G., et al., *Protein kinase N (PKN) and PKN-related protein rhophilin as targets of small GTPase Rho.* Science, 1996. **271**(5249): p. 645-8.

176. Mopert, K., et al., *Depletion of protein kinase N3 (PKN3) impairs actin and adherens junctions dynamics and attenuates endothelial cell activation.* Eur J Cell Biol, 2012. **91**(9): p. 694-705.

177. Scott, R.W., et al., *LIM kinases are required for invasive path generation by tumor and tumor-associated stromal cells.* J Cell Biol, 2010. **191**(1): p. 169-85.

178. Prudent, R., et al., *Pharmacological inhibition of LIM kinase stabilizes microtubules and inhibits neoplastic growth.* Cancer Res, 2012. **72**(17): p. 4429-39.

179. Manetti, F., *LIM kinases are attractive targets with many macromolecular partners and only a few small molecule regulators.* Med Res Rev, 2012. **32**(5): p. 968-98.

180. McCabe, A., et al., *Automated quantitative analysis (AQUA) of in situ protein expression, antibody concentration, and prognosis.* J Natl Cancer Inst, 2005. **97**(24): p. 1808-15.

181. Akers, A.L., et al., *Biallelic somatic and germline mutations in cerebral cavernous malformations (CCMs): evidence for a two-hit mechanism of CCM pathogenesis.* Hum Mol Genet, 2009. **18**(5): p. 919-30.

182. Davis, S., et al., *Isolation of angiopoietin-1, a ligand for the TIE2 receptor, by secretion-trap expression cloning.* Cell, 1996. **87**(7): p. 1161-9.

183. Maisonpierre, P.C., et al., *Angiopoietin-2, a natural antagonist for Tie2 that disrupts in vivo angiogenesis.* Science, 1997. **277**(5322): p. 55-60.

184. Zhang, J., et al., *Angiopoietin-1/Tie2 signal augments basal Notch signal controlling vascular quiescence by inducing delta-like 4 expression through AKT-mediated activation of beta-catenin.* J Biol Chem, 2011. **286**(10): p. 8055-66.

185. Hammes, H.P., et al., *Angiopoietin-2 causes pericyte dropout in the normal retina: evidence for involvement in diabetic retinopathy.* Diabetes, 2004. **53**(4): p. 1104-10.

186. Rajantie, I., et al., *Bmx tyrosine kinase has a redundant function downstream of angiopoietin and vascular endothelial growth factor receptors in arterial endothelium.* Mol Cell Biol, 2001. **21**(14): p. 4647-55.

187. He, Y., et al., *Critical function of Bmx/Etk in ischemia-mediated arteriogenesis and angiogenesis.* J Clin Invest, 2006. **116**(9): p. 2344-55.

188. Kim, O., J. Yang, and Y. Qiu, *Selective activation of small GTPase RhoA by tyrosine kinase Etk through its pleckstrin homology domain.* J Biol Chem, 2002. **277**(33): p. 30066-71.

189. Gorovoy, M., et al., *LIM kinase 1 coordinates microtubule stability and actin polymerization in human endothelial cells.* J Biol Chem, 2005. **280**(28): p. 26533-42.

190. Yang, N., et al., *Cofilin phosphorylation by LIM-kinase 1 and its role in Rac-mediated actin reorganization.* Nature, 1998. **393**(6687): p. 809-12.

191. Totsukawa, G., et al., *Distinct roles of ROCK (Rho-kinase) and MLCK in spatial regulation of MLC phosphorylation for assembly of stress fibers and focal adhesions in 3T3 fibroblasts.* J Cell Biol, 2000. **150**(4): p. 797-806.

192. Sun, H., et al., *Rho and ROCK signaling in VEGF-induced microvascular endothelial hyperpermeability.* Microcirculation, 2006. **13**(3): p. 237-47.

193. Yamada, A., et al., *Inhibition of smooth-muscle myosin-light-chain phosphatase by Ruthenium Red.* Biochem J, 2000. **349 Pt 3**: p. 797-804.

194. Hashimoto, T., et al., *Abnormal pattern of Tie-2 and vascular endothelial growth factor receptor expression in human cerebral arteriovenous malformations.* Neurosurgery, 2000. **47**(4): p. 910-8; discussion 918-9.

195. Uranishi, R., et al., *Expression of endothelial cell angiogenesis receptors in human cerebrovascular malformations.* Neurosurgery, 2001. **48**(2): p. 359-67; discussion 367-8.

196. Hashimoto, T., et al., *Regulation of tie2 expression by angiopoietin--potential feedback system.* Endothelium, 2004. **11**(3-4): p. 207-10.

197. Makinde, T.O. and D.K. Agrawal, *Increased expression of angiopoietins and Tie2 in the lungs of chronic asthmatic mice.* Am J Respir Cell Mol Biol, 2011. **44**(3): p. 384-93.

198. Nethe, M. and P.L. Hordijk, *The role of ubiquitylation and degradation in RhoGTPase signalling.* J Cell Sci, 2010. **123**(Pt 23): p. 4011-8.

199. Doye, A., et al., *CNF1 exploits the ubiquitin-proteasome machinery to restrict Rho GTPase activation for bacterial host cell invasion.* Cell, 2002. **111**(4): p. 553-64.

200. Lerm, M., et al., *Identification of the region of rho involved in substrate recognition by Escherichia coli cytotoxic necrotizing factor 1 (CNF1).* J Biol Chem, 1999. **274**(41): p. 28999-9004.

201. Ren, X.D., W.B. Kiosses, and M.A. Schwartz, *Regulation of the small GTP-binding protein Rho by cell adhesion and the cytoskeleton.* EMBO J, 1999. **18**(3): p. 578-85.

202. Perez-Sala, D., et al., *The C-terminal sequence of RhoB directs protein degradation through an endo-lysosomal pathway.* PLoS One, 2009. **4**(12): p. e8117.

203. Rolli-Derkinderen, M., et al., *Phosphorylation of serine 188 protects RhoA from ubiquitin/proteasome-mediated degradation in vascular smooth muscle cells.* Circ Res, 2005. **96**(11): p. 1152-60.

204. Forget, M.A., et al., *Phosphorylation states of Cdc42 and RhoA regulate their interactions with Rho GDP dissociation inhibitor and their extraction from biological membranes.* Biochem J, 2002. **361**(Pt 2): p. 243-54.

205. Fidalgo, M., et al., *Adaptor protein cerebral cavernous malformation 3 (CCM3) mediates phosphorylation of the cytoskeletal proteins ezrin/radixin/moesin by mammalian Ste20-4 to protect cells from oxidative stress.* J Biol Chem, 2012. **287**(14): p. 11556-65.

206. Soucy, T.A., et al., *An inhibitor of NEDD8-activating enzyme as a new approach to treat cancer.* Nature, 2009. **458**(7239): p. 732-6.

207. Nawrocki, S.T., et al., *MLN4924: a novel first-in-class inhibitor of NEDD8-activating enzyme for cancer therapy.* Expert Opin Investig Drugs, 2012. **21**(10): p. 1563-73.

208. Read, P.W., et al., *Human RhoA/RhoGDI complex expressed in yeast: GTP exchange is sufficient for translocation of RhoA to liposomes.* Protein Sci, 2000. **9**(2): p. 376-86.

209. Lampugnani, M.G., et al., *CCM1 regulates vascular-lumen organization by inducing endothelial polarity.* J Cell Sci, 2010. **123**(Pt 7): p. 1073-80.

210. Ma, X., et al., *PDCD10 interacts with Ste20-related kinase MST4 to promote cell growth and transformation via modulation of the ERK pathway.* Mol Biol Cell, 2007. **18**(6): p. 1965-78.

211. Li, R., et al., *A mesenchymal-to-epithelial transition initiates and is required for the nuclear reprogramming of mouse fibroblasts.* Cell Stem Cell, 2010. **7**(1): p. 51-63.

212. Nishino, K., et al., *DNA methylation dynamics in human induced pluripotent stem cells over time.* PLoS Genet, 2011. **7**(5): p. e1002085.

213. Itskovitz-Eldor, J., et al., *Differentiation of human embryonic stem cells into embryoid bodies compromising the three embryonic germ layers.* Mol Med, 2000. **6**(2): p. 88-95.

214. Levenberg, S., et al., *Endothelial cells derived from human embryonic stem cells.* Proc Natl Acad Sci U S A, 2002. **99**(7): p. 4391-6.

215. James, D., et al., *Expansion and maintenance of human embryonic stem cell-derived endothelial cells by TGFbeta inhibition is Id1 dependent.* Nat Biotechnol, 2010. **28**(2): p. 161-6.

216. Yang, L., et al., *Human cardiovascular progenitor cells develop from a KDR+ embryonic-stem-cell-derived population.* Nature, 2008. **453**(7194): p. 524-8.

217. Matsa, E., et al., *Drug evaluation in cardiomyocytes derived from human induced pluripotent stem cells carrying a long QT syndrome type 2 mutation.* Eur Heart J, 2011. **32**(8): p. 952-62.

218. Boyd, N.L., et al., *BMP4 promotes formation of primitive vascular networks in human embryonic stem cell-derived embryoid bodies.* Exp Biol Med (Maywood), 2007. **232**(6): p. 833-43.

219. Nourse, M.B., et al., *VEGF induces differentiation of functional endothelium from human embryonic stem cells: implications for tissue engineering.* Arterioscler Thromb Vasc Biol, 2010. **30**(1): p. 80-9.

220. Chin, M.H., et al., *Induced pluripotent stem cells and embryonic stem cells are distinguished by gene expression signatures.* Cell Stem Cell, 2009. **5**(1): p. 111-23.

221. Hochedlinger, K. and K. Plath, *Epigenetic reprogramming and induced pluripotency.* Development, 2009. **136**(4): p. 509-23.

222. Ohi, Y., et al., *Incomplete DNA methylation underlies a transcriptional memory of somatic cells in human iPS cells.* Nat Cell Biol, 2011. **13**(5): p. 541-9.

223. Panopoulos, A.D., et al., *Rapid and highly efficient generation of induced pluripotent stem cells from human umbilical vein endothelial cells.* PLoS One, 2011. **6**(5): p. e19743.

224. Lagarkova, M.A., et al., *Induction of pluripotency in human endothelial cells resets epigenetic profile on genome scale.* Cell Cycle, 2010. **9**(5): p. 937-46.

225. Asahara, T., et al., *Isolation of putative progenitor endothelial cells for angiogenesis.* Science, 1997. **275**(5302): p. 964-7.

226. Mead, L.E., et al., *Isolation and characterization of endothelial progenitor cells from human blood.* Curr Protoc Stem Cell Biol, 2008. **Chapter 2**: p. Unit 2C 1.

227. Veleva, A.N., et al., *Selective endothelial cell attachment to peptide-modified terpolymers.* Biomaterials, 2008. **29**(27): p. 3656-61.

228. Veleva, A.N., S.L. Cooper, and C. Patterson, *Selection and initial characterization of novel peptide ligands that bind specifically to human blood outgrowth endothelial cells.* Biotechnol Bioeng, 2007. **98**(1): p. 306-12.